LBL-28970

Lawrence Berkeley Laboratory
UNIVERSITY OF CALIFORNIA

Materials & Chemical Sciences Division

Density Effects on the Molecular Dynamics of the I_2 Geminate Recombination Reaction in Liquid Xe

M.E. Paige
(Ph.D. Thesis)

May 1990

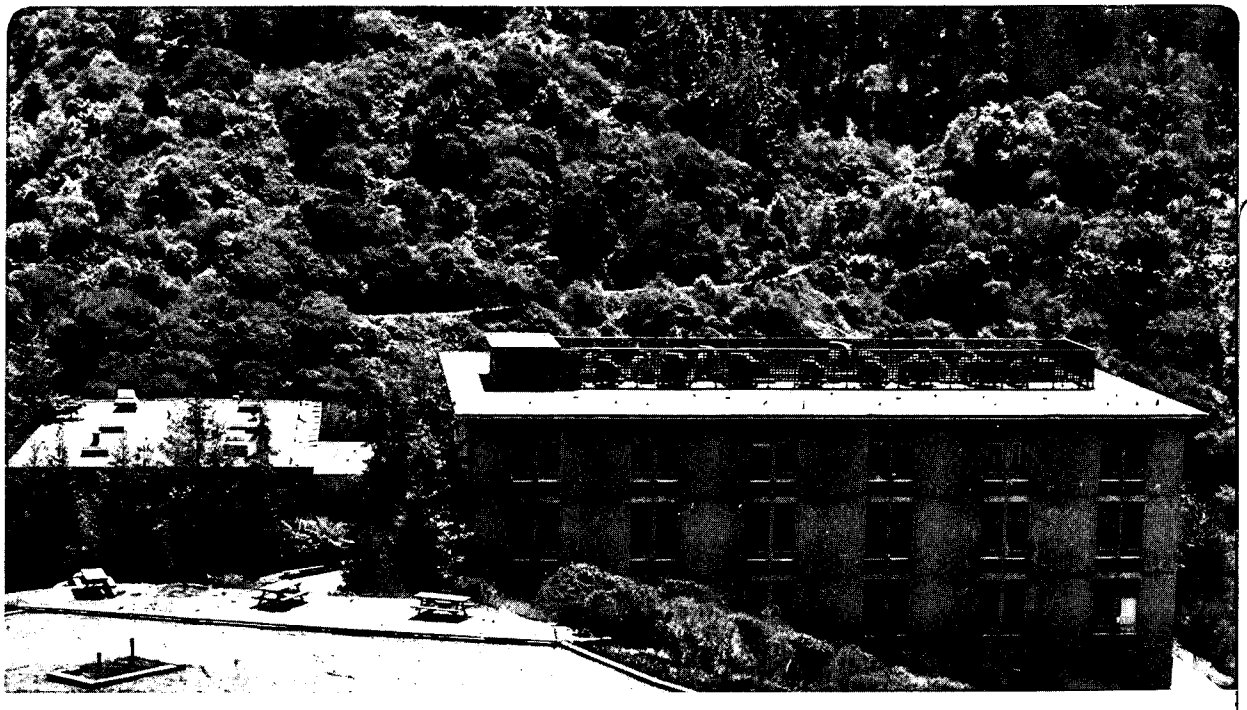

LOAN COPY
Circulates
for 2 weeks
LBL-28970
Copy 2
Bldg. 50 Library.

Prepared for the U.S. Department of Energy under Contract Number DE-AC03-76SF00098.

DISCLAIMER

This document was prepared as an account of work sponsored by the United States Government. While this document is believed to contain correct information, neither the United States Government nor any agency thereof, nor the Regents of the University of California, nor any of their employees, makes any warranty, express or implied, or assumes any legal responsibility for the accuracy, completeness, or usefulness of any information, apparatus, product, or process disclosed, or represents that its use would not infringe privately owned rights. Reference herein to any specific commercial product, process, or service by its trade name, trademark, manufacturer, or otherwise, does not necessarily constitute or imply its endorsement, recommendation, or favoring by the United States Government or any agency thereof, or the Regents of the University of California. The views and opinions of authors expressed herein do not necessarily state or reflect those of the United States Government or any agency thereof or the Regents of the University of California.

LBL-28970

Density Effects on the Molecular Dynamics of the I_2 Geminate Recombination Reaction in Liquid Xe

Mark Edward Paige

Ph.D. Thesis

Department of Chemistry
University of California

and

Lawrence Berkeley Laboratory
University of California
Berkeley, CA 94720

May 1990

This work was supported by the National Science Foundation and the Office of Naval Research. The U.S. Department of Energy, Office of Basic Energy Sciences, Chemical Sciences Division, under Contract No. DE-AC03-76SF00098

Density Effects on the Molecular Dynamics of the I_2 Geminate Recombination Reaction in Liquid Xe

by

Mark Edward Paige

Abstract

The dynamics of the I_2 geminate (original partner) recombination reaction in liquid Xe are examined as a function of solvent density and temperature through picosecond transient absorption spectroscopy. Specifically, the vibrational relaxation of I_2 on its ground state potential surface and the nonradiative curve crossing of molecules originally recombining on the A′ state to the ground state are studied. The experiments are performed at 280 K over a range of Xe densities which span the entire liquid phase portion of the Xe phase diagram. The temperature dependence of the dynamics is determined between 253 and 323 K at constant Xe density. Solvent density effects on the ground state absorption coefficients are calculated.

The vibrational relaxation of I_2 is much slower in Xe than it is in molecular solvents, requiring over 3 nsec at the highest Xe density. Measurement of the I_2 vibrational relaxation in CS_2 reveals that the rate of vibration to translation energy transfer can be much greater than that exhibited in the I_2/Xe system. The overall increase in I_2 relaxation rate in high density Xe to that in low density Xe is a factor of 4. Plots of vibrational energy vs. time at different Xe density can be overlapped by linearly scaling the time axis. This linear scaling

behavior for different solvent densities supports the validity of applying gas phase models of vibrational relaxation at liquid densities.

The nonradiative A'→X curve crossing requires ≈8 nsec in Xe and is surprisingly insensitive to changes in solvent density. Further information regarding the general mechanism of A'→X curve crossing is obtained by measuring the A' state lifetime in deuterated chloromethanes and hydrocarbons and comparing the results to those seen in the corresponding undeuterated solvents. The A' lifetime doubles upon deuteration of the solvent which reveals that the $I_2(A')$ is electronically deexcited through an electronic to vibration energy transfer to the solvent C-H stretch modes. Thus, nonadiabatic curve crossing is an important mechanism in the A'→X nonradiative transition.

Charles B. Harris
April 11, 1990

Table of Contents

I. Introduction 1

II. Experimental Details and Results 17

A. Picosecond Transient Absorption Technique 17

B. Further details regarding I_2/Xe 21

C. Further details regarding I_2/CS_2 24

D. Further details regarding Deuterated Solvents 25

E. High Pressure Apparatus 25

F. Spectra Interpretation and Decomposition 33

III. Conversion of I_2/Xe Spectra to Vibrational Energy Information 49

A. General Approach 49

B. Solvent Effects on the Extinction Coefficients 56

C. Solving for C[i](t) 69

IV. Ground State Vibrational Relaxation 72

A. I_2/Xe 72

i. Qualitative Features 72

ii. Comparison of Experimental Results to Theoretical Predictions and Simulations 80

iii. Consideration of Isolated Binary Collision Modeling .. 92

B. I_2/CS_2 102

V. A' and A State Dynamics 107

A. I_2/Xe 107

i. General Features 107

ii. Density and Temperature Dependence 112

B. Deuterium Isotope Effect on A' Lifetime 121

VI. Summary and Conclusions 129

Appendix 134

References 142

Acknowledgments 148

I. Introduction

The solution phase is the most practical and widespread medium in which chemical reactions are conducted. While development of synthetic methods and techniques in this phase has been largely successful, little is understood about the microscopic physical processes underlying chemical reactions in solution. For the most part, such knowledge is a matter of understanding the energy flow in the system as it occurs through molecular interactions and collisions. In the gas phase, major progress has been made in reaction dynamics because of molecular beam and laser techniques through which reactants are prepared in a particular energy state and then after a single collision, the energy states of the products determined. However, in solution, no comparable isolation technique exists since a solvated molecule is continually within the intermolecular potential range of several molecules at any given time. This non-isolated environment of molecules in liquids creates problems for both theorists and experimentalists who wish to understand the molecular dynamics in this phase. The theoretical difficulties include solving multibody interaction problems while also dealing with the dynamic nature of liquids, i.e., the constant molecular motion which eliminates the static lattice structure characteristic of solids. For experimentalists, the problems encountered are not having and being unable to determine accurate potential surfaces. Thus, accurate assignment of spectroscopic data is often difficult. In addition, until recent technological developments, experimentalists have been unable to resolve the fast timescales involved in many liquid processes as a

molecule in solution typically undergoes a collision every 0.1 psec. As a result, liquid phase dynamics is a very young and relatively undeveloped field which is still lacking the large experimental data base essential in developing and testing theories.

Because of the relatively undeveloped state of liquid dynamics, one wishes to to study a simple solution phase chemical reaction such as the photodissociation and geminate recombination of iodine in weakly interacting solvents. There are a number of advantages in studying this system. First, this "simple" reaction involves many processes which are important in larger systems. These processes include bond formation, vibrational energy transfer, electronic curve crossing, predissociation, and cage recombination. Second, the geometric simplicity of a homonuclear diatomic molecule makes I_2 much easier to model theoretically and numerically and thus, it has often been used as a prototype system for development of theories regarding a wide variety of liquid phase processes. Third, since I_2 contains only one vibrational mode, one can focus on the role of the solvent in dissipating the vibrational energy of the hot I_2 without competion from vibration to vibration intramolecular energy transfer. Naturally, this is an important effect to understand in developing solution phase chemical reaction theory and once understood, will allow for easier interpretation in larger molecular systems where intramolecular vibration to vibration energy transfer is involved. A fourth advantage of studying I_2 is that a large amount of information has been gathered regarding the gas phase potential surfaces of this molecule, particularly during the late 70's and early 80's by Tellinghuisen and coworkers.[1] While these potential surfaces will be

somewhat altered in the liquid phase, a point which will be addressed later in this thesis, these gas phase surfaces provide a good approximation, a luxury which experimentalists often must do without in more complicated molecules. Thus, firm spectroscopic assignments regarding transient absorption measurements can be made for this reaction. A last advantage of the I_2 system is that I_2 can be photodissociated with light frequencies which fall in the middle of the visible spectrum (500-600 nm), a region which is very well suited to the rather limited range of high power picosecond laser sources.

Interest in the I_2 recombination reaction as a prototype system for understanding liquid phase dynamics dates back to the 1930's when Rabinowitch and Wood cited the geminate recombination of I_2 as exemplifying the physical entrapment of two chemical species by the solvent around them, a process for which they coined the term "cage effect".[2] Twenty years later, Noyes and coworkers measured nongeminate yields as a function of solvent viscosity and photon excitation energy in order to understand the cage effect.[3-9] In the late 70's and early 80's, Troe and coworkers extended this work by conducting these studies in high pressure gases in order to determine the density dependence on the nongeminate yields.[10-13] However, not until the advent of picosecond lasers, were the dynamics of the geminate recombination investigated.

Such studies were initiated by Chuang, Hoffman, and Eisenthal in 1974.[14] Their experiment was designed to measure the geminate recombination time of the I atoms following dissociation. They measured the recombination time by monitoring the recovery of the ground state absorption following photodissociation. If the recombination process is

diffusive in nature, i.e., similar to a random walk within the solvent cage, a 100 psec decay would be expected (the time required to diffuse a molecular diameter in solution). On the other hand, if the recombination is ballistic, i.e., rebounding off the solvent cage followed by immediate recombination, a decay no longer than a few picoseconds would be observed. Since 50-200 psec was the typical absorption recovery time observed for I_2 in a variety of hydrocarbons and chloromethanes, the recombination process was thought to be diffusive in nature.

Subsequently, a number of molecular dynamics simulations of this system showed that recombination should occur within a few picoseconds.[15-17] These results indicated that the recombination was not a diffusive motion within the solvent cage. However, electronic transitions in these simulations were treated very artificially since the atoms were placed on the ground state surface once they were within kT of this potential surface while there are actually a large number of surfaces with the same asymptotic energy as the ground state. Nonetheless, the results of these simulations led Nesbitt and Hynes to question the interpretation of the bleach recovery as being a measure of the cage recombination time.[18] They noted that the recovery of the ground state absorption requires not only the recombination of the I atoms, but also vibrational relaxation down to the bottom of the ground state surface which entails a vibrational energy loss of 12500 cm^{-1}. They suggested that the vibrational relaxation dominated the observed timescale for this bleach recovery. Previously, it had been assumed that the relaxation would require not much more than a few picoseconds since I_2 is such a low frequency oscillator (ω_e=214 cm^{-1})[19]. Nesbitt and

Hynes' hypothesis of slow vibrational relaxation was based upon gas phase type modelling of the system (isolated binary collision model) which revealed that approximately 100 psec was required for I_2's vibrational relaxation in CCl_4. As a test of their interpretation of the ground state bleach recovery, Nesbitt and Hynes suggested that experimentalists look for ground state transient absorptions from excited I_2 vibrational levels. Because of the Franck-Condon factors for the B←X transition (the dominant transition in the ground state spectrum), these transient absorptions should shift from the near infrared at high vibrational levels to 520 nm at v=0 as the molecule vibrationally relaxed, thereby mapping out this process (see figure 1).

Shortly after this suggestion, Kelley et al. reported finding a transient absorption which peaked in the 600-750 nm region and showed no wavelength shift with time.[22] This absorption decayed exponentially with a 1/e lifetime which varied from 100 psec in hydrocarbon solvents to as long as 3 nsec in CCl_4. The origin of this absorption was postulated to be from the two low lying I_2 trap states, the A and A' states (see figure 2). Thus, I atoms could recombine onto the ground, A', or A states with those molecules forming on the A' and A states curve crossing back to the ground state with a time characterized by the decay of the transient absorption. Two years after Kelley's finding, Harris et al. and Bado et al. discovered an additional transient absorption component in the 600-1000 nm region.[25-27] This new absorption component shifted toward shorter wavelength with time, just as Nesbitt and Hynes had suggested would be indicative of vibrational relaxation in the system. From these

Figure 1 Classical Franck-Condon outer turning point transitions from the ground state to the B state for various wavelengths. Notice that as the vibrational energy of the I_2 increases, the transition moves toward longer wavelengths. The wavelengths shown in the figure are the probe wavelengths used in the experiments which will be described later. The potential surfaces are from references 20 and 21.

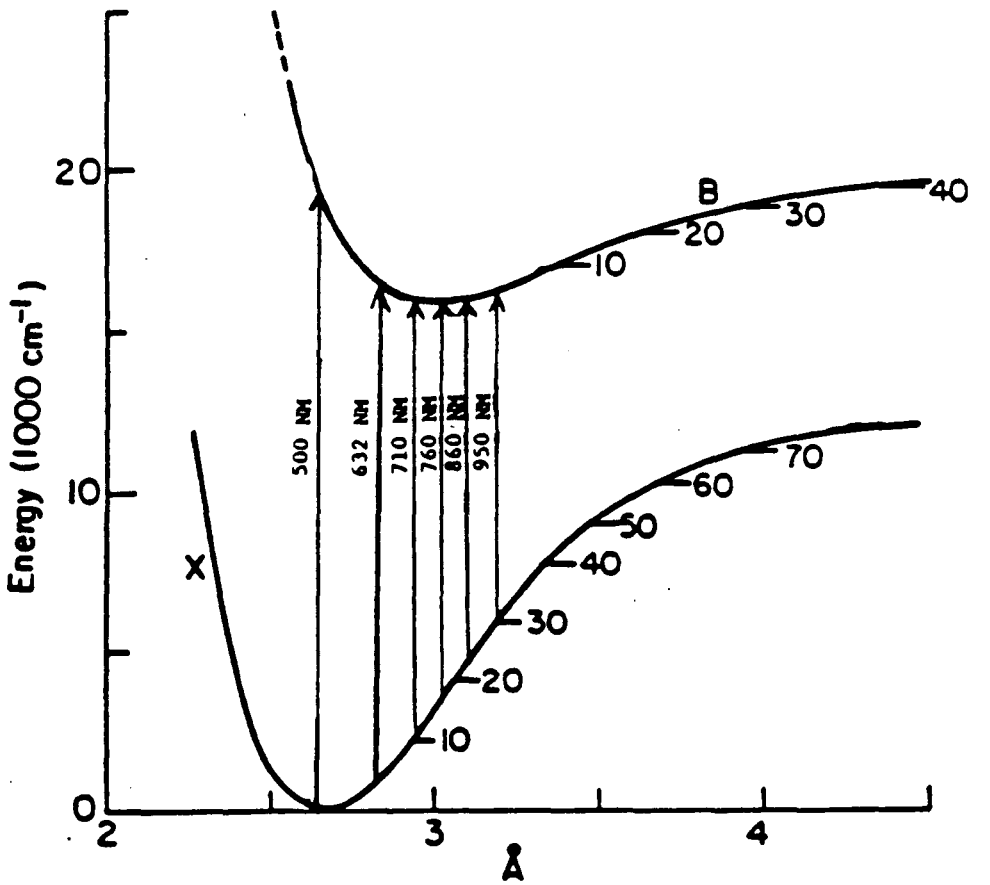
Energy (1000 cm⁻¹)
20
10
0
2
3
4
Å
X
B
500 NM
632 NM
710 NM
760 NM
860 NM
950 NM
10
20
30
40
10
20
30
40
50
60
70

Figure 1

Figure 2 The A and A′ state potentials of I_2.[23-24] The A and A′ state surfaces are the only potential surfaces which have well depths that are significantly larger than kT and have the same asymptotic energy as the ground state. Molecules which recombine on the A and A′ states eventually nonradiatively curve cross back to the ground state.

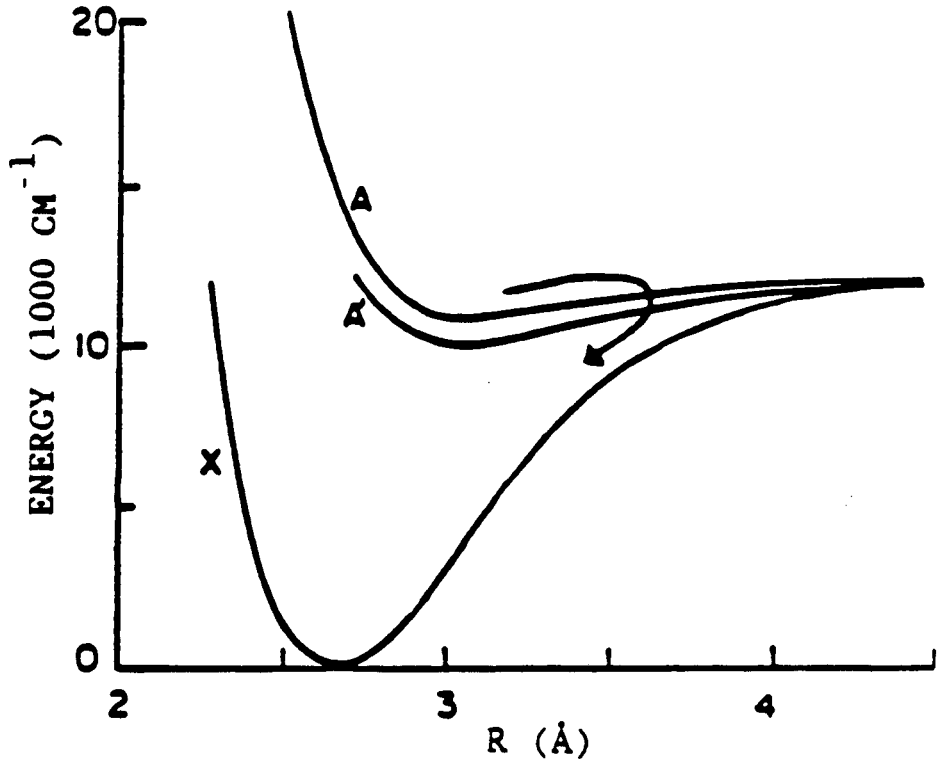

Figure 2

new measurements, the vibrational relaxation time was found to require from 50 to 200 psec in various weakly interacting hydrocarbon and chloromethane solvents while the cage recombination time was set at an upper limit of 10 psec and nonradiative electronic transition times from the A' and A states back to the ground state ranged from 100 to 3000 psec.

With the processes occurring in this reaction identified, emphasis can now be placed on understanding the factors controlling these dynamics. While the I_2 experiment has been performed in a variety of hydrocarbon and chloromethane solvents, little physical insight as to the mechanisms of the ground state vibrational relaxation or A'/A→X curve crossing has been gained. The primary reason for the lack of progress is the complexity of the solvents used in these studies and the large number of parameters which change with solvent such as I_2-solvent intermolecular potential, solvent mass, density, geometry, and the frequencies of the solvent molecule's internal degrees of freedom. Thus, conclusions from these studies regarding the mechanism of the dynamics occurring are difficult to make and typically ambiguous. For example, one would expect that as the solvent vibrational frequencies become resonant with the I_2 vibrational frequency that the I_2 vibrational relaxation would occur more quickly. The relaxation times observed in various chloromethane solvents do not follow this expectation as the relaxation in CCl_4 which has a vibrational mode resonant with the I_2 vibrational frequency is 3 times slower than that observed in CH_2Cl_2 whose lowest vibrational mode is 65 cm^{-1} higher than I_2's.[28] The findings are not altogether surprising as other modes of energy transfer and steric effects will influence the

relaxation time. As to the large variance of A'/A state lifetime observed in different solvents, no correlation with solvent parameters such as viscosity (which might control the time required to reach the large internuclear separation required for the curve crossing) or ionization potential (as a measure of electronic interaction) has yet been found which explains these dramatic changes.

Better control of the solvent parameters is therefore desirable. A natural method to establish such control is to perform these experiments in a pressure cell so that the solvent density and temperature can be independently varied using a single solvent and the effects of these fundamental parameters on the dynamics may be established. In general, few experiments have been performed thus far which have studied the independent effects of solvent density and temperature on vibrational relaxation or electronic curve crossing in solution. As a result, theoretical development regarding these processes has been limited. Establishment of the dependence of the dynamics on these parameters will therefore provide a basis for theoretical models.

Additionally, the I_2 experiment can be further simplified by using a monatomic solvent. A monatomic's spherical geometry and lack of internal degrees of freedom make theoretical and computational analysis much easier. Such a reduction in complexity of the system is very desirable given the relatively undeveloped state of theoretical molecular dynamics in solution and the difficulties inherent in trying to describe liquid phase dynamics. Also, the role of vibration to translation energy transfer in the vibrational relaxation process can be determined in a monatomic solvent since the internal degrees of freedom are eliminated.

The relative efficiency of vibrational energy transfer from the I_2 to solvent vibrational, rotational, and translational modes has not yet been experimentally established. As is illustrated by the relaxation times observed in the chloromethane series mentioned above, insight into the mechanisms of vibrational relaxation in these molecular solvents is obscured by their complexity and a lack of knowledge regarding the relative importantance of the various relaxation pathways (i.e., vibration to vibration, vibration to rotation, or vibration to translation energy transfer).

Xe is an apparent choice as the monatomic solvent since the entire liquid density range of Xe can be studied with pressures under 4000 atm. The I_2/Xe system has also been the subject of some controversy regarding the efficiency of vibrational relaxation in this system. Back when the bleach was thought to be a measure of the recombination time, Kelly and Rentzepis reported a 60 psec bleach recovery time for the I_2/Xe system.[29] This result is quite puzzling since a number of theoretical papers published afterward predicted that vibrational relaxation in this system would require over a nanosecond.[18,30-31] If Kelly and Rentzepis' results are correct, vibrational relaxation in Xe is faster than that observed in any molecular solvents and the relaxation must be dominated by vibration to translation energy transfer which directly contradicts the theoretical findings. Another reason for using Xe as the solvent is that it is a rare gas. Thus, a minimal amount of electronic interaction with the I_2 is expected as compared to previously studied solvents and the alteration of the gas phase potential surfaces should be smaller. Nature has also selected Xe as the solvent of choice since Xe is the only rare gas in

which I_2 is soluble enough to obtain the required concentrations for performing the experiment.

Thus, for these reasons, the I_2 experiment has been performed in liquid Xe and the results of this experiment are reported in this thesis. At a temperature of 280 K, the experiment has been repeated at five densities which cover the entire Xe liquid density range (1.8 to 3.4 g/ml). Conversely, the temperature dependence of the dynamics has been determined at four different temperatures between 253 and 323 K while the density was held constant at 3.0 g/ml. The Xe densities and temperatures studied are indicated on the Lennard-Jones phase diagram shown in figure 3.

In addition to studying the density and temperature dependence of the I_2 ground state vibrational relaxation and A'/A→X curve crossing in liquid Xe, also reported in this thesis are the findings of experiments using CS_2 as the solvent. As previously mentioned, little is known about the comparative importance of the solvent's various degrees of freedom in vibrationally relaxing the I_2. Intuitively, one expects the rotational and translational solvent modes to be effective in relaxing a low frequency oscillator while solvent vibrational modes would be effective in dissipating the energy of a high frequency vibrator. However, little experimental work has been done to establish this notion. The vibrational modes in CS_2 are much too high for efficient vibration to vibration energy transfer with I_2 and thus, the role of vibration to translation and vibration to rotation energy transfer from I_2 to solvent can be examined in this system.

Figure 3 Lennard-Jones phase diagram. The circles indicate the densities and temperatures used in the experiments for Lennard-Jones Xe (σ= 4.1 Å, ϵ= 154 cm^{-1}).[16,32-33] However, Xe is not well characterized by the Lennard-Jones potential and the experimental density which is a solid on this phase diagram is in reality a liquid which is near the solid-liquid transition.

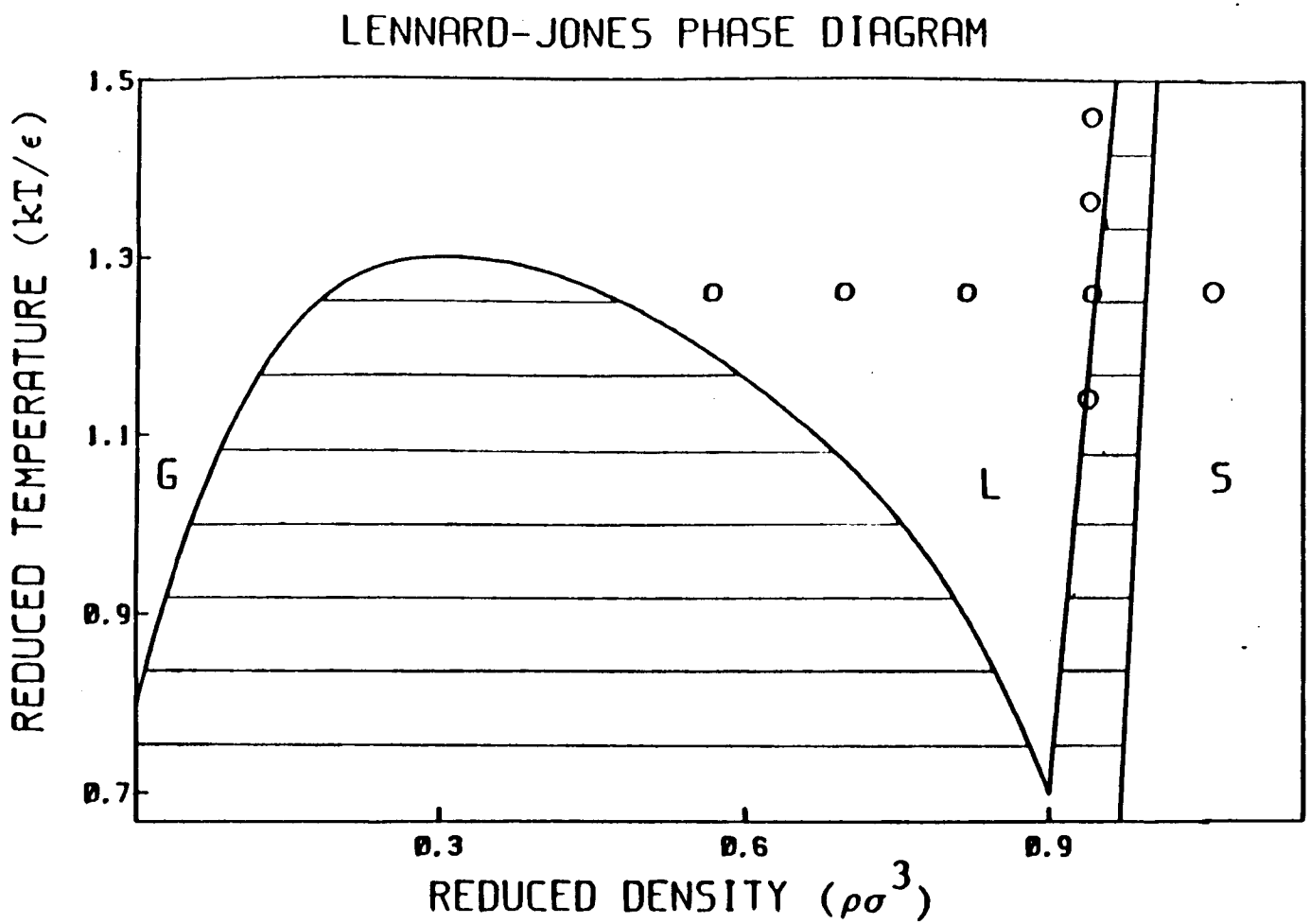
LENNARD-JONES PHASE DIAGRAM
REDUCED TEMPERATURE (kT/ε)
1.5
1.3
1.1
0.9
0.7
G
L
S
0.3
0.6
0.9
REDUCED DENSITY (ρσ³)

Figure 3

Also reported in this thesis are results on experiments in deuterated analogs of various hydrocarbon and chloromethane solvents. While the original intention in performing these experiments was to determine if the vibration to rotation energy transfer from the I_2 to solvent is very sensitive to changes in the solvent's moments of inertia, an unexpected effect was observed on the A'/A state lifetime. The findings of these experiments illuminate the mechanism of the A'/A→X curve crossing and suggest the reason a large range of curve crossing times has been observed in different solvents.

In chapter II of this thesis, the experimental techniques employed in these studies and the transient absorption spectra obtained in the aforementioned solvents are presented. In chapter III, the analysis required to convert the ground state transient absorptions observed in Xe into information regarding the time behavior of the I_2 vibrational energy is detailed. A large portion of this chapter investigates solvent effects on the spectroscopy. In chapter IV, the ground state vibrational relaxation findings in Xe and CS_2 are discussed. Of particular noteworthiness in chapter IV is a new test of the validity of gas phase vibrational relaxation models at liquid density. In Chapter V, the significance of the findings regarding A'/A state lifetimes in these solvents and in the deuterated solvents is explored. Lastly, a summary of the findings is presented in chapter VI.

II. Experimental Details and Results

A. Picosecond Transient Absorption Technique

Transient absorption spectra of the I_2/Xe and I_2/CS_2 systems were taken at 6 probe wavelengths - 500, 632, 710, 760, 860 and 950 nm. Transient absorption spectra for the deuterated hydrocarbons and chloromethanes were taken at 350, 632, and 710 nm. The optical setup is shown in figure 4. The laser source is a synchronously pumped dye laser whose output is amplified in a three cell dye amplifier chain with the second harmonic (532 nm) of a 10 Hz Nd:YAG laser.[34-35] The final pulse is 1 psec long, 1 mJ in energy, 590 nm in wavelength, and has single shot stability of ±10%. 40% of this pulse was used to excite the sample. 87% of the molecules excited at this wavelength are promoted to the predissociative B state and 7% and 6% to the directly dissociative $^1\pi_u$ and A states.[1] The remaining 60% of the laser pulse was focused into a cell containing water or acetone to generate the white light continuum source (350-950 nm) which was used as a probe pulse. Transient absorption spectra were taken one wavelength at a time by selecting a wavelength from the continuum source with a 10 nm bandpass filter, spatial filtering this beam, and then using the front surface reflections from two 1/2" thick silica flats to provide signal and reference beams. These beams were focused into their respective samples with 25 cm focal length lenses. Since 500 nm is near the peak of the I_2 room temperature spectrum where the extinction coefficient is quite sensitive to wavelength, a reference cell with an identically absorbing solution was

Figure 4 Laser system and optical setup used for detecting I_2 transient absorptions.

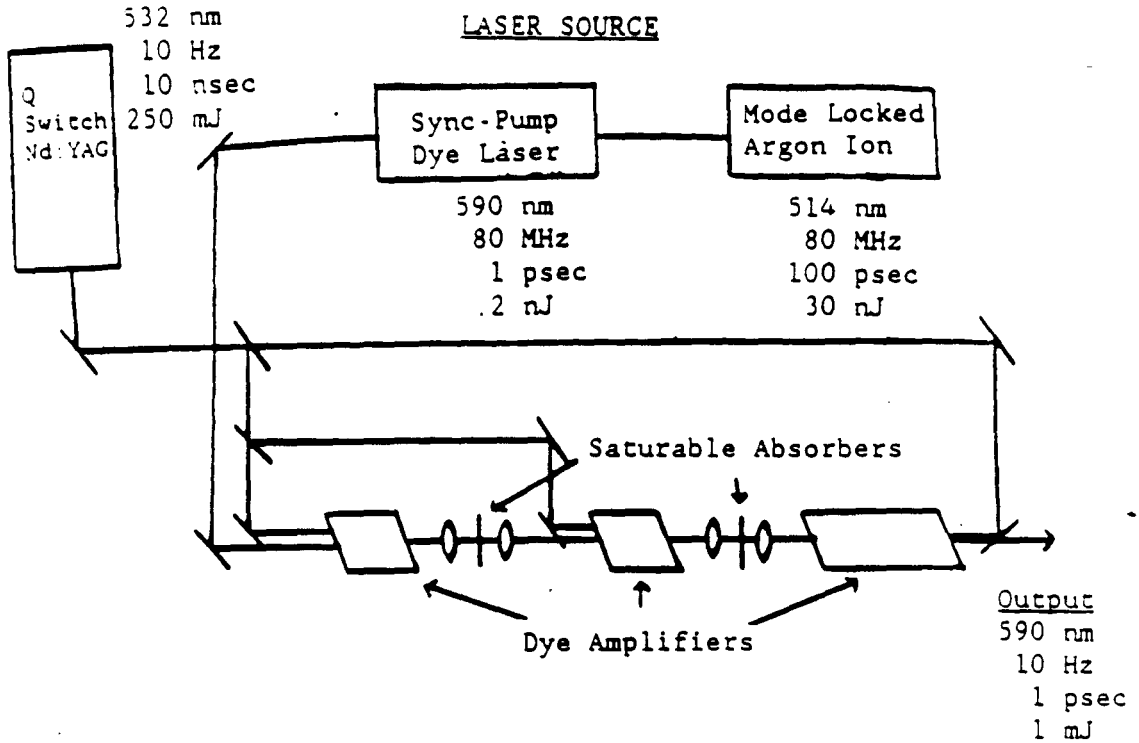

Optical Setup for Transient Absorption Measurements

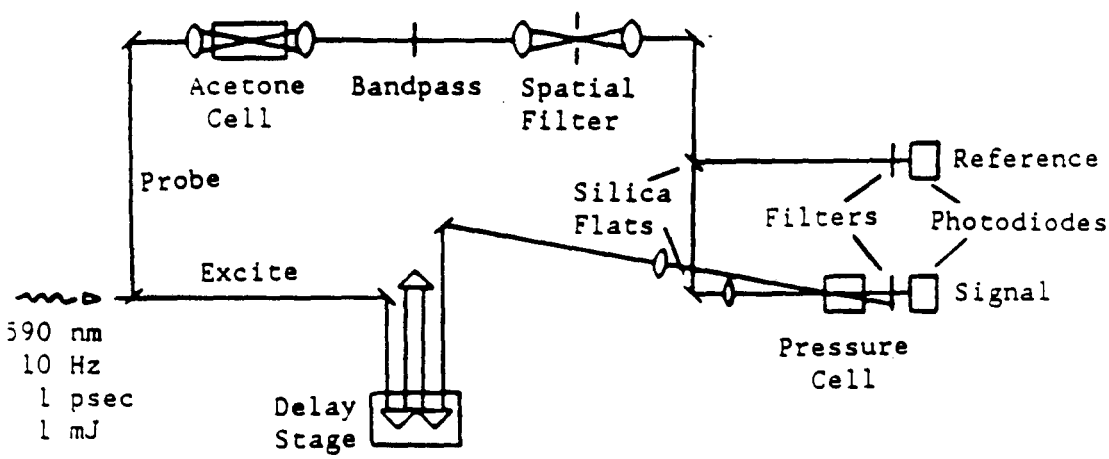

Figure 4

required to normalize out the continuum wavelength fluctuations at this wavelength. For I_2/Xe, this requirement poses a problem since only one pressure cell was available. However, it was empirically determined that an I_2/hexane solution has nearly the same room temperature absorption spectrum as the I_2/Xe solution and could be used as a reference sample when performing ground state bleach measurements at 500 nm. At other wavelengths, no reference sample was needed since the room temperature absorbance at these wavelengths is either insensitive to slight wavelength fluctuations or is nonexistent. After passing through identical colored filters which block the excite beam, the probe beams were detected on EG&G DT110 photodiodes. The photodiode signals were fed into a LeCroy 10 bit A/D converter which was interfaced to a LSI11 computer. With this setup, single shot changes of 0.2% between the signal and reference beams could be detected.

The excitation pulse made two round trips on a Klinger 1 meter variable path length delay stage before entering the sample, allowing for maximum time delays between excite and probe pulses of 11 nsec. Retroreflectors were used on this stage to make beam alignment easier. The excitation beam was focused into the sample at a 6° angle to the probe beam with a 50 cm focal length lens. The sample was placed 45 cm away from the excite beam's lens and in the focus of the probe beam. This off angle approach improved the signal size by approximately 4 times over a collinear excite-probe setup without the loss of any observable time resolution. The off angle method improves the signal because the excite can be more tightly focussed into the sample since small amounts of excite generated continuum in the sample do not reach the photodiodes

(and Xe appears to continuum generate easily). Using two different lenses for the excite and probe beams also allows tighter focussing of the poorer focal quality probe beam so that only the excited region of the sample is being probed. The I_2 used in these experiments is Mallinckrodt analytical reagent grade (>99.8%) and the solutions were prepared at I_2 concentrations of 4.5 mM. Nongeminate recombination at this concentration requires nearly a microsecond and thus, only appears in ground state bleach measurements as a long time offset.

B. Further details regarding I_2/Xe

The I_2/Xe sample is prepared by loading dry I_2 into a high pressure optical cell, evacuating the cell to 500 mtorr (200 mtorr above the I_2 vapor pressure), and then pressurizing with 99.9995% Xe. The cell is pressurized to 1000 atm with a Newport Scientific diaphragm compressor and further pressurized with a Nova Swiss piston intensifier. The pressure is measured within 2% accuracy with a Bourdon tube gauge or can be calculated from the oil pressure on the low pressure end of the intensifier. The Xe thermodynamic states used in these experiments are listed in table 1. To prevent I_2 corrosion, the cell body, valves and tubes connected to the cell, and all cell parts coming into contact with the I_2 solution were constructed from heat treated β C titanium alloy. The clear aperture through the cell is 6 mm and the sample pathlength is 1 cm. The windows were made from oriented sapphire (Union Carbide) and were 10 mm thick. These windows were sealed on an optically polished

Table 1

ρ (g/ml)	T (K)	ρ^*	T^*	P (atm)
1.8	280	0.57	1.26	48
2.2	280	0.70	1.26	163
2.6	280	0.82	1.26	577
3.0	253	0.95	1.14	1291
	280		1.26	1607
	303		1.37	1855
	353		1.46	2056
3.4	280	1.07	1.26	3006

Caption: PVT information for the Xe thermodynamic states used in the experiments.[37-38] ρ^* and T^* are the Lennard-Jones reduced density and temperature ($\rho\sigma^3$ and kT/ϵ respectively). The Lennard-Jones diameter(σ) for Xe is 4.10 Å and a well depth (ϵ) of 154 cm^{-1}.[16,32-33]

mushroom plug using the Bridgeman unsupported sealing technique. A low pressure/vacuum seal was obtained by tightening the windows against a teflon gasket. A magnetic stir bar loaded inside the cell was used to stir the solution. A copper coil bonded to the cell with thermal conducting epoxy and attached to a temperature regulated circulator was used to control the cell temperature to within ±1° C. Further details regarding the pressure system are described in a subsequent section.

The data collection time varied greatly with density (100 to 2000 laser shots per data point) since the amount of geminate recombination and continuum generation in the sample depends upon density. Generally, three types of scans were performed at each wavelength - an 11 nsec scan with 60 psec timesteps, a 1-2 nsec scan with 6 psec timesteps, and a 100-200 psec scan with 1 psec timesteps. Since the data analysis relies on the excitation intensity being the same at each wavelength and the data collection time for a given Xe thermodynamic state took several days to several months, the absorptions for the various wavelengths were calibrated to one another within a half hour time period by measuring the signal at one time delay for all wavelengths, only changing the necessary filters for the measurement at each wavelength. The transient absorptions were found to be linear over a range of 10 in excite intensity and were observed to be independent of I_2 concentration between 2 and 10 mM. No artifacts were found when the I_2 was removed from the cell and the experiment repeated. The 2.2 g/ml study proved to be the most troublesome experiment as the cell often leaked at this pressure which was too low to obtain a good Bridgeman seal and too high for the low pressure gasket seal. The signal to noise in the 500 nm bleach data

is significantly worse than in the transient absorptions because the sample concentration was halved in order to get enough probe light through the sample.

C. Further details regarding I_2/CS_2

These experiments were performed with a collinear excite-probe configuration. The I_2/CS_2 cuvette was sealed with parafilm and was always kept under a air suction system so that any poisonous CS_2 vapors were prevented from filling the laboratory. A 4 psec transient absorption which was solely due to CS_2 was observed in many of the spectra. This signal was seen to have a quadratic dependence on excitation intensity and thus, is due to a two photon excitation process in the CS_2. This two photon process in the CS_2 appeared to have no effect on the time behavior of the I_2 transient absorptions. At 500 nm, a large transient absorption was observed rather than the expected ground state bleach. After an initial 20 psec decay of about one third the signal, this absorption showed no decay on the timescale available with the delay stage. An excite-probe experiment using two Nd:YAG lasers revealed that this absorption decayed over a few microseconds, a typical nongeminate recombination time. Thus, as has been observed in some other solvents, this transient absorption is believed to result from a I atom-solvent complex.[38] A long lived component of the transient absorption (> 3 nsec) which was linearly dependent upon the excitation intensity was also observed at other wavelengths. Since the dynamics of geminately recombining I_2 were entirely completed long before the maximum time

delay, this offset is believed to be due to a weak I atom-solvent complex absorption.

D. Further details regarding deuterated solvent experiments

The solvents in which the I_2 experiment was performed were CH_2Cl_2, CH_3Cl, cyclohexane, and octane. These solvents were 98 to 100% deuterated (Aldrich Chemical Co.) and were used immediately after breaking the glass sealed vial. Corresponding experiments in the completely undeuterated solvents were performed immediately after the deuterated scans for comparison.

E. High Pressure Apparatus

When working at high pressure,[39-40] one should first consider safety. Catastrophic failure of a high pressure system can be equivalent to a hand grenade exploding. Precautionary steps have been taken to prevent overpressurization and to protect the user should an explosion occur. However, safety improvements to the system should always be considered. Unfortunately, the literature is very scarce and sketchy about proper safety barriers. Consultation with an expert is best (such as an author of a high pressure equipment book). In addition, "overbuilding" of the system increases safety. "Overbuilding" refers to using equipment which is work rated far above the pressure the user intends to work at (the work rating already includes a safety factor). Aside from increased safety, the working lifetime of valve packing and

stems are greatly increased when using valves which are rated for much higher pressures than the user will be working at. The lone drawback is that the equipment is larger and heavier. Overbuilding is probably not more costly in the long run as equipment replacement is not needed as often.

Rupture discs have been installed in the system to prevent accidental overpressurization by the operator or should a valve not seal properly. Valve failure is particularly dangerous since only proper system design can prevent catastrophe. The entire pressure system has been encased in 1/2 inch thick polycarbonate Lexan shielding (commonly known as bullet proof glass). 1/4 inch thick Lexan shielding will withstand the impact of most bullets fired from 10 ft. Additionally, the pressure cell has been enclosed around its sides by 1/8" thick steel or 3/8" thick aluminum. This metal shield is surrounded by the Lexan (otherwise more shrapnel will be flying around than there would be without the metal shielding). The most dangerous part of the system is possible window or endcap failure in the pressure cell. The user should avoid standing in a direct line to the cell path. Several layers of shields have been mounted on the optical table to protect along this path. The optics around the cell area have also been encased in Lexan to protect the user from flying fragments should the window blow out. In addition, hearing protectors are recommended when the system is at high pressure as the shock wave from an explosion at close range can rupture an eardrum.

A schematic of the high pressure system is shown in figure 5. The system includes a high pressure optical cell, a pressure generation

Figure 5 High pressure system capable of performing optical experiments up to 100,000 psi.

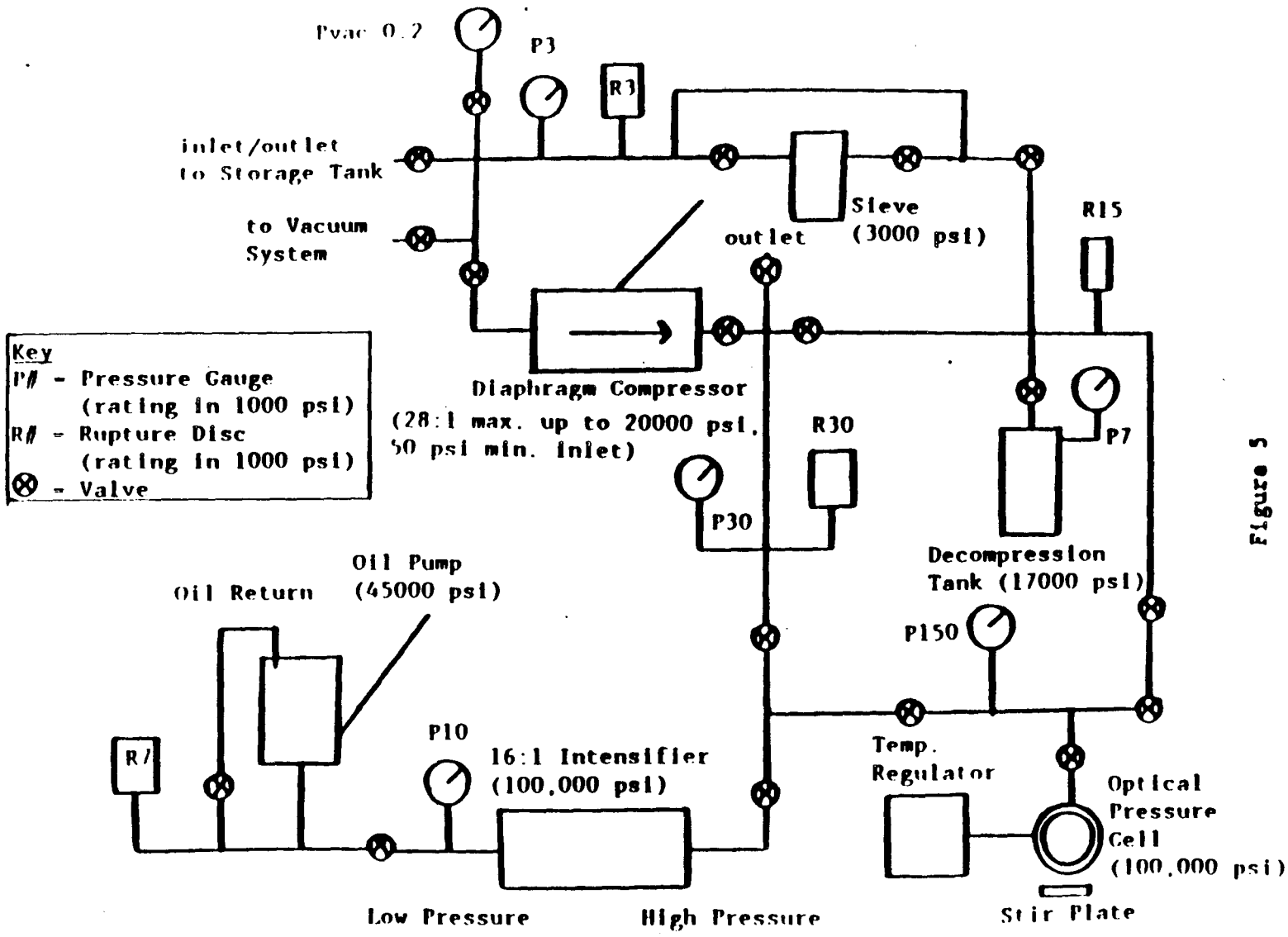
Pvac 0.2
P3
R3
inlet/outlet
to Storage Tank
to Vacuum
System
Sieve
(3000 psi)
outlet
R15
Key
P# - Pressure Gauge
(rating in 1000 psi)
R# - Rupture Disc
(rating in 1000 psi)
⊗ - Valve
Diaphragm Compressor
(28:1 max. up to 20000 psi,
50 psi min. inlet)
R30
P7
P30
Decompression
Tank (17000 psi)
Oil Pump
(45000 psi)
Oil Return
P150
R7
P10
16:1 Intensifier
(100,000 psi)
Temp.
Regulator
Optical
Pressure
Cell
(100,000 psi)
Low Pressure
High Pressure
Stir Plate

Figure 5

system, a vacuum system, and a temperature regulator for the pressure cell. This apparatus is capable of producing pressures of up to 100,000 psi although the valve packing which is rated to 100,000 psi tends to leak at pressures above 85,000 psi when using compressed gases. The gas input to the system is first cold trapped out with liquid nitrogen into a small high pressure cylinder (approximately 100-1000 ml in volume). After warming to room temperature, the gas in this cylinder provides a 750-1000 psi pressure source to feed into the system. Extreme care has to be taken that the cylinder pressure does not become too high upon warming. A relief valve on the tank insures that this situation will not occur. This tank is then connected to the high pressure apparatus. After vacuuming out the air in the system, pressures of 15,000 psi are generated using the two stage diaphragm compressor (from Newport Scientific). Company specifications for the compressor state that a pressure of 20,000 psi can be attained with this device but in practice, hand pumping the last 5,000 psi is more suited for an Olympic event. After using the diaphragm compressor to obtain a high density fluid, the compressor section of the system is sealed off and the pressure intensifier (from Nova Swiss) is used to reach pressures of up to 100,000 psi. The intensifier is a piston type device in which a high pressure piston is pushed by a larger area low pressure piston. The large area piston is moved with a hydraulic oil hand pump. The cross sectional area ratio of the low pressure to high pressure piston is 16:1. A significant amount of friction exerted on the piston by packing accounts for approximately 10% of the oil pressure required to move the pistons. Thus, the actual intensification of the oil pressure used to move the low

pressure piston is approximately 15:1 at the high pressure outlet. A pressure of 750 psi is required to reset the piston toward the low pressure end. The volume of the high pressure end is 40 ml. The pressure at the high pressure end is measured with a 150,000 psi Bourdon tube gauge (from Pressure Products Industries).

A schematic of the 100,000 psi optical pressure cell is shown in figure 6. The cell was built by the departmental machine shop. The cell design was provided by J. Troe and B. Otto from the University of Gottingen. This design is very similar to that of the high pressure optical cell which is made by Nova Swiss. Clearances between mating parts are set to 0.002 ± 0.001 inches. The cell body, mushroom plug, and all other parts which come into contact with the high pressure fluid are made from β C titanium alloy which has been heat treated to obtain a tensile strength of approximately 185,000 psi. After a considerable search, this alloy was the strongest alloy found which resists iodine corrosion. No signs of corrosion have been evident after several thousand hours of use. The tube and valve attached to the cell were also made of titanium alloy. The cell part under the most pressure is the pressure cap. Deformation of this part is avoided if it is made of an ultra high strength alloy such as drill rod which can be heat treated to attain a tensile strength of 300,000 psi. The clear aperture of the cell is 1/4 inch and the cell pathlength is approximately 1 cm. The sapphire windows are 10 mm thick and are oriented with the c axis at 0 degrees.

To pressurize the optical pressure cell, the cell is first pumped to approximately 750 psi and then sealed off with the valve directly attached to it. At this pressure the teflon gasket can hold the gas pressure provided that the cell endcaps have been tightened sufficiently

Figure 6 High pressure optical cell. 1) guide case made from β C titanium alloy, 2) mushroom plug made from β C titanium alloy, 3) triangular anti-extrusion rings made from β C titanium alloy, 4) support ring made from 17-4 PH steel, 5) cell body made from β C titanium alloy, 6) endcap made from 17-4 PH steel, 7) pressure cap made from heat treated drill rod (nickel plated to prevent rusting), 8) teflon O-ring, 9) sapphire window, 10) teflon gasket. The figure is drawn to scale (1:1) except for the cell body diameter.

Figure 6

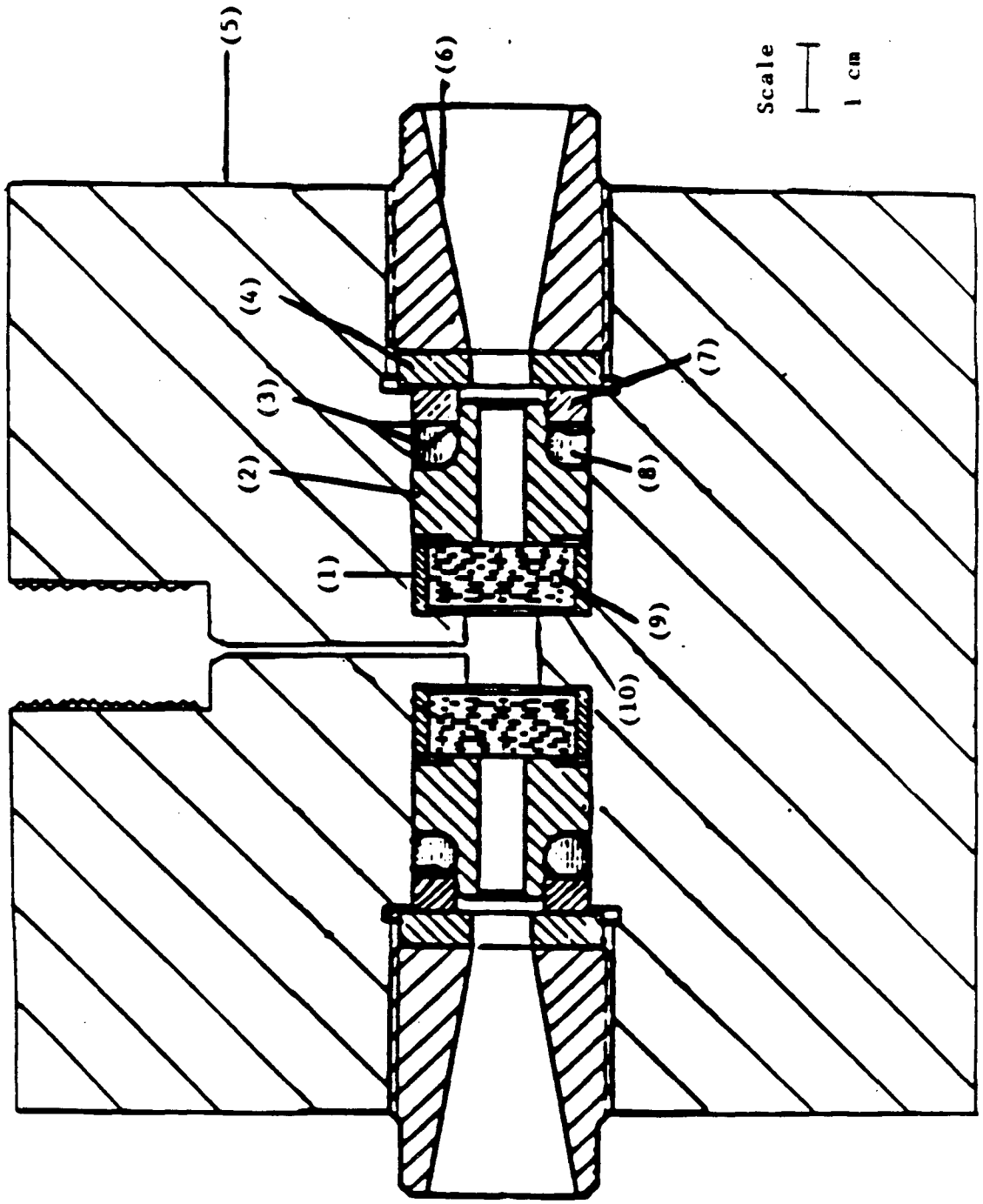

(300 inch-pounds is more than enough torque). At pressures above 1500 psi however, the teflon gasket will no longer seal. At 10,000 psi the windows will seal against the optically polished window mounts. Thus, high cell pressures are attained by pressurizing the rest of the system above 10,000 psi with the cell valve closed and then opening the cell valve. Once the desired pressure is attained in the cell, the pressurization equipment is sealed off to protect it from iodine corrosion. Depressurization of the cell was performed in a slow and controlled manner through the use of several valves. Slow depressurization of the windows is important as windows are most likely to blow out when depressurizing (although sapphire is not known to do this). The gas is cold trapped back in the storage tank through a return loop and not through the pressurization part of the system in order to avoid iodine corrosion of the pressurization units.

F. Spectra Interpretation and Decomposition

The long time transient absorption spectra taken at the six probe wavelengths for Xe densities of 1.8 and 3.0 g/ml at 280 K are shown in figure 7. Interpretation of these spectra is based upon the previous studies of the I_2 system in weakly interacting molecular solvents as was discussed in the introduction (see figure 8).[22,26,41] To recapitulate, these experiments have shown that predissociation occurs 1 psec following excitation and that the subsequent geminate recombination occurs in under 20 psec onto either the X, A, or A' states. Those molecules initially

Figure 7 I_2/Xe transient absorption spectra at 280 K at Xe densities of 3.0 and 1.8 g/ml. The short time component of the spectra originates from the ground state and the long tail from the A and A′ states. The shift of the ground state component toward longer wavelength with time reflects vibrational relaxation of the hot I_2. Notice that the ground state component at the lower density is much slower than that at the higher density.

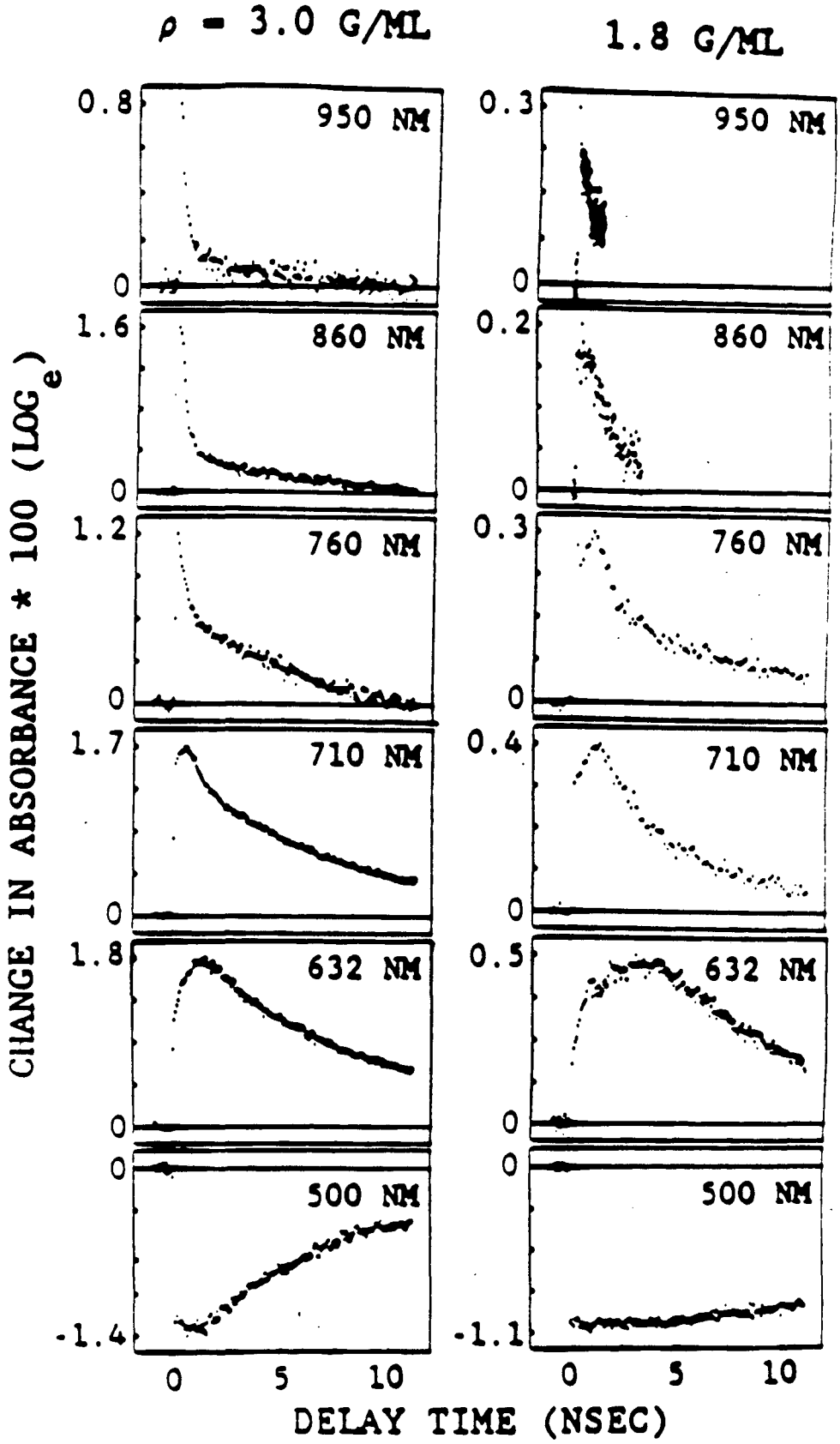
ρ = 3.0 G/ML
1.8 G/ML
950 NM
860 NM
760 NM
710 NM
632 NM
500 NM
0.8
0
1.6
1.2
1.7
1.8
-1.4
0.3
0.2
0.4
0.5
-1.1
CHANGE IN ABSORBANCE * 100 (LOG$_e$)
0
5
10
DELAY TIME (NSEC)

Figure 7

Figure 8 I_2 geminate recombination reaction as observed in molecular solvents: 1) excitation with 1 psec laser pulse to the B state, 2) predissociation (under 1 psec), 3) recombination onto X, A, or A' states (under 20 psec), 4) X state vibrational relaxation (100-200 psec), and 5) A'/A→X nonradiative curve crossing (100-3000 psec). Potential surfaces are from references 20, 21, 23, 24, and 42.

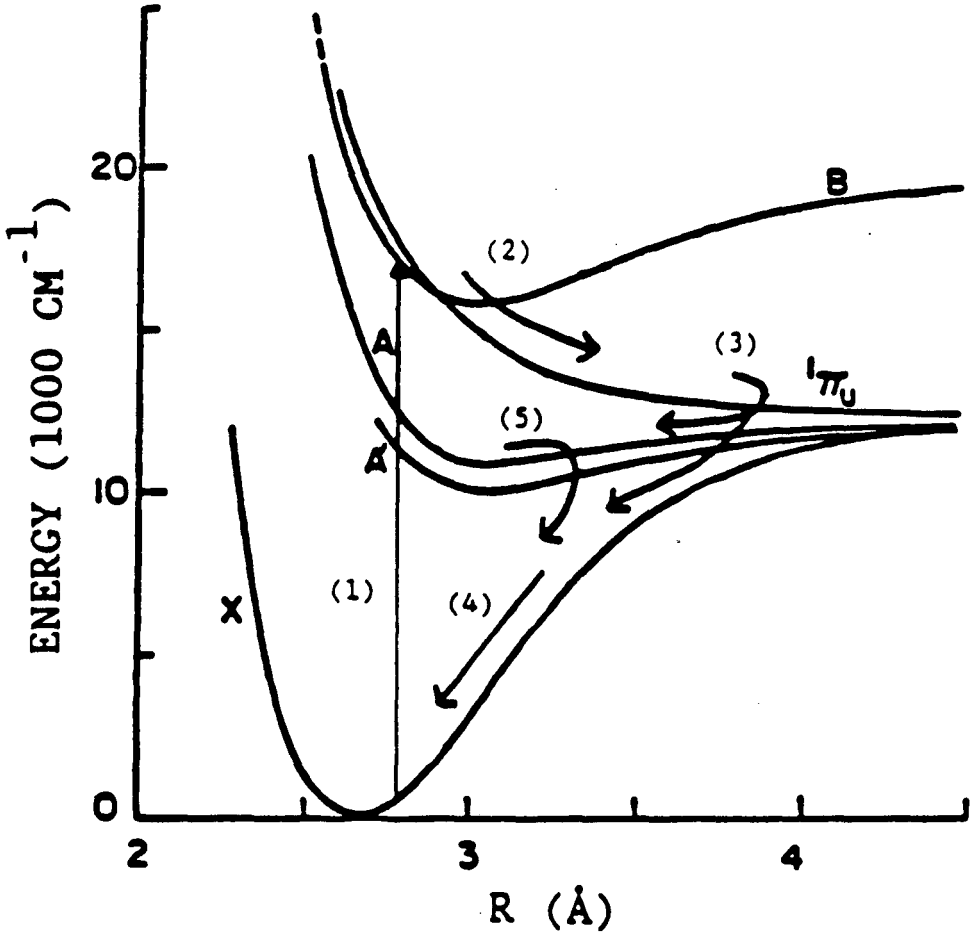

Figure 8

forming on the A and A' states eventually nonradiatively curve cross back to the ground state. This curve crossing time appears in the spectra as a long time exponential tail whose magnitude peaks in the 600 - 720 nm region and shows the same time behavior at all wavelengths. The A and A' lifetimes have never been separately distinguished and vary from 100 to 3000 psec dependent on solvent. Those molecules originally recombining on the ground state appear in the spectra as a short time peak which smoothly shifts from the near infrared to 520 nm as delay time increases. This time dependent behavior of the ground state absorption results from the vibrational energy dependence of the Franck-Condon factors for the B←X transition which smoothly shifts from the near infrared at high vibrational energy to 520 nm at v=0. Thus, the vibrational relaxation of the I_2 can be followed by monitoring the time dependence of this spectral shift. In molecular solvents, the ground state absorption peaks at 1000 nm in a few picoseconds followed by a 10-15 psec decay as the absorption shifts toward shorter wavelength. This shift continues until the v=0 absorption which appears as a 100-200 psec decay in the ground state bleach.

With this interpretative scheme, the transient absorptions for the I_2/Xe system can be separated into ground state and A'/A state components as presented in table 2. In the spectra taken at wavelengths greater than and including 760 nm, the ground state component peaks and decays within the first nanosecond and is easily distinguished from the more slowly decaying A'/A state component. At shorter wavelengths the ground state component's decay can be difficult to discern from that of the A'/A states. While in other solvents the decay of the A'/A state absorption

Table 2 Caption:

Fits of I_2 transient absorption spectra in various Xe thermodynamic states. The numbers in parentheses are the Gaussian error ranges in which the parameters may be perturbed without increasing the χ^2 error by more than a factor of 4 (90% confidence limits). A question mark after a number means that value could not be determined from the spectra because it was obscured by an unresolved absorption component or a scan was not performed on an appropriate timescale. Except for F=5, the fitting functions, F, are segmented into an X state component (x subscript) and an A/A' state component (A subscript) with C representing the magnitude, R being the rise time, and D being the decay time. The A'/A component sometimes shows a double rise. The F=5 function is for fitting X state bleaches with C_{1A} being the nongeminate offset and the C_{2A} term representing hole burning requilibration in unexcited molecules.

Fitting Functions (F)

A'/A state component= $C_A = (C_{1A}e^{-t/R_{1A}} + C_{2A}e^{-t/R_{2A}})e^{-t/D_A}$

$t' = t - t_c$

	for $t' \leq 0$	for $t' > 0$
1)	$C_x(1-e^{-t/R_x}) + C_A$	$C_x(1-e^{-t/R_x})e^{-t'/D_x} + C_A$
2)	$C_x e^{-(t'/R_x)^2} + C_A$	$C_x e^{-(t'/D_x)^2} + C_A$
3)	$C_x(1-e^{-t/R_x}) + C_A$	$C_x(1-e^{-t/R_x})e^{-(t'/D_x)^2} + C_A$
4)	$C_x e^{-(t'/R_x)^2} + C_A$	$C_x e^{-t'/D_x} + C_A$

Table 2 Caption (continued)

	for $t' \leq 0$	for $t' > 0$
5)	$[1 + C_{2A}(1-e^{-t/R_{2A}})][C_x + C_{1A}]$	$[1+ C_{2A}(1-e^{-t/R_{2A}})][C_x e^{-t'/D_x} + C_{1A}]$

Table 2

ρ (g/ml)	T (K)	λ (nm)	F	C_x ($\Delta A*100$)	R_x (psec)	D_x (psec)	t_c (psec)	C_{1A} ($\Delta A*100$)	R_{1A} (psec)	C_{2A} ($\Delta A*100$)	R_{2A} (psec)	D_A (psec)
3.4	280	950	1	0.56(.11)	7(8)	270(90)	0	0.79(.50)	1?	-	-	7500?
		860	1	0.80(.10)	9(6)	300(80)	0	0.14(.06)	1?	-	-	7500?
		760	1	1.13(.35)	215(140)	320(90)	0	0.73(.05)	5?	-	-	6900(850)
		710	1	0.19(.12)	250(230)	375(240)	390(250)	1.09(.04)	11(5)	-	-	7400(600)
		632	1	0.36(.23)	640(430)	775(440)	825(360)	1.00(.12)	14(3)	0.73(.19)	525(250)	7600(850)
		500	5	-0.45(.14)	-	5750(3200)	1600(1100)	-0.54(.13)	-	0.16(.09)	745(670)	-
3.0	280	950	1	1.23(.15)	35(20)	155(45)	0	0.21(.91)	40?	-	-	3900(2600)
		860	1	1.64(.10)	77(14)	250(20)	0	0.22(.03)	10?	-	-	4700(1500)
		760	1	0.88(.16)	245(95)	430(180)	0	0.57(.06)	7?	-	-	3900(1100)
		710	3	0.40(.11)	485(310)	790(340)	480(220)	1.74(.07)	12(1)	-	-	7460(300)
		632	2	0.26(.20)	790(590)	1530(570)	1385(500)	1.57(.17)	26(6)	1.30(.25)	640(275)	9100(650)
		500	5	-2.59(.17)	-	6250(850)	1370(520)	-0.41(.17)	-	0.10(.07)	240(165)	-
2.6	280	950	1	2.14(.34)	88(25)	170(20)	0	0.07	20?	-	-	7000(2600)
		860	1	1.97(.25)	160(30)	265(30)	0	0.18(.26)	20?	-	-	6900?
		760	1	0.38(.10)	135(70)	640(185)	510(205)	0.85(.07)	5?	-	-	5900(640)
		710	1	0.43(.14)	1080(335)	1085(250)	1290(250)	1.22(.07)	20(3)	-	-	4500(650)
		632	1	0.31(.23)	1950(950)	1755(640)	1940(570)	1.18(.11)	38(10)	1.56(.23)	1050(270)	8850(900)
		500	5	-2.11(.40)	-	8000(3600)	2400(1100)	-1.99(.45)	-	0	1	-
2.2	280	950	1	0.33(.12)	105(90)	385(140)	0	0.06(.04)	33(16)	-	-	7500(3800)
		860	3	0.18(.03)	73(70)	350(160)	535(150)	0.11(.02)	11?	-	-	8250(4000)
		760	1	0.23(.14)	400(300)	700(390)	1070(490)	0.73(.09)	175(95)	-	-	5400(1450)
		710	1	0.30(.08)	635(365)	1155(400)	1555(420)	0.50(.05)	7?	-	-	9900(1200)
		632	1	0.30(.05)	860(420)	2280(570)	2620(500)	0.33(.04)	60()	-	-	9500(1200)
		500	5	-0.33(.20)	-	7100(4500)	3800(2400)	-0.64(.17)	-	0.10(.06)	1610(1340)	-
1.8	280	950	1	0.20(.18)	100(230)	290(280)	0	0.09(.03)	20?	-	-	7500?
		860	1	0.14(.04)	75(70)	1015(565)	650(550)	0.02(.04)	3?	-	-	7500?
		760	1	0.18(.06)	955(860)	625(185)	950(890)	0.18(.02)	16(8)	-	-	7500(900)
		710	4	0.19(.04)	1000(565)	1670(820)	1390(356)	0.35(.05)	56(23)	-	-	6400(800)
		632	4	0.30(.11)	1800(290)	8690(2400)	4000(950)	0.56(.15)	270(180)	-	-	6300(2400)
		500	5	-0.36(.15)	-	7200(3600)	4400(2300)	-1.51(.14)	-	0	1	-

Table 2 (continued)

ρ (g/ml)	T (K)	λ (nm)	F	C_x (AA*100)	R_x (psec)	D_x (psec)	t_c (psec)	C_{1A} (AA*100)	R_{1A} (psec)	C_{2A} (AA*100)	R_{2A} (psec)	D_A (psec)
3.0	323	950	1	0.94(.16)	27(11)	105(30)	0	0.15	1?	-	-	4500?
		860	1	1.11(.11)	37(16)	175(30)	0	0.23(.04)	25?	-	-	6500(2100)
		760	1	0.36(.11)	195(200)	250(130)	195(175)	0.57(.04)	12(5)	-	-	4350(550)
		710	1	0.32(.23)	500(400)	265(250)	460(240)	1.20(.09)	9()	0.15(.10)	230(240)	3770(425)
		632	1	0.32(.17)	910(430)	635(390)	910(350)	1.10(.12)	23(5)	0.84(.15)	430(160)	4420(275)
		500	5	-0.85(.11)	-	4500(2000)	1200(515)	-0.72(.09)	-	0.19(.06)	340(240)	-
3.0	303	950	1	0.82(.11)	22(10)	165(45)	0	0.11(.06)	1?	-	-	5000?
		860	1	1.15(.22)	53(30)	185(25)	0	0.21(.03)	1?	-	-	4700(1300)
		760	1	0.40(.24)	200(230)	260(135)	390(190)	1.06(.13)	6?	-	-	4200(750)
		710	3	0.50(.11)	335(140)	450(135)	390(140)	1.17(.06)	12()	-	-	5250(490)
		632	1	0.29(.15)	645(340)	540(330)	1045(370)	1.22(.14)	18(3)	1.13(.14)	520(160)	5250(420)
		500	5	-1.29(.19)	-	5000(1600)	1250(800)	-1.15(.10)	-	0.13(.06)	960(1090)	-
3.0	253	950	1	0.51(.10)	27(18)	340(70)	0	.10(.04)	16?	-	-	9000?
		860	1	0.69(.07)	91(30)	440(60)	0	0.14(.03)	23?	-	-	6000(2100)
		760	1	1.33(.36)	580(300)	510(140)	410(200)	1.25(.86)	16?	-	-	8050(1820)
		710	1	0.27(.15)	840(920)	705(360)	975(350)	0.91(.05)	15(3)	-	-	11650(1350)
		632	1	0.29(.17)	2100(1130)	1500(1050)	2115(1100)	0.83(.07)	32(9)	0.86(.18)	1395(415)	12300(1100)
		500	5	-0.70(.10)	-	9675(2800)	3350(1700)	-0.43(.09)	-	0.25(.10)	1100(600)	-

shows the same time behavior throughout the experimentally observed spectral region, in some thermodynamic states of Xe, the decay time lengthens as the wavelength is shortened, thus compounding the separation problem. In addition, in some 632 nm spectra a fast rise (20 psec) followed by a slower rise (>400 psec) is observed for the A/A' absorption. The slow A'/A rise cannot be uniquely determined since it is similar to the ground state absorption rise. No attempt was made to fit the A/A' state component in the 500 nm bleach data since a meaningful fit would require scans with greater time delays than could be performed with the translation stage.

The I_2/CS_2 spectra shown in figure 9 have been interpreted in the same fashion as the I_2/Xe data. With this data, the X and A'/A state components are easily distinguished. These fits are listed in table 3.

Sample spectra in the deuterated and corresponding undeuterated hydrocarbon and chloromethane solvents are shown in figure 10. The A'/A state lifetime in these solvents were determined by fitting the long tail on the transient absorptions at 710 and 632 nm. Harris et al. have shown that the A' and A states also absorb in the 350 nm wavelength region and that this absorption has a decay time identical to that observed in the red to near infrared region.[26] In cases where the ground state absorption at 632 and 710 nm decay obscured the fit of the A'/A lifetime, the transient absorption at 350 nm was used to determine this lifetime. The A' lifetimes determined from these spectra will be listed in a chapter V.

Figure 9 I_2/CS_2 transient absorption spectra. The energies noted in the figure are those associated with the classical Franck-Condon transition from the ground state to the B state. v is the vibrational level and Do is the dissociation energy.

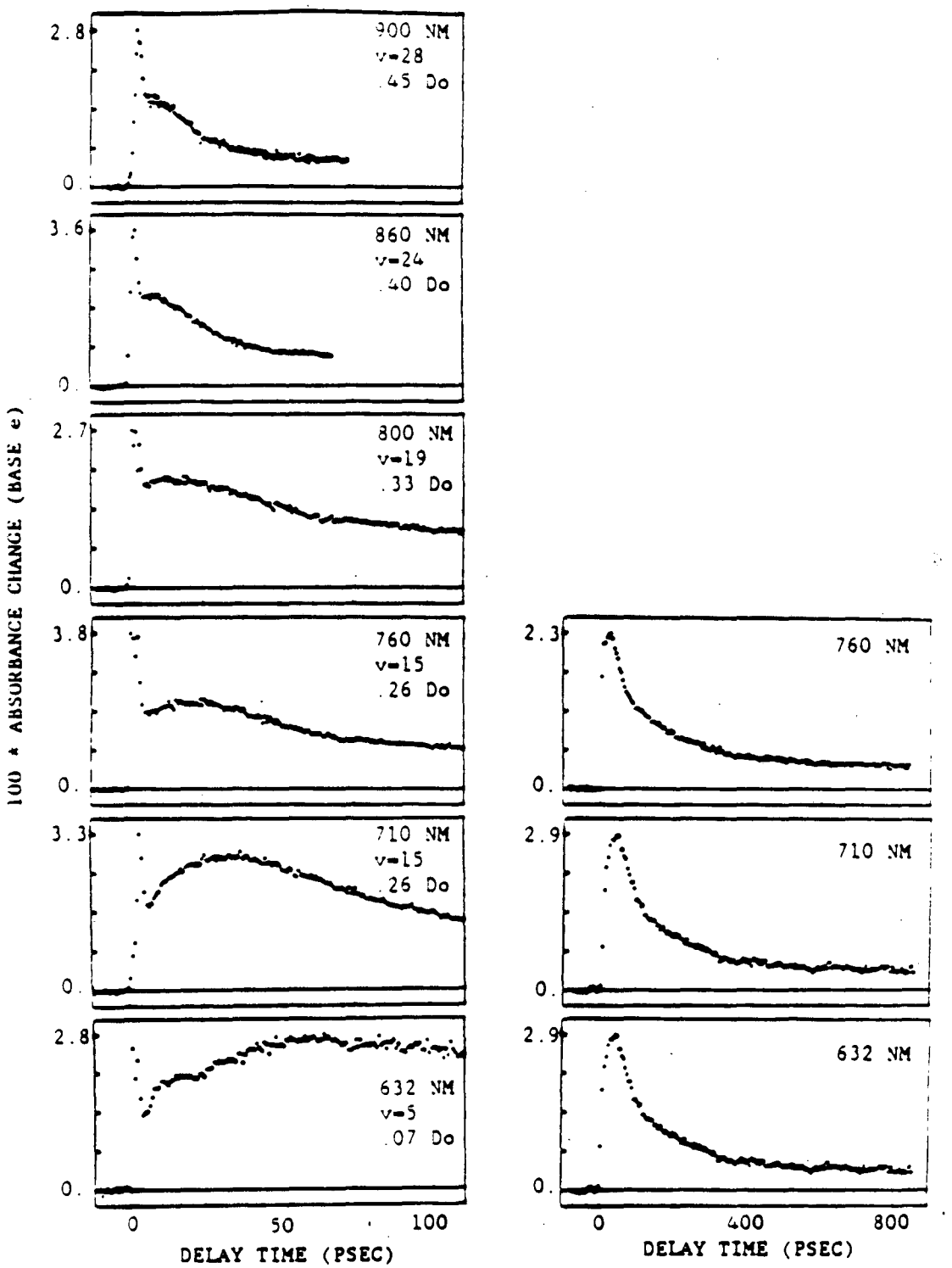
100 * ABSORBANCE CHANGE (BASE e)
2.8
0.
900 NM
v=28
.45 Do
3.6
0.
860 NM
v=24
.40 Do
2.7
0.
800 NM
v=19
.33 Do
3.8
0.
760 NM
v=15
.26 Do
3.3
0.
710 NM
v=15
.26 Do
2.8
0.
632 NM
v=5
.07 Do
0
50
100
DELAY TIME (PSEC)
2.3
0.
760 NM
2.9
0.
710 NM
2.9
0.
632 NM
0
400
800
DELAY TIME (PSEC)

Figure 9

Table 3

λ (nm)	C_X $\Delta A*100$	R_X (psec)	D_X (psec)	t_c (psec)	C_A $\Delta A*100$	R_A (psec)	D_A (psec)
900	4.43(.89)	9.0(2.7)	12.3(1.3)	0	0	.	.
860	3.59(.57)	8.6(2.6)	15.1(1.9)	0	0.55(.12)	2	151.2(50.)
760	0.95(.16)	20.4(6.8)	21.8(5.7)	25.5(6.9)	1.35(.14)	5.5(3.4)	157.9(15.)
710	0.84(.13)	38.3(13.)	27.6(7.5)	40.8(8.6)	2.91(.13)	9.5(1.2)	158.4(17.)
632	1.56(.51)	70.1(56.)	96.2(52.)	66.8(45.)	2.89(.74)	18.8(17.)	155.1(25.)

Fitting Function

$$C_X(1-e^{-t/R_X})e^{-(t-t_c)/D_X} + C_A(1-e^{-t/R_A})e^{-t/D_A}$$

Caption: Fits of transient absorption spectra of I_2/CS_2 at various probe wavelengths (λ). Subscript X indicates ground state parameters while subscript A represent the A'/A state parameters. ΔA is absorbance (base e), R is a rise time, and D is a decay time. The numbers in parentheses represent the Gaussian error ranges in which the parameters may be perturbed without increasing the χ^2 by more than a factor of 4 (90% confidence limits). The absorbances listed here have not been calibrated (i.e., measured at the same excitation intensity).

Figure 10 I_2 transient absorption spectra in deuterated and undeuterated dichloromethane. The exponential decay of the transient absorption shown by the solid line fit is a measure of the A'/A lifetime. Notice that the lifetime in the deuterated solvent is exactly twice that of the undeuterated solvent.

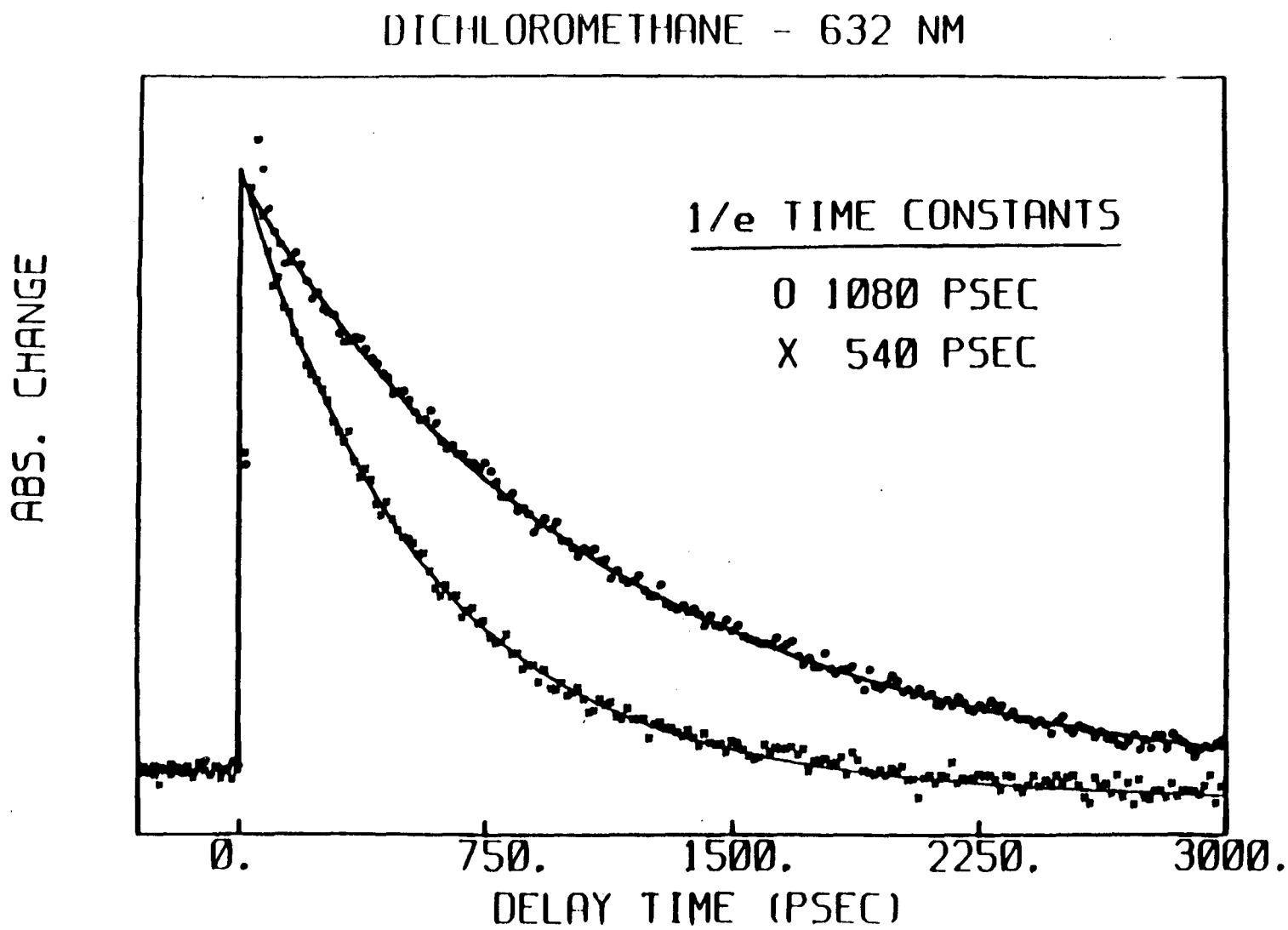
DICHLOROMETHANE - 632 NM
1/e TIME CONSTANTS
O 1080 PSEC
X 540 PSEC
ABS. CHANGE
0.
750.
1500.
2250.
3000.
DELAY TIME (PSEC)

Figure 10

III. Conversion of I_2/Xe Spectra to Vibrational Energy Information

A. General Approach

To determine the I_2 vibrational energy as a function of time, the time evolving population distribution must be found. This distribution is calculated from the transient absorption spectra by applying Beer's law and solving the matrix equation:

$$1) \qquad A[\lambda](t) = \epsilon[\lambda,i] \cdot C[i](t)$$

where $A[\lambda](t)$ is the absorbance vector at time t which is composed of elements for each probe wavelength λ, $\epsilon[\lambda,i]$ is the extinction coefficient matrix with elements for each λ and vibrational level i, and $C[i](t)$ is the relative concentration vector at time t of the vibrational levels. Since the number of vibrational levels greatly exceeds the number of experimental probe wavelengths, the ground state potential surface must be divided into a number of sections equal to the number of probe wavelengths so that a unique solution for the $C[i](t)$ may be found from equation 1. Since six probe wavelengths have been used in these experiments, the ground state surface is divided into six sections and the averaged extinction coefficients over each section are used as the elements of $\epsilon[\lambda,i]$.

The molar extinction coefficient for a specified vibronic transition is calculated using the equation

$$\epsilon(\lambda,\Psi(e_1,v_1)\rightarrow\Psi(e_2,v_2)) =$$

$$C\ g\ \lambda^{-1}\ |\mu_{e_1,e_2}|^2\ |\langle\Psi(e_1,v_1)|\Psi(e_2,v_2)\rangle|^2\ \Gamma(E_2-E_1 - hc/\lambda)$$

where λ is the transition wavelength, $\Psi(e,v)$ are the wavefunctions for electronic state e and vibrational level v, C is a constant, g is the electronic degeneracy, μ is the electronic transition moment, and Γ is the line broadening function which depends upon the energy difference between the two vibronic states and the photon.[43-44] According to Tellinghuisen, the three excited states involved in the ground state absorption spectrum are the A,B, and $^1\pi_u$ states.[1] The RKR gas phase potential surfaces for all of these states are known and were used in calculating the wavefunctions for these states.[20-21,23,42,45-46] The bound wavefunctions were calculated every 0.0025 Å by numerically solving the Schroedinger equation with a Cooly integrator. The unbound wavefunctions were calculated every 0.000125 Å at energy intervals of 50 cm^{-1} using a second order integrator and wavefunction normalization was performed at asymptotic r.[47] The transition moments to the A and $^1\pi_u$ states were assumed to be independent of vibrational energy while that to the B state was assumed to have an R centroid dependence which has been noted in the literature:[48-49]

$\mu_{X,A} = 0.202$ D $\qquad\qquad \mu_{X,^1\pi_u} = 0.369$ D

$\mu_{X,B} = 1.62\ R - 3.51$; $\qquad R < 3.1$ Å

$\qquad = -1.745\ R + 6.91$; $\qquad 3.1 \leq R \leq 3.3$ Å

$$= -0.781\ R + 3.74; \qquad 3.3 < R < 4.6\ \text{Å}$$

where $R = \langle\Psi(v_1)|r|\Psi(v_2)\rangle$ (the R centroid integral)

400 cm^{-1} Gaussian broadening was used to model the solvent line broadening. This amount of broadening was required to remove any spectral features from the calculated room temperature ground state spectrum and duplicate the featureless experimental spectral profile. The constant C was determined by matching the peak magnitude of the calculated room temperature spectrum to that in the literature.[50] The value of this scaling factor has no effect on the vibrational energy calculation since only the relative extinction coefficients are required for this purpose.

The vibrational energy dependence of the extinction coefficients at the six probe wavelengths is shown in figure 11. The extinction coefficient for each probe wavelength is strongly peaked near the Franck-Condon classical turning point with a long tail extending up to high vibrational energies and a sharp decay at energies below the turning point. Thus, the transient absorption decay at a given wavelength indicates when the population has relaxed below the energy corresponding to the Franck-Condon turning point. The peaked shape of the extinction coefficients suggests that the most sensible way of segmenting the ground state surface into six regions and keeping $\epsilon[\lambda,i]$ as nonsingular as possible is to separate the peaks of the different probe wavelengths into different sections. This segmentation is shown in figure 12 where the averaged extinction coefficient over each section for 760 nm is superimposed upon the calculated extinction coefficient. These averaged

Figure 11 Ground state gas phase extinction coefficients at experimental probe wavelengths as a function of vibrational energy.

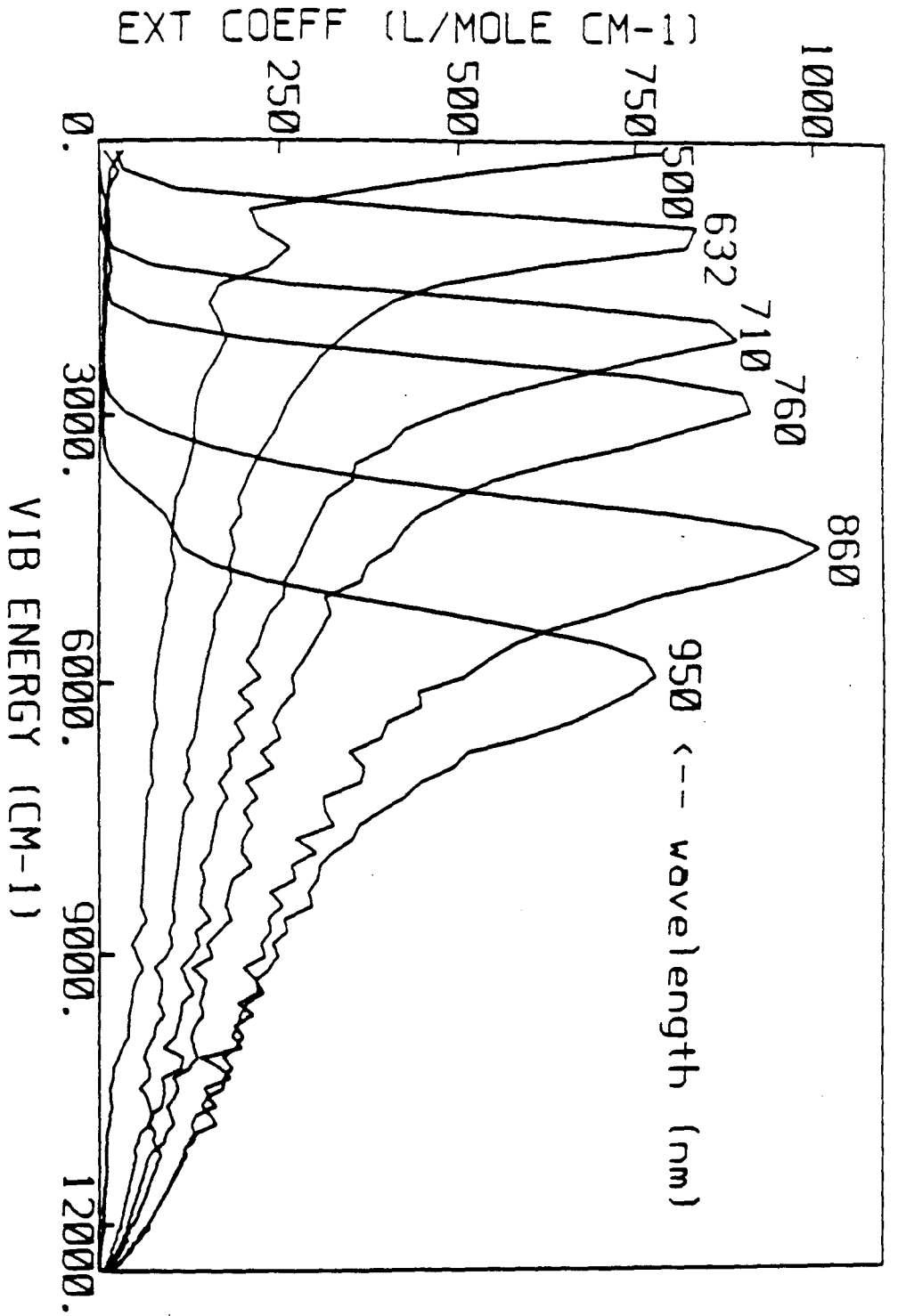
EXT COEFF (L/MOLE CM-1)
1000
750
500
250
0.
500
632
710
760
860
950 <-- wavelength (nm)
3000.
6000.
9000.
12000.
VIB ENERGY (CM-1)

Figure 11

Figure 12 Segmentation of 760 nm ground state extinction coefficient.

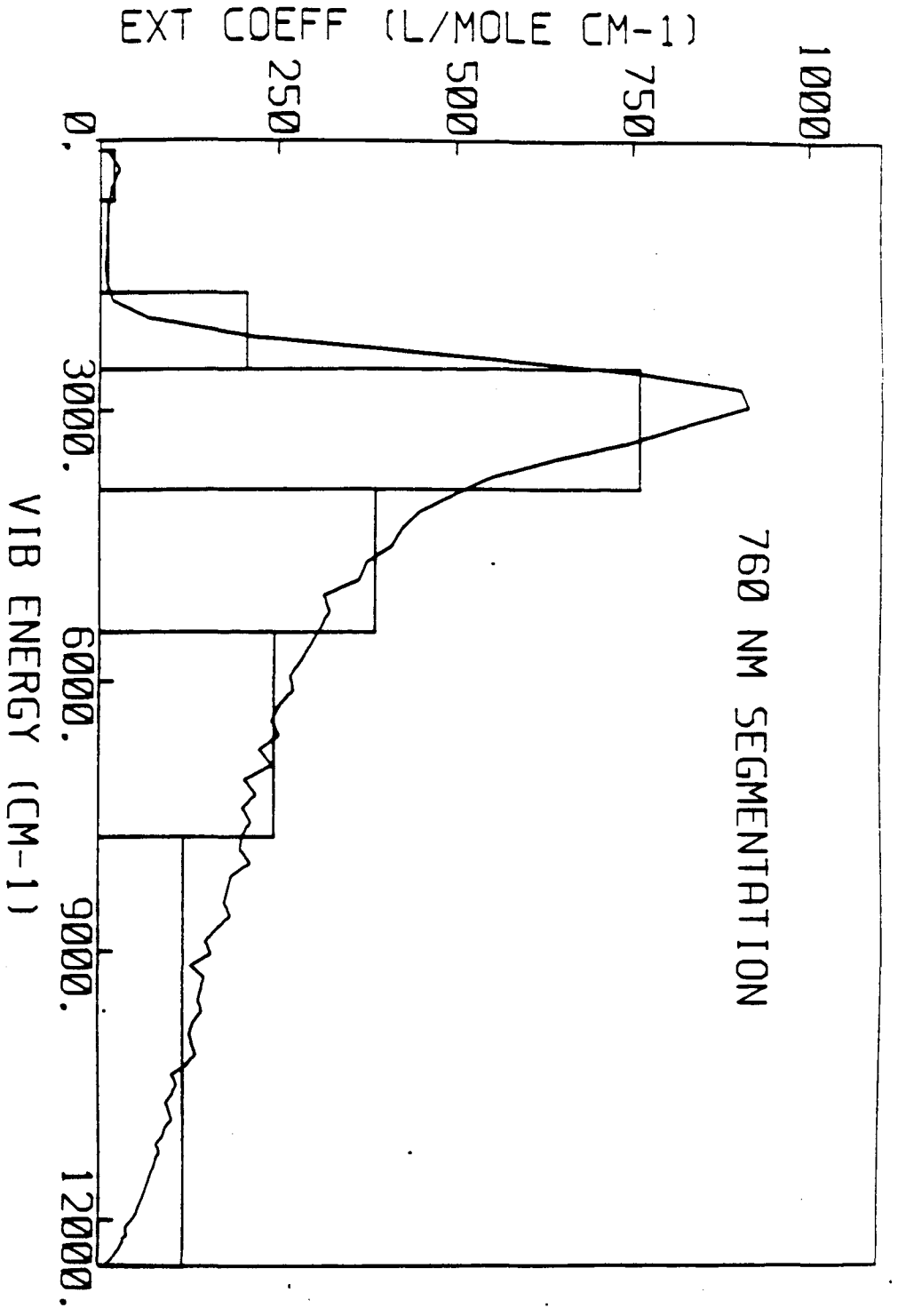
760 NM SEGMENTATION
EXT COEFF (L/MOLE CM-1)
1000
750
500
250
0.
3000.
6000.
9000.
12000.
VIB ENERGY (CM-1)

Figure 12

values are used as the elements of $\epsilon[\lambda,i]$. Since no probe wavelength is peaked in the upper region of the ground state potential surface, only the lower 7000 cm^{-1} of the potential surface was divided into sections for the calculation. Thus, information from these calculations regarding the vibrational energy of the I_2 as a function of time is not quantitatively accurate until the population has relaxed below this energy. The decay of the 950 nm transient absorption which primarily probes the 6000 cm^{-1} vibrational energy region indicates when the population has relaxed below this point. The 950 nm decay ranges from 100-300 psec in these experiments.

B. Solvent Effects on the Extinction Coefficients

In order to assess the solvent's effect on the ground state absorption, potential surfaces of mean force were calculated for the ground state using the classical molecular dynamics simulations of this system which were performed in this laboratory by Brown, Harris, and Tully.[51] Briefly, these simulations contain 1 I_2 and 254 Xe with the interaction between all the atoms in the system assumed to be the sum of the two body Lennard-Jones forces and the I-I interaction being that of the RKR gas phase potential surface. Following equilibration of the system, the atoms are placed on the $^1\pi_u$ dissociative surface with an energy corresponding to the laser pulse. Once the atoms have lost enough energy to be within kT of the ground state surface, they are put on that potential surface. The simulation is continued until the hot I_2 has lost all of its excess vibrational energy. The potential surfaces of mean

force at 280 K were calculated from these simulations for all experimental solvent densities except for 3.4 g/ml Xe which is a Lennard-Jones solid. The ground state potential surface of mean force for the 1.8 and 3.0 g/ml Xe solution and the gas phase RKR potential surface are shown in figure 13. As expected, the potential surface becomes more harmonic as the solvent density is increased due to the growing solvent pressure along the bond axis. The density effect is rather modest in the lower portion of the potential surface with only a few hundred wavenumbers energy difference between high and low density potential surfaces. In the upper portion of the potential surface, the solvent effect becomes quite large - a few thousand wavenumbers - and the difference between high and low densities is substantial.

With the solvent effects on the ground state surface calculated, the remaining problem to be resolved before calculating $\epsilon[\lambda,i]$ is determining the solvent's effect on the excited state potential surface. Since the solvent does not move an appreciable amount during an electronic transition, the effect on the excited state surface was determined by stopping the computer simulation of the I_2 relaxation at various times, inserting the excited state intermolecular potential between I_2 and Xe, calculating the solvent force on the I_2, and then continuing the simulation by reinserting the ground state intermolecular potential.[52] In this manner, the solvent force as a function of internuclear separation was determined. Unfortunately, the intermolecular potential between electronically excited I_2 and Xe is not known. However, since 90% of the ground state absorption strength is to the B state, the alteration in the intermolecular potentials for I_2 in the A or $^1\pi_u$ state

Figure 13 I_2 ground state potential surfaces of mean force at 280 K for Xe densities of 3.0 g/ml (upper surface) and 1.8 g/ml (middle surface). The lower surface is the gas phase RKR potential. The bottom of each well has been set to zero in energy. The solvation energy of the 3.0 g/ml surface is approximately -1700 cm^{-1} and that of the 1.8 g/ml potential surface is approximately -1150 cm^{-1}.

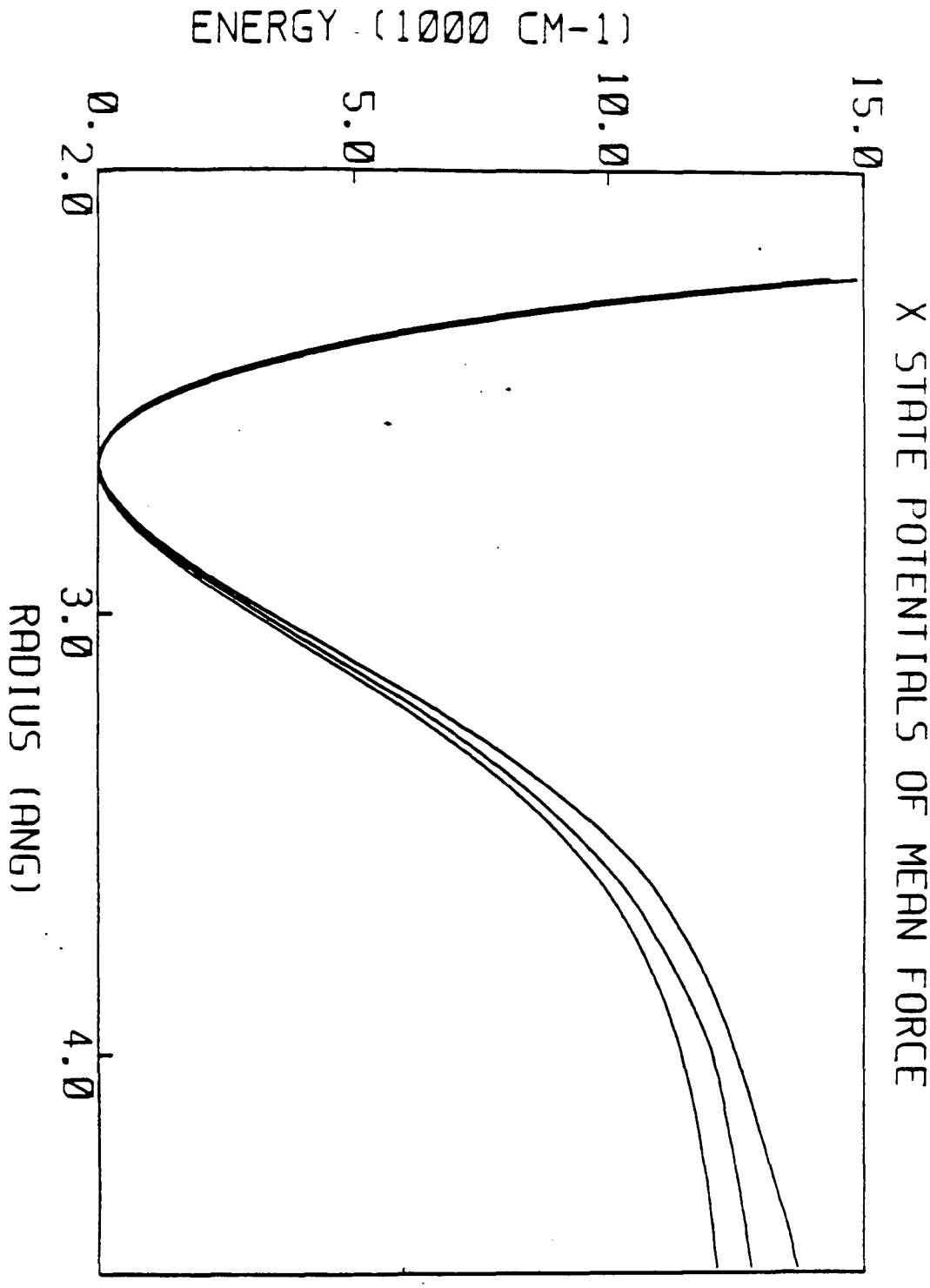
X STATE POTENTIALS OF MEAN FORCE
ENERGY (1000 CM-1)
15.0
10.0
5.0
0
2.0
3.0
4.0
RADIUS (ANG)

Figure 13

is probably not important in calculating the ground state extinction coefficient. Thus, the change in the intermolecular potential for I_2 in the B state is the primary concern and the solvent effects on the A and $^1\pi_u$ states are assumed to be the same as on the ground state. Levy and others have performed molecular beam experiments in which the intermolecular potential for B state I_2 and light rare gas atoms have been determined.[53] These experiments indicate that there is a very small change in the intermolecular potential for I_2 in the B state as opposed to the ground state, with typical changes in the potential parameters of about 2%. Xe though is much more polarizable than the lighter rare gases and therefore larger changes may occur. For this reason, a variety of Lennard-Jones parameters was used to determine the sensitivity of the solvent forces along the bond axis to intermolecular potential. The effects of different intermolecular potentials on the B state surface and the calculated 760 nm extinction coefficient for the 3.0 g/ml Xe density are shown in figures 14 and 15. At the probe wavelengths in these experiments, the effect is mostly to shift the peak of the extinction coefficient up or down in vibrational energy while the extinction coefficient shape and magnitude are only slightly changed.

There is little current experimental evidence to verify the accuracy of these extinction coefficient calculations and to help in determining which intermolecular potential is most accurate for I_2(B) and Xe. The room temperature ground state absorption spectrum has been calculated and compared to the experimentally determined spectrum at a Xe density of 3.0 g/ml. These results are tabulated in table 4. The calculated spectrum which is closest to the experimental spectrum is that in which the

Figure 14 Instantaneous B state surfaces following absorption of a photon from the ground state for various Lennard-Jones I_2-Xe intermolecular potentials at 280 K and a Xe density of 3.0 g/ml: a) gas phase RKR potential, b) σ=3.94 Å, ϵ=225 cm^{-1} (X state intermolecular parameters), c) σ=4.24 Å, ϵ=225 cm^{-1}, d) σ=3.94 Å, ϵ=450 cm^{-1}, e) σ=3.64 Å, ϵ=450 cm^{-1}.

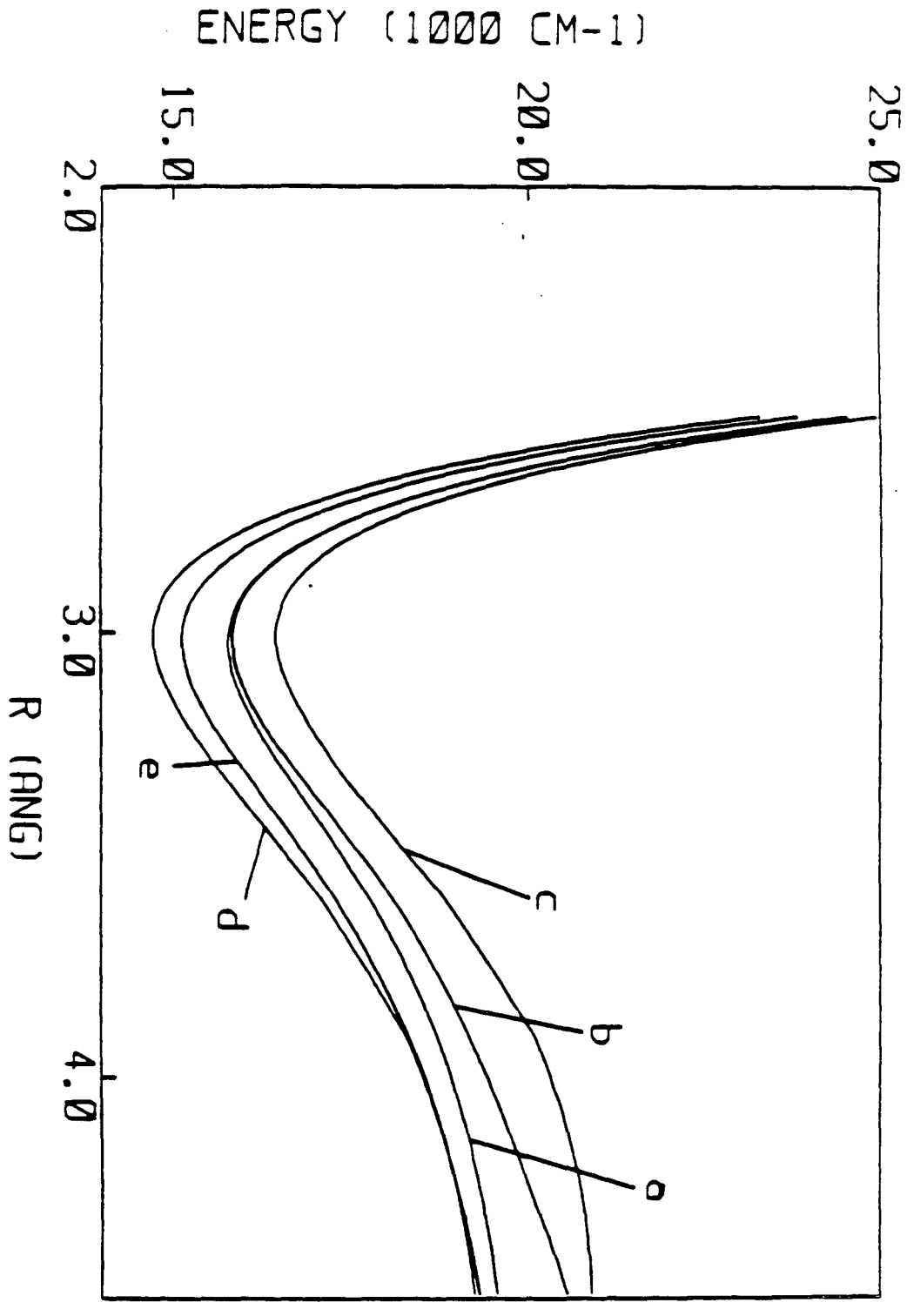

Figure 14

Figure 15 I_2 ground state extinction coefficient at 760 nm using the ground state potential surface of mean force in 3.0 g/ml Xe and the B state surfaces a,b,c,d in figure 14.

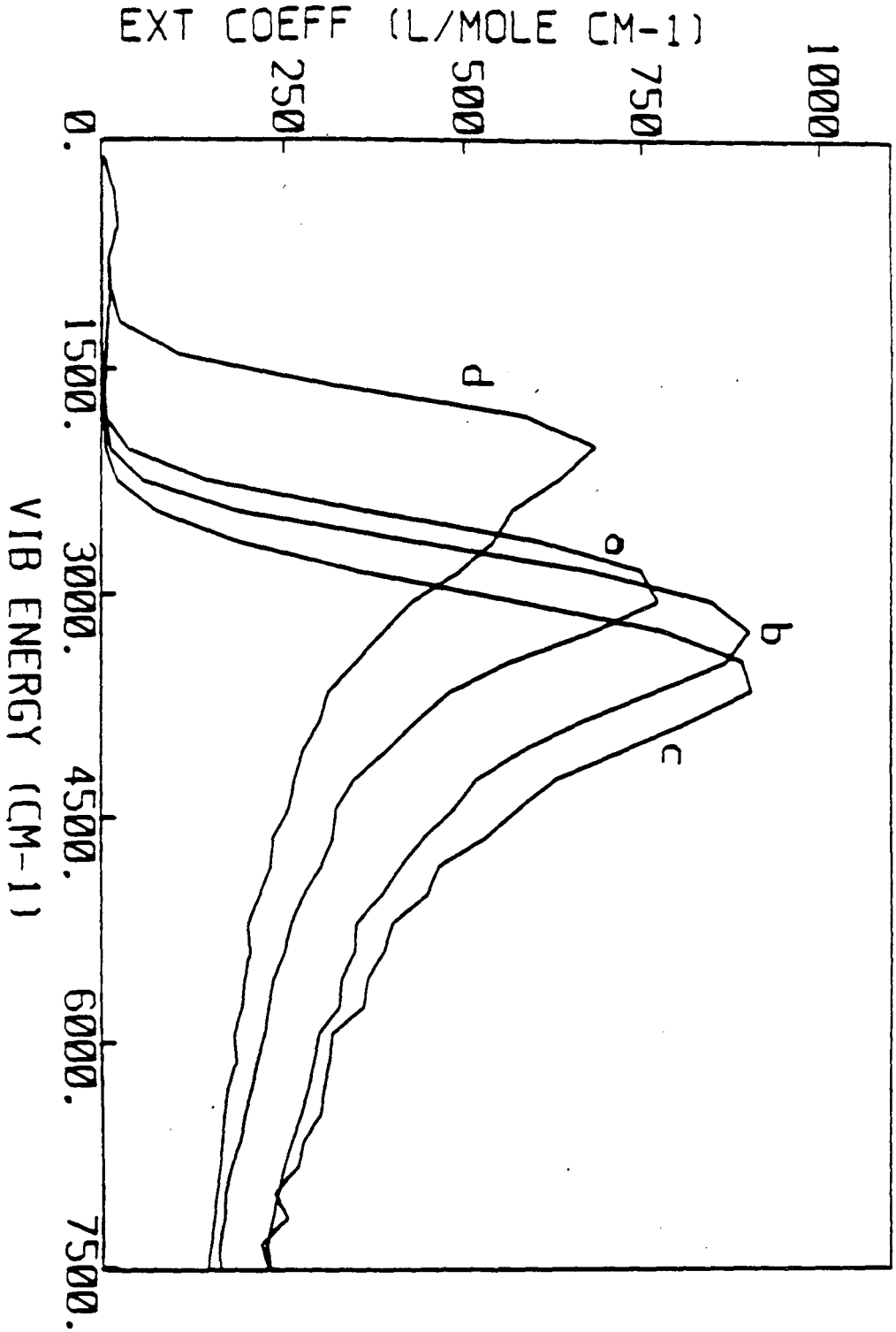
EXT COEFF (L/MOLE CM-1)
1000
750
500
250
0.
1500.
3000.
4500.
6000.
7500.
VIB ENERGY (CM-1)
a
b
c
d

Figure 15

Table 4

Source	ρ (g/ml)	Spectrum Peak (nm)
Experimental	1.8	522 ± 2
	3.0	519 ± 2
Calculated		
ϵ^*=225 cm^{-1}, σ^*=3.94 Å	1.8	518.0
	3.0	514.25
ϵ^*=225 cm^{-1}, σ^*=4.24 Å	3.0	504.75
ϵ^*=450 cm^{-1}, σ^*=3.94 Å	3.0	550.0

Caption: Experimental and calculated Peaks of the room temperature I_2 spectrum. ρ is the Xe density and ϵ^* and σ^* are the Lennard-Jones parameters used to model the B state I_2-Xe intermolecular potential.

excited state intermolecular potential was assumed to be the same as the ground state intermolecular potential. Thus, as is the case with other rare gases, the I_2-Xe intermolecular potential does not seem to change very substantially for I_2 in the ground or B state and the same intermolecular potential for both I_2 states has been used for the remaining calculations. The room temperature ground state spectra using the single intermolecular potential have been calculated for all densities. They are slightly blue shifted relative to the experimental spectra (about 4 nm). This result is not surprising as the actual intermolecular potential is probably not quite as repulsive as the Lennard-Jones potential which was used in the simulation (the reason for believing this will be discussed in the next chapter).

Further experimental verification of the accuracy of the potential surfaces used for these calculations is the A→X fluorescence of I_2 in a Xe matrix which has been reported by Beeken et al.[54] The florescence is entirely from v'=0 of the A state to v''=15-25 of the ground state. The vibrational energy for the v"=15-25 levels as calculated from the X state potential surface of mean force at the 3.0 g/ml Xe density are generally within 50 cm^{-1} of the the experimental data. In addition, the calculated A state electronic origin is within 100 cm^{-1} of the experimental origin. Thus, the solvent altered potential surfaces used for these extinction coefficient calculations appear to be within a few hundred wavenumbers of the actual surfaces at internuclear separations spanned in the lower half of the ground state potential surface.

The density dependence of the 760 nm extinction coefficient is shown in figure 16. The net effect of increasing solvent density is to shift

Figure 16 Density dependence of the 760 nm ground state extinction coefficient. The lowest energy curve is the gas phase curve, the middle curve is at a Xe density of 1.8 g/ml, and the highest energy curve is at a Xe density of 3.0 g/ml.

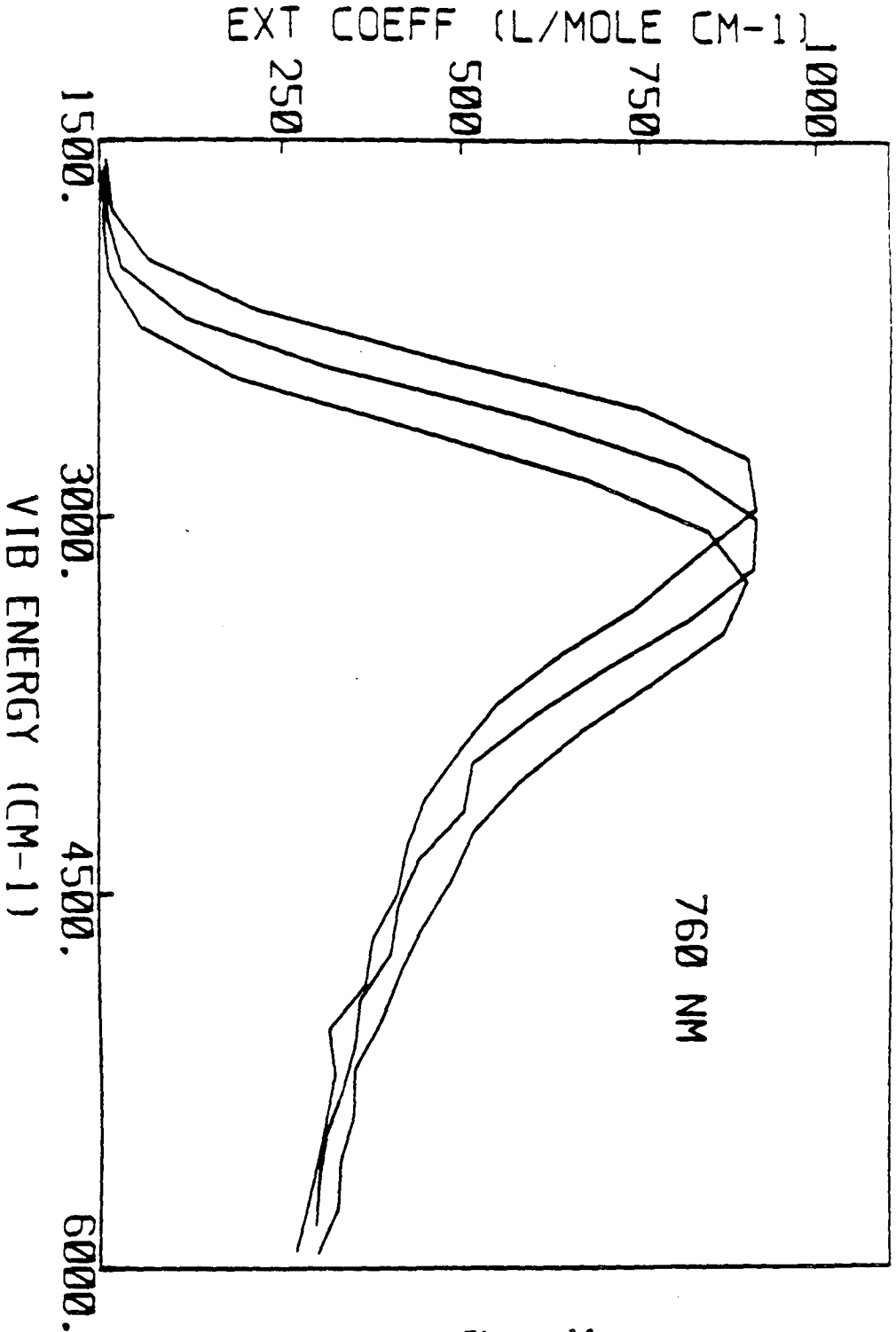
EXT COEFF (L/MOLE CM-1)
1000
750
500
250
760 NM
6000.
4500.
3000.
1500.
VIB ENERGY (CM-1)

Figure 16

the extinction coefficient profile to slightly higher vibrational energy without altering the shape. The shift in the 1.8 g/ml Xe is less than 100 cm^{-1} relative to the gas phase while that at a Xe density of 3.0 g/ml is approximately 300 cm^{-1}.

C. Solving for C[i](t)

With the ground state component of the transient absorptions identified and $\epsilon[\lambda,i]$ calculated, the C[i](t) were determined by solving equation 1 with the singular value decomposition method.[55] The condition number of $\epsilon[\lambda,i]$ was approximately 3. Since geminate recombination onto the ground state surface occurs within a few picoseconds, the sum of the C[i] components should be constant at all times. At short times, a low total population was compensated by assuming that the unaccounted population was in the upper region of the potential surface which had been excluded from this calculation. During the first few nanoseconds of delay time, the 500 nm bleach data shows a hole burning effect which results from primarily exciting v=2 of the ground state with the 590 nm laser pulse and mostly probing v=0 with 500 nm.[41] This causes a slow rise on the bleach while the unexcited population reequilibrates. Thus, no information regarding geminately recombined I_2 can be determined from the 500 nm data during this time period (1-3 nsec) and this data is initially excluded from the matrix equation.

The two major problems with the calculated C[i](t) were that the total population dropped by over 50% by the time the 950 and 860 nm absorptions decayed and during this time, large negative concentrations

occurred in the low energy sections. These negative concentrations occur because the transient absorptions at the shorter wavelengths which mainly probe the low energy sections were not large enough to account for the large populations in the higher energy sections which result from the large transient absorptions at the longer wavelengths. Empirically, it was determined that the 950 and 860 nm transient absorptions needed to be reduced in magnitude by a factor of 3 to eliminate the decreasing population problem. Such a reduction mostly eliminated the negative concentration problem also. The seemingly overly large transient absorptions at 950 and 860 nm can be explained if the calculated extinction coefficients for these two wavelengths were too small or if there is another transient absorption source at these wavelengths which has similar time behavior as the ground state component and has not been separated. The latter proposition may occur from recombination on the many shallow trap states which have the same asymptotic energy as the ground state. As to the former suggestion, the alternative B state potential surfaces calculated earlier do not cause large changes in the magnitude of the extinction coefficients. However, another possibility is that the B←X transition moment is very different than the function used for the calculations since it has a strong R centroid dependence which has not yet been thoroughly investigated. An additional problem with the transition moments which were used for these calculations is that they were determined in gas phase experiments and they will change when the molecule is put into solution.[56-58] However, it was determined empirically that a 170% increase in the 3.1 Å R centroid region of the transition moment without altering the other R centroid regions is

required to solve the concentration problem. Such a radical change seems doubtful. Thus, the reason for the overly transient absorptions at 950 and 860 nm would appear to be the result of some short-lived trap state. For the purposes of this analysis, the problem has been circumvented by adjusting the magnitudes of the transient absorptions so that the concentration is approximately constant over time. However, the calculated average energy of the system is not very sensitive to these adjustments and the main benefit of these adjustments is too reduce noise in the calculated C[i](t).

IV. Ground State Vibrational Relaxation

A. I_2/Xe

i. Qualitative Features

The time dependence of the calculated average I_2 vibrational energy and population distribution (within 1 standard deviation of the average) at a Xe density of 3.0 g/ml at 280 K are shown in figure 17. The loss of vibrational energy is very rapid in the top half of the potential surface (< 150 psec) followed by much slower energy loss over the bottom half of the potential surface (> 3000 psec). The stagnation in the lower half of the potential surface is a consequence of the increase in oscillator frequency as the molecule vibrationally relaxes. In the top half of the potential surface, the oscillator frequency ranges from 100-170 cm^{-1} whereas in the lower portion the frequency spans 170-220 cm^{-1}. Since the I_2-Xe intermolecular force contains a greater magnitude of frequency components at the lower vibrational frequencies than at the higher vibrational frequencies, relaxation is more efficient in the anharmonic portion of the potential surface. The dramatic decrease in energy transfer as the I_2 vibrational frequency increases indicates how quickly the magnitude of the I_2-Xe force decreases at higher frequencies.

Compared to I_2 relaxation times seen in molecular solvents such as the chloromethanes and hydrocarbons, the relaxation in Xe is over 20 times slower. This small rate of energy transfer in Xe is due to two reasons. First, there are not any internal degrees of freedom to help accommodate the I_2 energy. One might then conclude from this experiment

Figure 17 I_2 vibrational relaxation in 3.0 g/ml Xe at 280 K. The solid line is the average vibrational energy, the dotted line is the 65% confidence limits for the average energy (representing fitting error of the transient absorptions), and the circles show the population distribution for 1 standard deviation from the average.

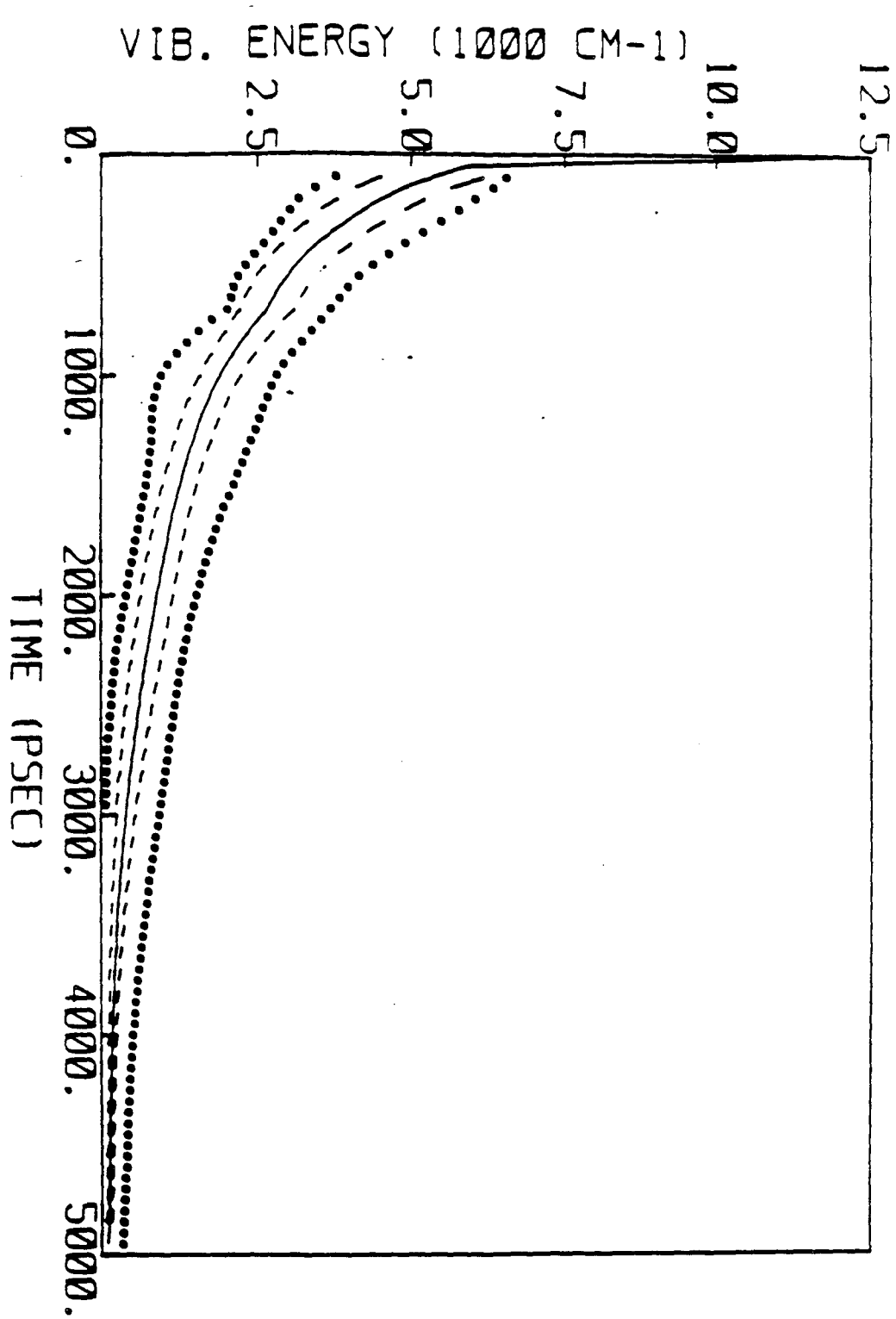
VIB. ENERGY (1000 CM-1)
12.5
10.0
7.5
5.0
2.5
0.
TIME (PSEC)
0.
1000.
2000.
3000.
4000.
5000.

Figure 17

that vibration to translation energy transfer is not very important in solution, particularly when the oscillator frequency is greater than 200 cm^{-1}. However, the second reason for the slow vibrational relaxation in Xe is that the repulsive part of the intermolecular potential is relatively "soft" and therefore the I_2-Xe force has a comparatively small magnitude at frequencies of 200 cm^{-1} or more. Vibration to translation energy transfer might be efficient in solvents which have more repulsive intermolecular potentials. Some evidence for this hypothesis can be found from the relaxation of I_2 in CS_2 which occurs in approximately 200 psec. Fast relaxation occurs in this solvent even though vibration to vibration energy transfer does not occur since the vibrational frequencies of CS_2 are more than twice that of I_2 and the rotational degreees of freedom appear to add no new frequencies to the I_2-solvent force (further discussion regarding the CS_2 experiment is presented later in this chapter). Thus, a large part of the increased relaxation observed in the chloromethanes (70-140 psec)[26] could be the result of the more repulsive solvent-solute intermolecular potential (particularly the I-H interaction). Experiments in lighter rare gases would help resolve this issue, however, I_2 is not soluble enough in these compressed gases to perform such experiments.

The density and temperature dependence of the vibrational relaxation is shown in figures 18 and 19. The functional form of the relaxation is identical for all thermodynamic conditions, which means that the time axis can be linearly scaled to make the energy decay curves overlap for the different Xe thermodynamic states. Examples of scaled energy curves

Figure 18 Density dependence of the I_2 ground state vibrational relaxation for Xe densities between 1.8 and 3.4 g/ml at 280 K.

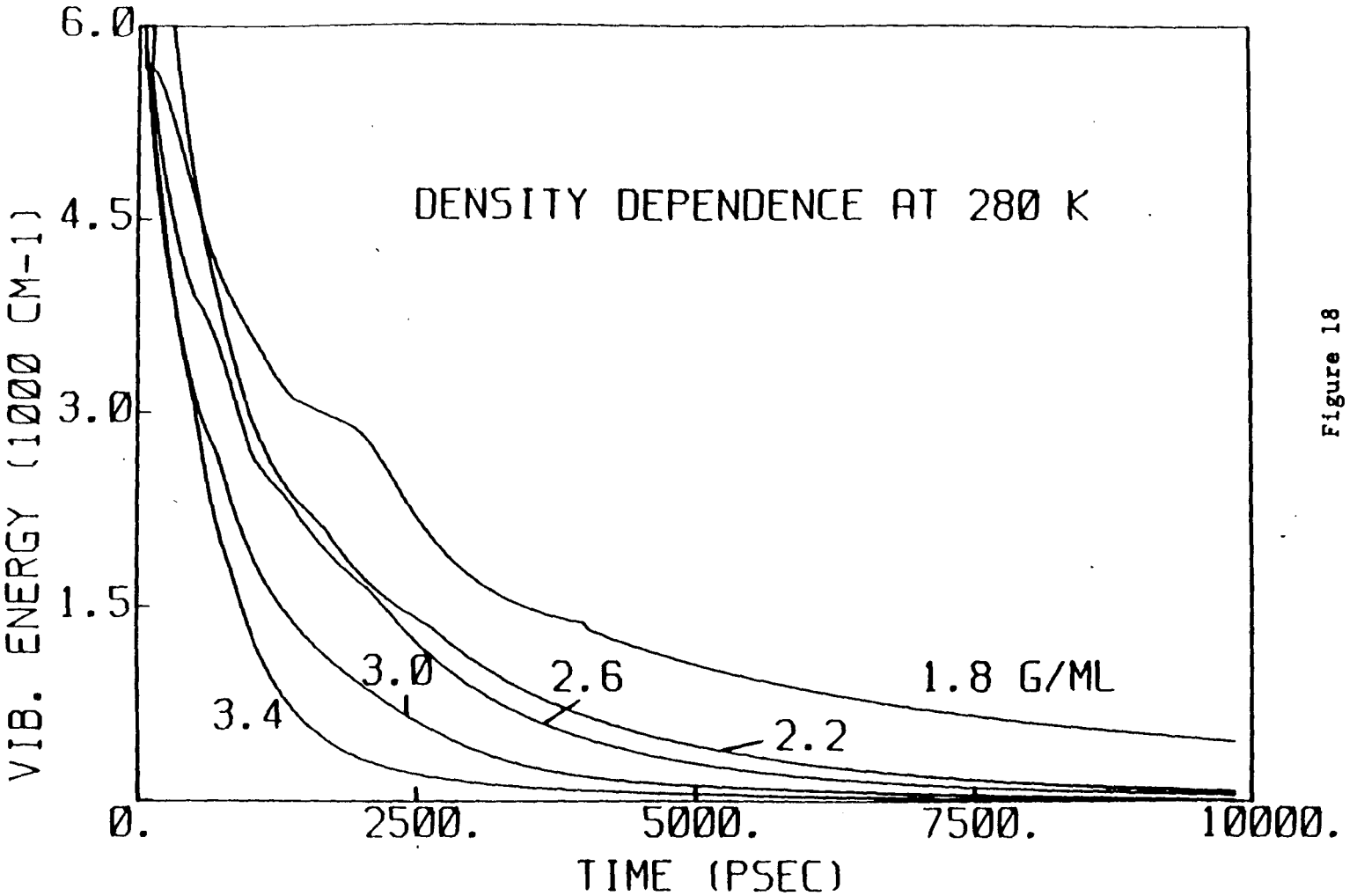
DENSITY DEPENDENCE AT 280 K
VIB. ENERGY (1000 CM-1)
6.0
4.5
3.0
1.5
0.
2500.
5000.
7500.
10000.
TIME (PSEC)
1.8 G/ML
2.2
2.6
3.0
3.4

Figure 18

Figure 19 I_2 ground state vibrational relaxation between the temperatures of 253 and 323 K at a Xe density of 3.0 g/ml.

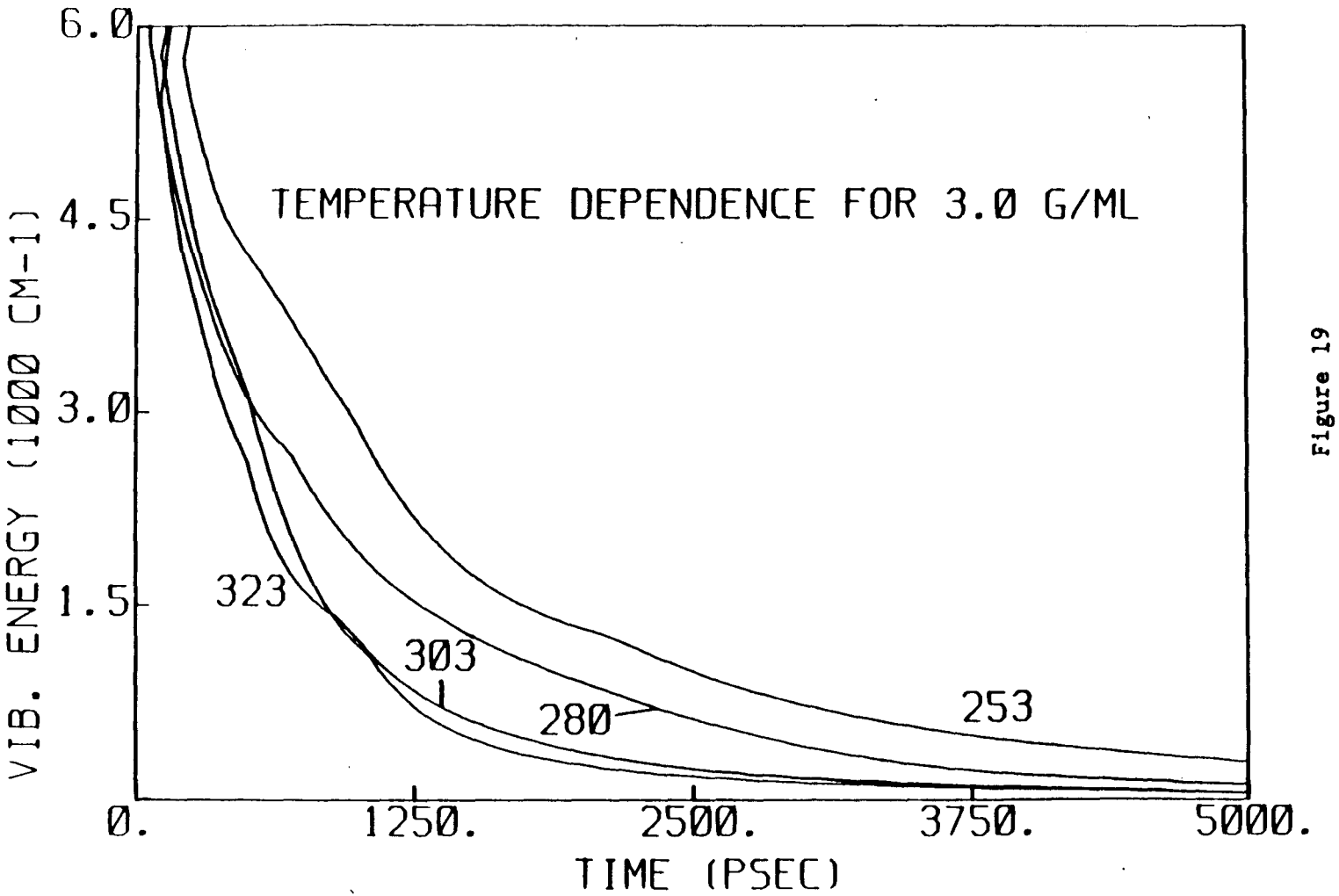
TEMPERATURE DEPENDENCE FOR 3.0 G/ML
VIB. ENERGY (1000 CM-1)
6.0
4.5
3.0
1.5
0.
1250.
2500.
3750.
5000.
TIME (PSEC)
323
303
280
253

Figure 19

are shown in figures 20 and 21 where t=0 is assigned to the time when the vibrational energy reaches 6000 cm^{-1}. As expected, the relaxation quickens as the density and temperature increases because the solvent-solute collisions become more frequent and violent. At 280 K, the relaxation rate increases by a factor of 4 from low to high density, a change which is like that seen in hydrogen and nitrogen relaxation experiments over the same Lennard-Jones reduced density range.[59-60] The relaxation is also fairly sensitive to temperature as the rate doubles from 253 to 323 K (a Lennard-Jones reduced temperature range of 1.14 to 1.46) at a density of 3.0 g/ml.

ii. Comparison of Experimental Results to Theoretical Predictions and Simulations

The I_2/Xe system has received a substantial amount of attention from theorists interested in vibrational relaxation in solution. The obvious attractions to this system for theorists are its geometrical simplicity and its isolation of the solvent's role in vibration to translation energy transfer. The approaches taken for modeling this system range from gas phase models in which the individual molecular interactions are emphasized, to modified hydrodynamic theories in which the solvent is treated as a continuous media, to 3 dimensional molecular dynamics simulations of the system. Here, the various predictions which have been made using these techniques are compared with the experimental results.

Nesbitt and Hynes performed the first calculation on the role of vibration to translation energy transfer in the I_2 relaxation. They

Figure 20 I_2 vibrational energy decay in 3.0 g/ml Xe scaled to that in 1.8 g/ml Xe at 280 K. The time axis of the 3.0 g/ml curve has been multiplied by 3.0.

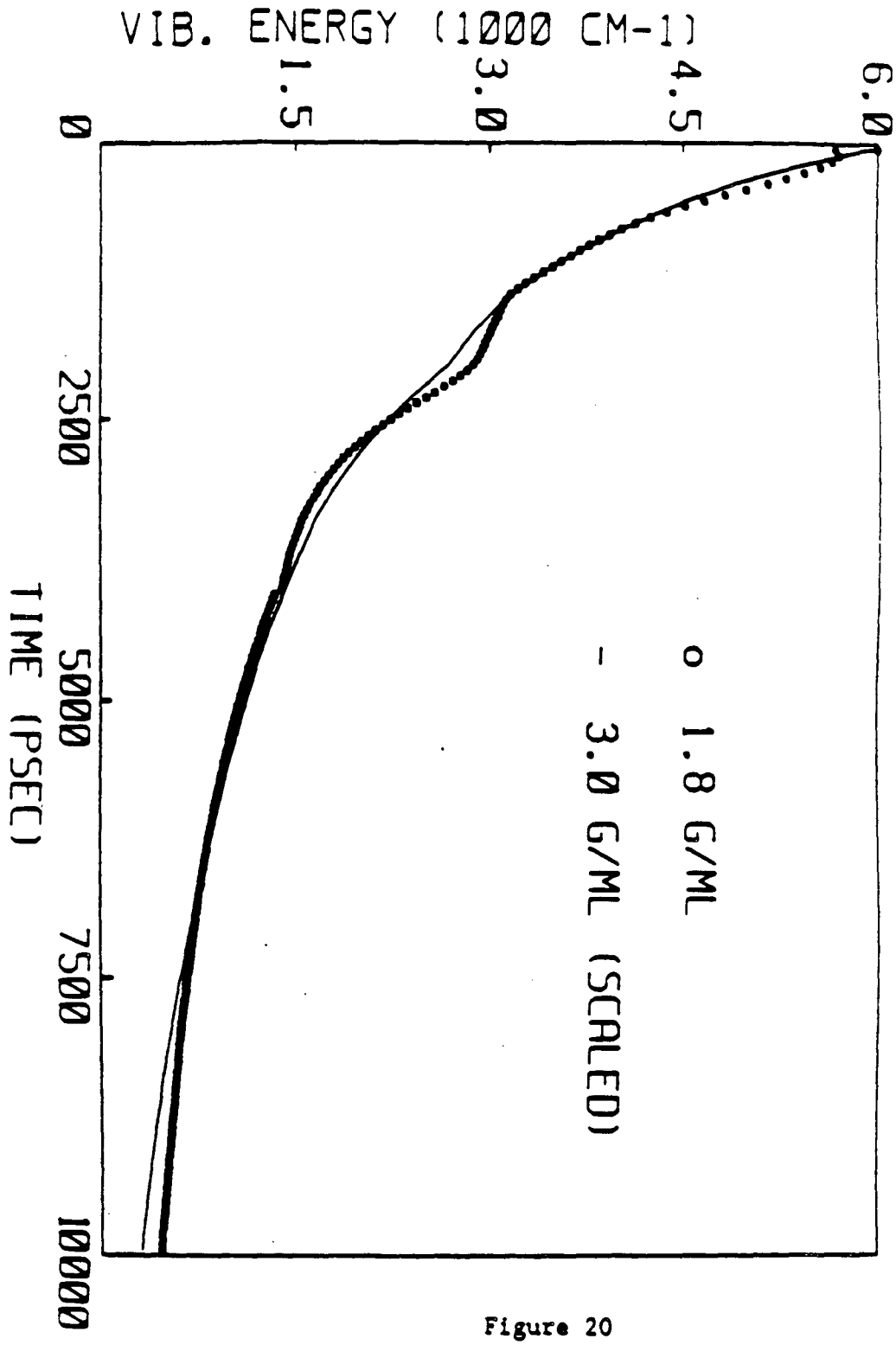
VIB. ENERGY (1000 CM-1)
6.0
4.5
3.0
1.5
0
2500
5000
7500
10000
TIME (PSEC)
o 1.8 G/ML
- 3.0 G/ML (SCALED)

Figure 20

Figure 21 I_2 vibrational energy decay at 323 K scaled to that at 253 K in 3.0 g/ml Xe. The time axis of the 323 K curve has been multiplied by 2.2.

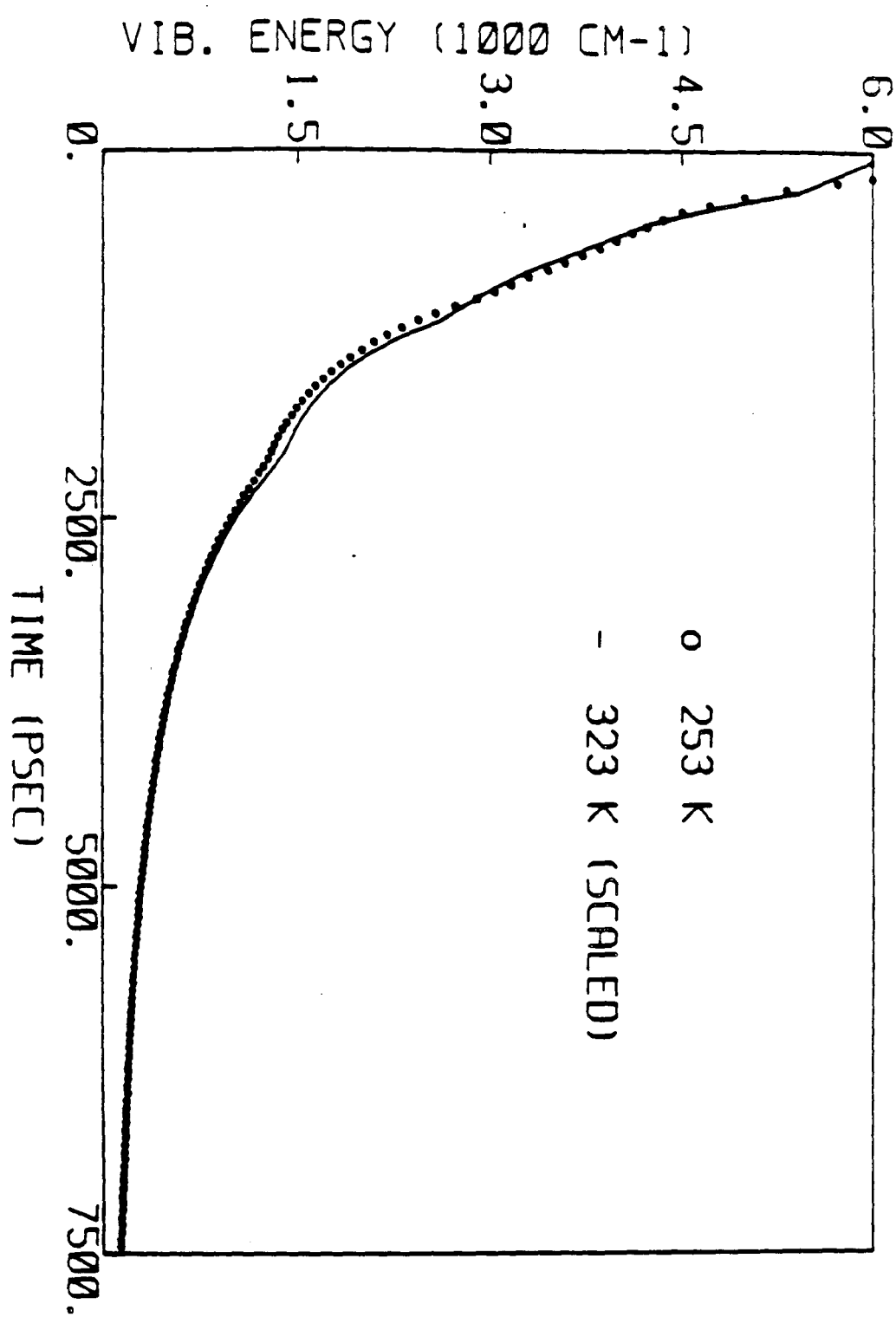
VIB. ENERGY (1000 CM-1)
6.0
4.5
3.0
1.5
0.
o 253 K
- 323 K (SCALED)
2500.
5000.
7500.
TIME (PSEC)

Figure 21

calculated the energy transfer per collision as a function of vibrational energy using two body molecular dynamics trajectories and then assumed an appropriate solution phase collision frequency to calculate the energy of the system as a function of time. While their calculation was based on the I_2/CCl_4 system in which the CCl_4 were modeled as structureless particles, the authors state that their results should give "a reasonable facsimile" for the I_2/Xe system.[61] Their results show that relaxation down to 7500 cm^{-1} of vibrational energy occurs in under 100 psec, followed by extremely slow relaxation down the remainder of the potential surface (requiring over a nanosecond). Thus, the authors predict that "in liquid Xe, the observed characteristic time scale [for vibrational relaxation] would be in the nanosecond range." This prediction and the stagnation half way down the well have certainly been verified in the present experiments. The qualitative success of this prediction warrants further investigation into the merits of applying gas phase models of vibrational relaxation to liquids and further comments regarding these models are made in the next section of this thesis.

Next, the experimental findings are compared with the results of classical molecular dynamics simulations performed by Brown, Harris and Tully which were described previously.[51] Simulations of the vibrational relaxation were performed at the same densities at 280 K as the experiments (except for the 3.4 g/ml Xe which is a Lennard-Jones solid) and for a temperature range of 280 - 320 K. As is shown in figure 22, the functional form of the molecular dynamics vibrational energy decay is the same as the experimentally determined curve when the time axis of molecular dynamics decay is multiplied by 12.4. Thus, the relaxation in

Figure 22 I_2 vibrational energy decay from the molecular dynamics simulations scaled to the experimental curve for 3.0 g/ml Xe at 280 K. The time axis of the molecular dynamics simulation curve has been multiplied by 12.4.

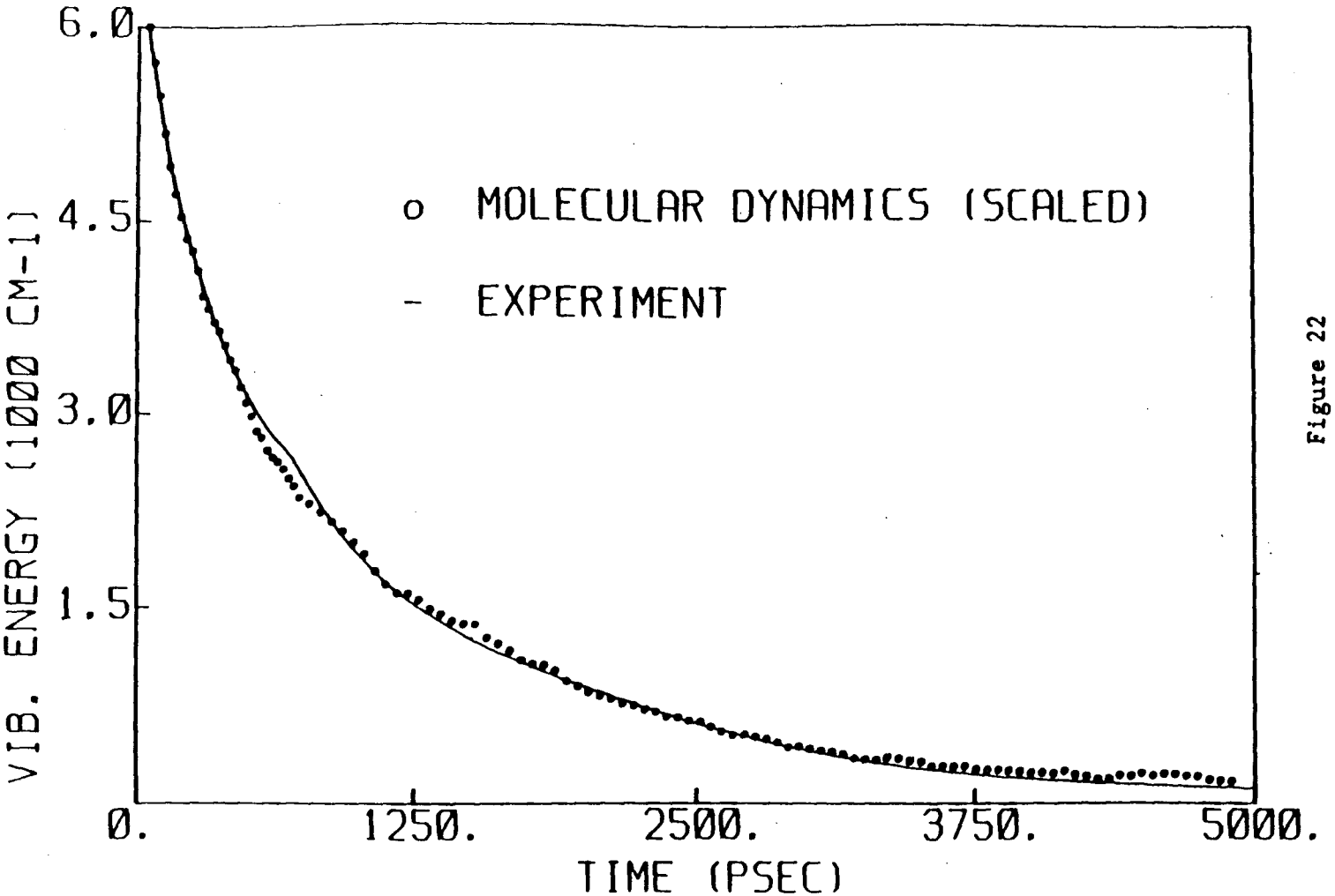
6.0
4.5
3.0
1.5
VIB. ENERGY (1000 CM-1)
o MOLECULAR DYNAMICS (SCALED)
- EXPERIMENT
0.
1250.
2500.
3750.
5000.
TIME (PSEC)

Figure 22

the simulated I_2 is more than an order of magnitude faster than the experimental findings. The most likely reason for this discrepancy is that the actual I_2-Xe potential is not quite as repulsive as the Lennard-Jones potential which has been used in the simulations. If this assumption is true and if the I_2-Xe intermolecular force in the region important to the vibrational relaxation (the repulsive wall) has the form $C\gamma f(r)$ where C is a constant, γ is a parameter which describes the difference between the force in the simulation and the actual force, and f(r) is a function of the intermolecular separation, then the similiarity of the functional form of the relaxation for the simulation and experiment can be explained using a first order coupling approximation in the Golden Rule.[62] According to the Golden Rule, k_{ij}, the relaxation rate between two vibrational levels i and j is:

$$k_{ij} = (4\pi^2/h) \sum_{\alpha} P_{\alpha} \left|V_{i\alpha,j\beta}\right|^2 \delta(E_{i\alpha} - E_{j\beta})$$

where P_{α} is the density of initial bath states α, $V_{i\alpha,j\beta}$ is the coupling potential between the initial and final oscillator and bath states, and $\delta(E_{i\alpha} - E_{j\beta})$ is the Dirac delta function for the energy difference between these states. A power series expansion of the coupling potential in terms of the vibrational coordinate Q yields:

$$V_{i\alpha,j\beta} = \Sigma(\partial^n V_{\alpha,\beta} / \partial Q^n) \ (Q_{i,j})^n$$

Keeping only the first order term in the coupling and inserting the functional form of the force assumed above, the rate expression becomes:

$$k_{ij} = (4\pi^2/h) \ \gamma^2 \sum_{\alpha} P_{\alpha} \left|\partial f/\partial Q\right|^2 Q^2 \ \delta(E_{i\alpha} - E_{j\beta})$$

Thus, the relative relaxation rate for forces characterized by γ_1 and γ_2 is:

$$k_{ij}(\gamma_1)/k_{ij}(\gamma_2) = (\gamma_1/\gamma_2)^2$$

For vibrational relaxation over a multilevel system, N(t), the vibrational level population vector at time t is:

$$N(t) = e^{-kt} \cdot N(t=0)$$

where the exponential term is a matrix composed of elements $e^{-k_{ij}t}$. If the time is specified in units of 1/k then the resultant N(t') is identical for all k. Thus, if the change in the force is represented by the change in γ, a plot of the average vibrational energy of the system vs. time for the force characterized with γ_1 can be overlapped to the same plot for the force characterized by γ_2 by a linear scaling of the time axis with the scaling factor being $(\gamma_1/\gamma_2)^2$. In the case of a Lennard-Jones intermolecular potential γ is the well depth. Molecular dynamics simulations of the I_2/Xe system have shown that the relaxation for a well depth of ϵ is 4 times faster than the relaxation when the well depth is $\epsilon/2$ and that the energy decay curves can be overlapped by linearly scaling the time axis as is predicted by this first order Golden Rule formulation.[51] If the same comparison is made between the experimental vibrational relaxation results and those of the computer simulations, then the well depth of the actual intermolecular potential would be $(12.4)^{0.5}$ times smaller than that assumed in the simulation and the overlap of the energy decay curves by linearly scaling the time axis would be expected. Note that this characterization of the intermolecular potential only applies for internuclear separations corresponding to collisions distances and not for longer separations.

The overall increase in vibrational relaxation rate over the liquid density range is a factor of 4 for both computer simulation and experiment. Individual scaling factors between identical densities for the experiment and simulation differ from density to density which is not surprising since the Xe phase diagram does not conform to a Lennard-Jones phase diagram. The change in relaxation rate with temperature in the simulations is similar to that observed experimentally. A factor of 2 increase in relaxation rate is seen in the simulations when the temperature is raised from 280 to 320 K at a Xe density of 1.8 g/ml as compared to a factor of 1.6 ± 0.2 over the same temperature range for the experimental 3.0 g/ml Xe density. These comparisons demonstrate the utility of molecular dynamics in calculating relative trends as a function of the physical parameters but the difficulty in obtaining results which are correct in absolute magnitude without very accurate potential surfaces.

Lastly, the experimental results are compared with the calculations of Brooks and Adelman, who applied their molecular timescale generalized Langevin approach to the relaxation of I_2 in Xe for a Xe density of 1.8 g/ml at 280 K.[30] This method reduces the motion of the solvent atoms to a set of chain equations which describe the fluctuations of the solvent shells about the oscillator. Their results are similar in nature to those of Nesbitt and Hynes with stagnation occurring at 9000 cm^{-1} of vibrational energy after 50 psec. However, they only calculate the relaxation for the first 120 psec. Since the decay of the 950 nm data which indicates when the system has relaxed below 6000 cm^{-1} is approximately 300 psec for the 1.8 g/ml, 280 K Xe solution, no

quantitative comparison between Brooks and Adelman's calculations and experimental results is possible. However, Stote and Adelman have more recently developed another generalized Langevin model which they use to calculate the v=1→0 vibrational relaxation time of I_2 in Xe for a variety of solvent thermodynamic states.[63] The relaxation time is related to the magnitude of the I_2-Xe force autocorrelation function at the I_2 vibrational frequency. The force autocorrelation function is modeled as a Gaussian function and is estimated from the pair correlation functions. While the experiments do not measure individual level to level relaxation rates, the functional form of the relaxation does not change with thermodynamic state of the solvent and so comparisons of relative rate changes with density and temperature changes may be made between Stote and Adelman's results and the experimental findings. For the 1.8 g/ml Xe solution, they calculate v=1→0 relaxation times of 4.5 nsec at 280 K which decreases to 2.07 nsec at 350 K. This factor of 2.2 decrease for a 70 K change agrees with the 2.2 ± 0.2 factor experimentally observed for the 3.0 g/ml density over a 70 K change from 253 K to 323 K. As for density dependence, their results show a factor of 8 increase in the v=1→0 rate between 1.8 to 3.0 g/ml Xe at 298 K which is a much greater effect than the experimental increase of 3.0 ± 0.2 for the same density range at 280 K. Note that these comparisons between the experimental findings and Stote and Adelman's are less meaningful than comparing their results to those of the molecular dynamics simulations since both calculations employ the same I_2-Xe intermolecular potential. Thus, ideally these generalized Langevin calculations should provide the same results as the molecular dynamics simulations and currently they do not.

iii. Consideration of Isolated Binary Collision Modeling

As a first approximation for understanding vibrational relaxation in solution, theorists and experimentalists have considered the extension of the gas phase relaxation model known as the isolated binary collision (IBC) model to liquid densities. For the past 30 years, the applicability of this model of vibrational relaxation to the condensed phase has been widely debated. The IBC model states that $K_{i\rightarrow j}$, the relaxation rate from vibrational level i to j is:

$$K_{i\rightarrow j}(\rho,T) = P_{i\rightarrow j}(T)\cdot Z(\rho,T)$$

where $P_{i\rightarrow j}$ is the probability of $i\rightarrow j$ per collision which is determined at low gas density, Z is the solvent-solute collision frequency, ρ is the solvent density, and T is the temperature. Since the $P_{i\rightarrow j}$ is independent of density, the difference between relaxation in liquid and gas phases is solely given by $Z(\rho)$. Thus, in this framework, vibrational relaxation in solution is still dominated by two body collisions between the solute and solvent and multibody effects are considered to be inconsequential. Since molecules in solution are constantly within the range of the many other molecules' intermolecular potentials at a given time, the IBC model's validity at liquid densities would appear doubtful at first glance. However, Herzfeld's argument supporting the applicability of the IBC model to liquid density is that the hard collisions which dominate the vibrational relaxation are much longer apart in time than the oscillator period.[64] Therefore, from Herzfeld's perspective any correlations in oscillator phase or solvent-solute relative velocities

between these hard collisions which would alter the $P_{i\to j}$ in the liquid density regime are annihilated by the many "soft" collisions which occur between relaxation events. While the accuracy of this argument has been debated and some have suggested that the hard collisions would occur in sets due to the solvent cage effect so that correlations may exist between some collisions, Herzfeld's comments are very relevant to past experiments which have been performed to test the IBC model in solution. In these studies, only the relaxation of high frequency oscillators have been measured where the oscillator frequency is expected to be much shorter than the collision frequency. In the I_2 experiment, the oscillator frequencies involved (150 - 220 cm^{-1}) are much more comparable to the solvent-solute collision frequency and a breakdown of the IBC model may occur.

Additionally, all previous experimental studies designed to test the IBC model at liquid densities have only measured relaxation between vibrational levels 1 and 0.[65] The difficulty with interpreting such results as a function of density is that a calculation of $Z(\rho)$ is necessary in order to ascertain the validity of the IBC model since the relative change in relaxation rates between two densities ρ_1 and ρ_2 according to the IBC model is given by:

$$K_{i\to j}(\rho_1) \;/\; K_{i\to j}(\rho_2) \;=\; Z(\rho_1) \;/\; Z(\rho_2)$$

In solution, a collision is a nebulous concept and calculations of Z vary widely in magnitude with model and are very sensitive to parameters such as molecular size. Thus, studies in which the relaxation rate between two levels is measured as a function of density do not test the underlying assumption of the density independence of $P_{i\to j}$ separately from

the model of the collision frequency employed. In this experiment, the relaxation has been measured over approximately 30 vibrational levels for Xe densities covering the entire liquid phase region of the phase diagram. Following the relaxation over a large number of vibrational levels as a function of solvent density eliminates the need of a determination of Z in testing the density dependence of the $P_{i \to j}$.

To understand this distinction, consider the relaxation process over many vibrational levels in the IBC framework. After $Z(\rho) \cdot t$ binary collisions, N(t), the vibrational population distribution vector at time t would be

$$N(t) = P \cdot P \cdot P \ldots \cdot P \cdot N(t=0) = P^{Z \cdot t} \cdot N(t=0)$$

where P is the matrix of relaxation probabilities per collision for transitions between all levels of the system. The role of $Z(\rho)$ in this description of the relaxation is to control the timescale of the relaxation process. If the time were normalized by $Z(\rho)$, i.e. $t' = t/Z(\rho)$, then the resulting $N(t')$ would be identical for all ρ. Hence, plots of the average energy of the system as a function of time for different densities should show the same functional form, differing only by a linear scaling of the time axis which accounts for the change in $Z(\rho)$. Provided $Z(\rho)$ does not vary with vibrational energy, any deviation from linear scaling would be an indication of nonbinary behavior. The timescaling factor S necessary to overlap the energy decay curve at ρ_2 to that of ρ_1 can be determined from

$$Z(\rho_1) \cdot t = S \cdot Z(\rho_2) \cdot t$$

which leads to

$$S = Z(\rho_1)/Z(\rho_2)$$

As has been stated earlier in this chapter, the functional form of the relaxation is identical for all thermodynamic states of the Xe which have been studied. Thus, the $P_{i \rightarrow j}$ are density independent over the entire liquid density portion of the Xe phase diagram as is assumed in the IBC model. This result is particularly surprising because of some of the physical insights which the molecular dynamics simulations provide regarding the manner in which the solvent-solute collisions are occurring.[51] In the simulations, a collision was considered to have occurred when a Xe atom comes within a specified distance of the I_2. The collision frequency calculated in this fashion at a variety of contact distances was observed to be constant as a function of vibrational energy until the energy drops below 1000 cm^{-1}, at which point the collision frequency falls by about 50% over the remainder of the relaxation. This behavior of the collision frequency with vibrational energy suggests that the collisions at vibrational energies over 1000 cm^{-1} are being caused by the large amplitude motions of the vibrationally excited I_2 rather than by random solvent motions. Conversely, at vibrational energies below 1000 cm^{-1} where the vibrational amplitudes have become greatly diminished, the collisions occur as a result of random solvent motion. If this description is correct and the collisions are being caused by oscillator rather than solvent motions above 1000 cm^{-1} in vibrational energy, correlations between collisions would be expected to occur over that region of the potential surface. In particular, collisions may occur at the outer turning points of the oscillator motion at a much higher rate than they would if the solvent were presumed to approach the solute at random intervals as occurs in the gas phase. Such a change in

the nature of solvent-solute collisions with increasing solvent density would necessitate a change in the $P_{i\rightarrow j}$. However, our results indicate that the $P_{i\rightarrow j}$ do not change with density. Thus, these correlation effects must have an insignificant effect on the relaxation or the contact model of calculating the collision frequency is an inappropriate method of calculating the number of collisions which contribute to the relaxation.

As a test of the contact model of evaluating $Z(\rho)$ and of the predictive value of the IBC model in determining vibrational relaxation rates, the experimentally determined scaling factors, S_e, for the energy curves are compared to S_z, the scaling factors determined from the calculated collision frequencies using the molecular dynamics simulations. While the computer simulations were shown to be very far off in magnitude in calculation of the relaxation time because of the potential inaccuracies, Z may not be as sensitive to this problem. S_z for a variety of contact distances have been tabulated from the molecular dynamics simulations for the energy region between 6000 and 1000 cm^{-1} and are listed in table 5. Z has not been calculated for the 3.4 g/ml density since Xe at this density is a Lennard-Jones solid. The scaling factors cited are those by which the 3.0 g/ml Xe density data timebase is multiplied in order to overlap the 3.0 g/ml energy decay curve to the decay curves at other densities. The 3.0 g/ml Xe density timebase has been selected as the standard for comparison since the best signal/noise was obtained in experiments at that density. S_z for a collision radius of ≈3.8 Å matches the most S_e (see table 6). The agreement at this

Table 5

R (Å)	$Z_{3.0}$ (1/psec)	S_z at 2.6 g/ml	2.2 g/ml	1.8 g/ml
3.70	0.86	1.31	2.76	3.18
3.75	1.68	1.39	2.63	3.04
3.80	3.03	1.50	2.51	3.15
3.85	4.77	1.46	2.42	3.14
3.90	6.72	1.45	2.27	3.34
3.95	8.84	1.41	2.16	2.82
4.00	10.86	1.39	2.08	2.90
4.05	12.97	1.39	2.01	2.60
4.10	14.33	1.34	1.90	2.43
4.15	15.33	1.31	1.80	2.27

Caption: Calculated scaling factors $S_z = Z(\rho=3.0\ g/ml)/Z(\rho)$ generated from molecular dynamics simulations for a variety of I_2-Xe contact distances (R). S_z should be compared to the experimentally determined scaling factors needed to multiply the time axis of the 3.0 g/ml vibrational energy curve to that at other densities. $Z_{3.0}$ is the collision frequency for a Xe density of 3.0 g/ml at 280 K.

Table 6

ρ (g/ml)	ρ^*	S_e	S_z	Z (1/psec)
3.4	1.07	0.67 ± .07	-	-
3.0	0.95	1.00 ± .09	1.00	3.03
2.6	0.82	1.56 ± .12	1.50	2.01
2.2	0.70	1.66 ± .16	2.51	1.20
1.8	0.57	3.00 ± .22	3.15	0.96

Caption: Comparison of the timescaling factors for the I_2 vibrational relaxation at various Xe density (ρ). S_e are the experimentally determined scaling factors and S_z are the calculated scaling factors using collision frequencies (Z) determined for a contact distance of 3.8 Å . The timescaling factors are relative to the relaxation at 3.0 g/ml. ρ^* is the Lennard-Jones reduced density of the Xe.

contact distance is within experimental error for the 2.6 and 1.8 g/ml Xe while the 2.2 g/ml density relaxation is about 1.5 times too fast for the calculated collision frequency. The 2.2 g/ml density was also the most problematic density at which to perform the experiment because of difficulties in getting a good seal with the pressure cell at the appropriate pressure and thus, the data at that density is the least reliable. The distance of 3.8 Å corresponds to an energy above the I_2-Xe dissociation limit of 270 cm^{-1} (1.4 kT). For this contact distance to be the appropriate distance to evaluate the collision frequency, the intermolecular velocity required to attain this separation should be the velocity which contributes the most to the vibrational relaxation, i.e. the maximum product of the relative velocity distribution and the probability of the vibrational transition for a given velocity. Two body molecular dynamics which are currently being calculated in this laboratory indicate that 3.8 Å is approximately the correct contact distance.[66]

The scaling factors for the temperature dependence of the relaxation rate are listed in table 7. The linear scaling behavior with temperature does not have the same implications regarding the IBC model as it did when varying solvent density. Since the thermal velocity dependence of the individual $P_{i \rightarrow j}$'s may not be the same, the IBC model does not predict that the energy decay curves at different temperatures should necessarily linearly scale with time. While the molecular dynamics simulations indicate that the collision frequency at a given contact distance is constant over the experimental temperature range, one would expect that the contact distance at which the collision frequency should be

Table 7

T (K)	T^*	S_e
323	1.46	1.00 ± .12
303	1.37	1.03 ± .11
280	1.26	1.56 ± .18
253	1.14	2.22 ± .22

Caption: Experimental scaling factors (S_e) by which the time base of the 323 K vibrational energy curve is multiplied to overlap it to the energy curves at the other temperatures and the same Xe density (3.0 g/ml). T^* is the Lennard-Jones reduced temperature.

evaluated, i.e, the distance at which the most important energy transferring collisions occur, will decrease as the temperature rises due to higher average intermolecular velocities. Thus, at first glance, the fact that the decays scale does not provide information regarding the temperature dependence of the $P_{i\rightarrow j}$ since the collision frequency will also change with temperature.

However, if, as suggested earlier, the I_2 oscillations are driving the collisions, then the Xe velocity over the experimental temperature range contributes little to the relative I-Xe velocity because the I atom velocities attained during the oscillation are much larger. According to the IBC model, if the intermolecular velocity does not change, then there will be no change in the relaxation rate as neither the $P_{i\rightarrow j}$ or Z will be altered. From this perspective, the temperature dependence of the relaxation is surprising. However, given that the I_2 oscillations are causing the collisions, most collisions would be expected to occur near the outer turning point. In this region, the I atoms will be moving relatively slowly and the Xe velocity will be higher (I_2 is almost twice the weight of Xe so the I_2 center of mass motion will be slower). Thus, the I_2-Xe force during the collisions in this region will be sensitive to the Xe velocity and the $P_{i\rightarrow j}$ will display a temperature dependence. Furthermore, the appropriate contact distance at which to evaluate the collision frequency will decrease as was previously indicated. Usually collisions near the outer turning points are considered to be unimportant in vibrationally relaxing a molecule since there is little internal kinetic energy in the molecule to transfer to the collider at that time in the oscillation. Collisions closer to the equilibrium separation of

the oscillator atoms are required so that oscillator atoms are moving at high enough velocity to insure the necessary high frequency components in the force during the collision and that the internal kinetic energy exceeds the minimum required energy for vibrational energy loss (a vibrational quanta). However, I_2 is such a low frequency oscillator that little internal kinetic energy is required to lose a vibrational quanta of energy and it is quite possible that the most important I_2 internuclear separation for vibrational energy loss is just inside of the outer turning point.

B. I_2/CS_2

Experimental findings of I_2 in various alkanes and chloronated methanes have shown that relaxation in the top half of ground state potential surface occurs within 10 psec while relaxation in the bottom half of the potential surface requires an additional 50-150 psec.[26] In these studies, the solvent has always contained a vibrational mode within thermal energy of the I_2 frequency. The lone study performed to determine the role of the solvent's translational degree of freedom is the I_2/Xe experiment just described. In that experiment, a 150 psec vibrational relaxation time in the anharmonic part of the potential surface was observed, followed by a 3 nsec relaxation time in the bottom portion of the potential surface (for high density Xe). At first glance, these results suggest that the solvent's translational degrees of freedom may be particularly inefficient in accepting I_2's vibrational energy in the harmonic region of the potential surface.

However, in the I_2/CS_2 system, the decay of the 632 nm ground state transient absorption which indicates when the I_2 has relaxed below v=5 (a loss of 85% of the dissociation energy) is approximately 160 psec. This 160 psec recovery time of the bottom of the ground state is similar to that observed for I_2 in other molecular solvents while being 15 times faster than the relaxation time observed in the I_2/Xe system. In the I_2/CS_2 system, the only channels accessible for accepting I_2's energy are the solvent's rotational and translational degrees of freedom since CS_2's vibrational frequencies (400, 800, and 1200 cm^{-1})[28] are much higher than I_2's (≈200 cm^{-1})[19]. Since the CS_2 vibrational frequencies are much too high for efficient energy transfer with I_2, the huge increase in relaxation rate relative to that seen in Xe may be attributable to: 1)the lighter mass of CS_2 compared to Xe, 2)the CS_2's added rotational degrees of freedom, and/or 3)a steeper repulsive intermolecular potential of I_2 with CS_2 than with Xe. Since CS_2's occupied volume[67] is identical to the high density Xe system studied (70%), density dependent effects are probably small. Molecular dynamics simulations of the I_2/Xe system show a factor of 2 increase in relaxation for fictitious half mass xenon atoms compared to full mass xenon.[51] Thus, the lighter molecular weight of CS_2 (76 amu) compared to that of Xe (131 amu) probably halves the relaxation rate. Tildesley and Madden have performed molecular dynamics simulations of a rigid rotor CS_2 solution and have tabulated the torque and center of mass force autocorrelation functions.[68] The fourier transform of these functions are shown in figure 23. The spectra of these two forces are very similar, suggesting each rotational degree of freedom is equivalent to a translational degree of freedom in its effect on the I_2 vibrational

Figure 23 Fourier transform of the center of mass force (solid line) and the torque (broken line) autocorrelation functions for rigid rotor CS_2.

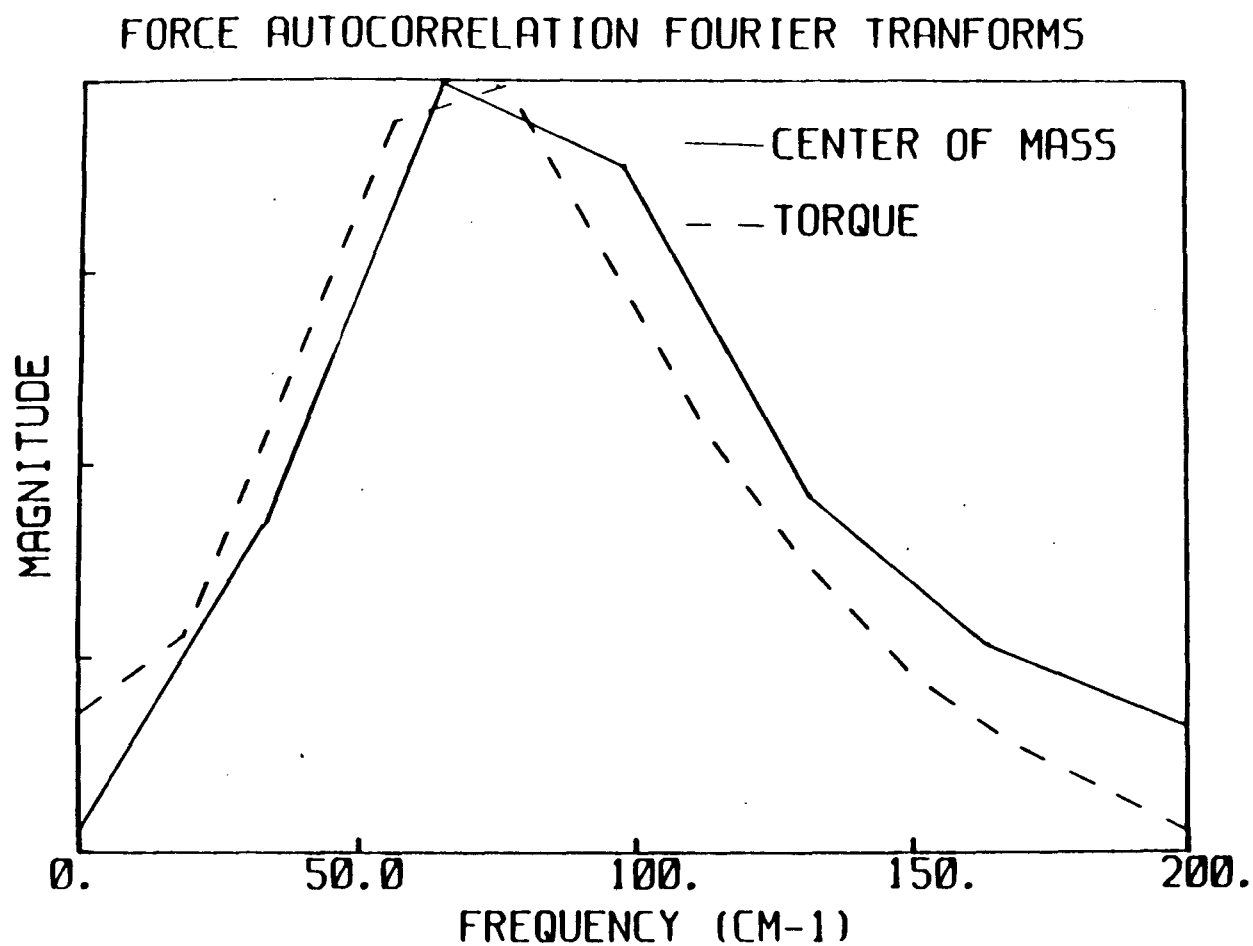
FORCE AUTOCORRELATION FOURIER TRANFORMS
CENTER OF MASS
TORQUE
MAGNITUDE
0.
50.0
100.
150.
200.
FREQUENCY (CM-1)

Figure 23

relaxation. Unfortunately, the autocorrelation functions calculated by Tildesley and Madden have been normalized so that no comparison of the magnitudes of the rotational and translational forces can be made. Assuming that each degree of freedom contributes equally to the magnitude of the solvent-solute force, a further 3/5 reduction of the I_2 relaxation time would occur in CS_2 relative to that in Xe. The differences in intermolecular potential between the I_2-CS_2 and I_2-Xe are unknown since the former has yet to be determined, however, the CS_2 probably has a more steeply repulsive interaction with the I_2 than the rather polarizable Xe. Since the slope of the intermolecular potential's repulsive region is important in determining the vibrational relaxation rate, the energy dissipation would be expected to be faster in CS_2. This difference probably accounts for the remaining factor of 2/9 reduction in I_2/CS_2 relaxation time.

Thus, this experiment demonstrates that the solvent's translational and rotational degrees of freedom can efficiently quench the solute's vibrational energy at even higher frequencies than had been expected. In particular, relaxation times of under half a nanosecond can occur solely through coupling to the solvent translation modes.

IV. A′ and A State Dynamics

A. I_2/Xe

i. General Features

As has been observed in molecular solvents, the A′/A absorption component in Xe is characterized by a fast rise followed by a slow exponential decay.[22,26] The 1/e rise and fall times in the various Xe thermodynamic states are listed in table 8. In molecular solvents, the rise time is ≈20 psec and is a combined measure of the recombination and vibrational relaxation times on the A and A′ surfaces. In these solvents, the exponential decay varies from 100-3000 psec and reflects the A′→X nonradiative electronic curve crossing time. As will be demonstrated later in this chapter, the A′/A lifetime in molecular solvents is dramatically shortened through electronic to vibration energy transfer from the I_2 to the solvent. Xe contains no internal degrees of freedom and as a consequence the lifetimes are extraordinarily long, ≈8 nsec. The rise times in Xe vary from 20 psec at high density to 300 psec at low density. Molecular dynamics simulations indicate that recombination in Xe occurs under 10 psec and is slightly slower at higher density because the solvent impedes motion of the I atoms to the large internuclear separation necessary for recombination.[51] Since the rise time becomes faster as the density increases, the change in rise time with density probably reflects differences in vibrational relaxation rates on the A′ and A state surfaces. If this assessment is correct, there is a large difference in the density dependence of relaxation on

Table 8

ρ	T	η	τ_1	τ_2	R_{12}	τ_D
(g/ml)	(K)	(cP)	(psec)	(psec)		(psec)
3.0	323	0.5	20 ± 5	> 370	1.5 ± 0.4	4500 ± 520
3.0	303	0.5	18 ± 3	> 570	1.1 ± 0.2	5260 ± 420
3.0	253	0.5	32 ± 9	> 900	1.0 ± 0.1	12250 ± 2000
3.4	280		14 ± 3	> 370	1.5 ± 0.2	7625 ± 830
3.0	280	0.5	26 ± 6	> 500	1.3 ± 0.2	9100 ± 2000
2.6	280	0.25	38 ± 10	> 850	0.85 ± 0.2	8850 ± 1500
2.2	280	0.12	82 ± 20	-	-	9530 ± 2000
1.8	280	0.03	270 ± 70	-	-	6900 ± 2000

Caption: Measured constants for A' and A state transient absorption at various thermodynamic states of Xe. ρ and T are the Xe density and temperature respectively. The viscosity, η, is estimated from the reduced state correlation.[71] τ_1 is the fast rise time and τ_2 is the slow rise time characterizing the double rise behavior of the absorption. R_{12} is the ratio of the magnitude of the fast rising component to that of the slow rising component and τ_D is the decay time of the absorption.

the A′ and A states surfaces (a factor of 20 change) as compared to the ground state surface where a factor of 4 increase was observed. Since ω_e in the A′ and A states is 100 cm^{-1} as opposed to 200 cm^{-1} in the ground state, the relative overlap of the A′ and A states vibrational frequencies with the solvent-solute force frequencies at different Xe densities may be quite different from that in the ground state.[20,23-24] Since the rise time in the high density Xe is similar to that in molecular solvents, vibration to translation energy transfer can be as efficient as other methods of energy transfer in the 100 cm^{-1} frequency range. There appears to be a slight slowing down of the rise time as the temperature decreases although the differences are within experimental error. Such a variation could be due to differences in cage recombination time as well as vibrational relaxation rate since the changes are only a few picoseconds at most.

In molecular solvents, the A→A′ transition has always been assumed to be fast since these states are only separated by 1000 cm^{-1} near their potential surface minima and only a single exponential decay of the transient absorption assigned to these states has been observed. In Xe, evidence of a relatively slow A→A′ transitions is apparent in some of the 632 nm transient absorption spectra where a fast and slow rise is required to fit the A′/A state component. An example where a double rise time is required to fit the A′/A component is shown in figure 24, the 632 nm transient absorption in 3.0 g/ml Xe at 323 K. The second slow rise of the A′/A state absorption cannot be uniquely separated from the rise of the ground state absorption which is similar in timescale. Thus, only a lower limit of ≈370 nsec can be placed on the slow A′/A rise. This slow

Figure 24 I_2 transient absorption at 632 nm in 3.0 g/ml Xe at 323 K shown in three different timescales. In the long time scan (top spectra), the exponential decay of the A'/A state absorption is fit. In the short time scan (bottom spectra), a 20 psec rise is observed for the A'/A state absorption. However, as shown in the intermediate time scan (middle spectra), a slower rise (>350 psec) is also needed to fit the magnitude of the A'/A absorption. The presence of the ground state absorption (the residual absorption in the spectra) makes a unique assignment of the slower rise time impossible and only a lower limit for it can be established.

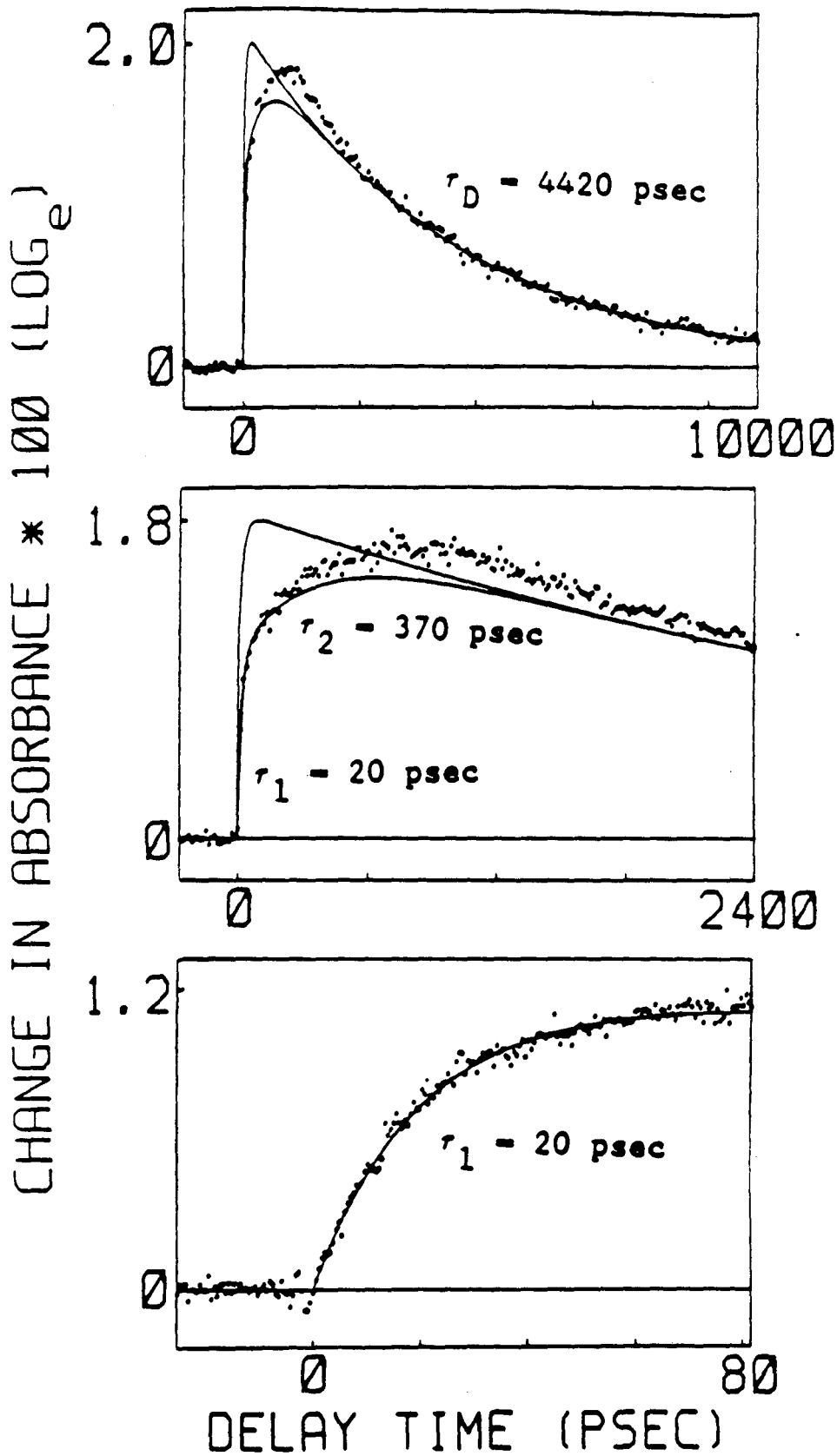
2.0
0
0
10000
τ_D = 4420 psec
1.8
0
0
2400
τ_2 = 370 psec
τ_1 = 20 psec
1.2
0
0
80
τ_1 = 20 psec
CHANGE IN ABSORBANCE * 100 (LOG$_e$)
DELAY TIME (PSEC)

Figure 24

rise probably represents the timescale of A→A′ dynamics and is a consequence of the A′ state having a larger extinction coefficient than the A state at that wavelength. This double rise behavior on the A′/A absorption does not appear at the lower Xe densities where it most likely becomes obscured by the ground state absorption. The relative magnitudes of the quickly rising component to that of the slowly rising component shows a general trend of increasing with density and temperature although most of the differences are within experimental error. If the slowly rising component is due to molecules originally recombining on the A state which later curve cross to A′ state, then these trends of relative magnitudes provide qualitative information regarding the preference of recombination onto the A versus A′ surface as a function of density and temperature. Specifically, these trends suggest that A′ state becomes increasingly preferred as the temperature and density increase. The temperature increase seems reasonable since the viscosity will decrease and recombination onto the A′ surface requires greater internuclear separation as compared to the A state. However, the density effect is contrary to this explanation since the viscosity increases with density.

ii. <u>Density and Temperature Dependence</u>

The discussion of the density and temperature effects on the A′ state lifetime is prefaced by highlighting the salient physical mechanisms involved in controlling barrier crossing rates as outlined by Kramers in 1940.[69] Kramers' theory of barrier crossing emphasizes the

two different limits of solvent density. At low solvent densities such as in the gas phase, the rate of barrier crossing increases with solvent pressure because of the increase in solute-solvent collisions which are activating the solute. In this density regime, the initial state is not in thermal equilibrium with the transition state because of a lack of the necessary number of collisions. On the other hand, at high solvent densities such as in the liquid phase, the rate of barrier crossing decreases with solvent density because the crossing process has become diffusive in the transition state region. In this regime, the solvent obstructs any large solute motion along the reaction coordinate through its attractive forces and physical presence. While the solvent provides adequate thermal activation of the reaction at high density, the viscous drag it exerts on the solute is the dominate factor in determining the crossing rate. Between the high and low density regimes, a region is expected where thermal activation is achieved, but the solvent does not exert significant viscous drag. In this region the reaction rate obeys transition state theory and does not vary with density.

The A and A' lifetimes in the Kramers' high density and transition state regimes have been calculated by Dawes and Sceats.[70] In this study, the I atom motion is simulated through use of the Langevin equation in which solvent effects are characterized by the coefficient of viscosity and a random force. R dependent nonadiabatic curve crossing probabilities were determined using a model in which the transitions occur as a result of Corriolis coupling at short r where the energy difference between the states is large and through solvent-I_2 complex rotational coupling at large r where the energy difference is small. Due

to computational limitations, only transitions at surface crossing points are included in calculation of the A and A' lifetimes although their crossing model shows nonzero probabilities for off resonance transitions. In the Kramers' high density limit, the lifetimes become much longer with density. Over a viscosity range of 0 to 3.34 cP, the A state lifetime increases from 250 to 6900 psec while the A' lifetime lengthens from 6 to 257 nsec. In the transition state regime, the density dependence of the lifetimes is negligible with the calculated A state lifetime varying from 133 to 147 psec and A' lifetime changing from 3340 to 3760 psec for the same viscosity range.

An additional consideration which Dawes and Sceats have not included in their calculations is the added barrier height resulting from solvent force along the bond axis. Recall that figure 13 (p. 58) showed that the potential surface of mean force is strongly density dependent at large r where transitions can occur most easily. Thus, at higher density, the solvent increasingly obstructs the I_2 in attaining large internuclear separation, effectively adding to the barrier height, and lengthening transition times. Near the surface crossing points for the A and A' states with the ground state, the added barrier height in the 3.0 g/ml Xe density over that in the 1.8 g/ml Xe solution is estimated to be several hundred to a thousand wavenumbers. An increase of barrier height in this range would decrease the rate of thermal activation by a factor of 4-100 as the density is increased. Thus, even in the transition state region, a lengthening of the excited state lifetimes is expected as the density is increased.

Surprisingly though, within experimental error, the A' lifetime is nearly density independent over the entire liquid density range (see figure 25). Given the added barrier height at higher density and the increase in viscosity from 0.03 cP at 1.8 g/ml Xe density to >0.5 cP at the 3.0 g/ml density [71], the insensitivity of lifetime to density appears rather puzzling unless the solution is considered to be in the Kramers' low density regime. In that limit, the predicted increase of rate with density could be offset by the added barrier from the solvent force along the bond axis. However, a few further factors must be considered with relation to the Dawes and Sceats calculations. First, the relevance of any single parameter characterizing solvent viscosity to some liquid phase processes has been highly questioned. When the time which the reactant spends in the barrier crossing region is short in relation to the solvent's ability to respond to this motion (which may be the case if the transitions occur after a few consecutive violent collisions), the solvent will not exert the same viscous effect as it does in slower processes. Thus, the frequency dependence of the solvent response to solute motions must be considered. Typically, the high frequency viscosity is much smaller than the macroscopic viscosity. Simulation of the I atom motion should be calculated through the generalized Langevin equation which includes the frequency dependence of the viscous forces and recognizes that there is a nonzero solvent reequilibration time. Secondly, the barrier crossing may occur nonadiabatically at r which are shorter than the surface crossing points Such crossings would significantly decrease the density dependence of the added barrier height due to the solvent force along the bond axis. Dawes and Sceats state

Figure 25 Density dependence of the A' state lifetime at 280 K.

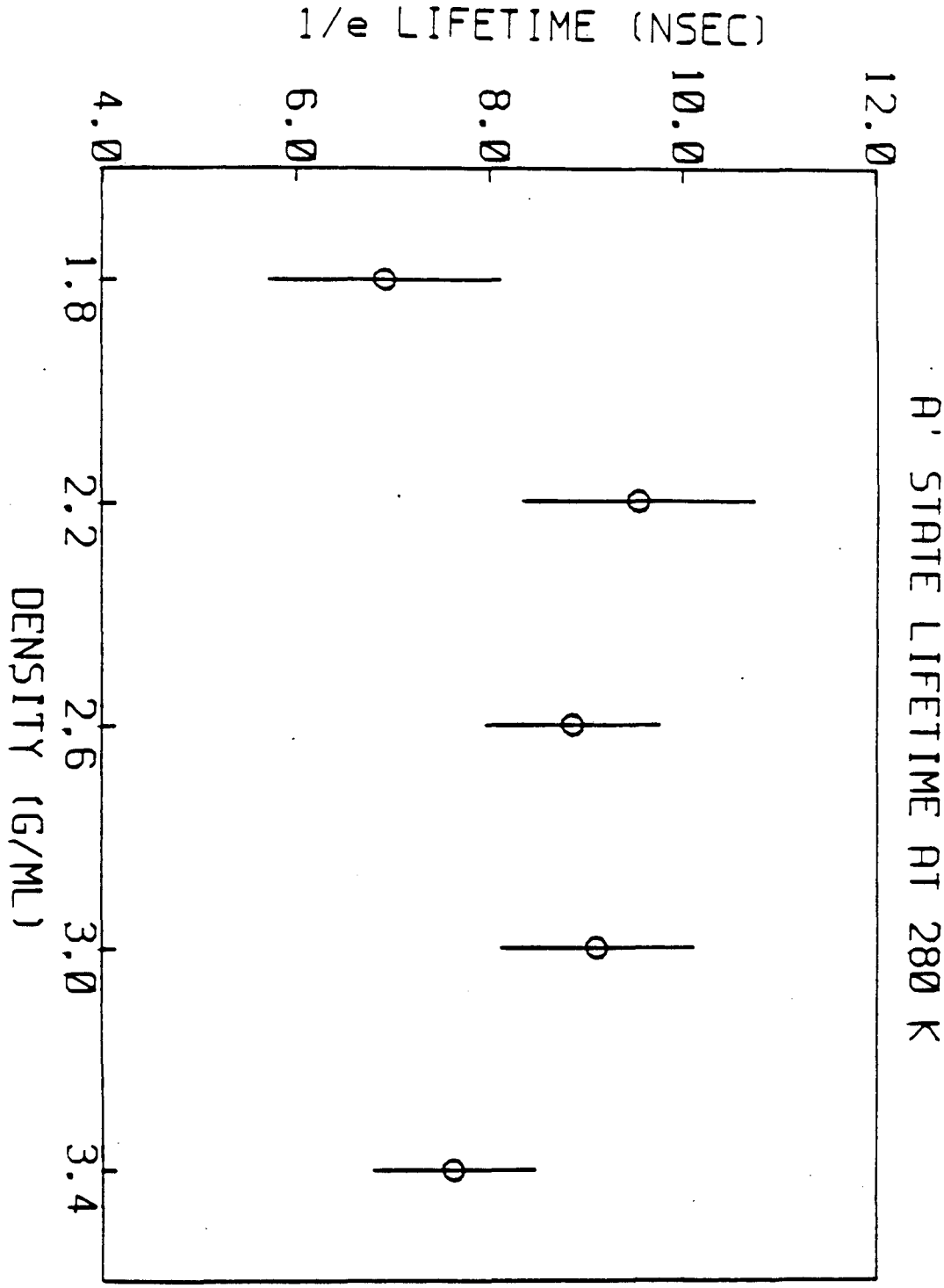
A' STATE LIFETIME AT 280 K
12.0
10.0
8.0
6.0
4.0
1/e LIFETIME (NSEC)
1.8
2.2
2.6
3.0
3.4
DENSITY (G/ML)

Figure 25

that their curve crossing model applies when the solvent mass is much less than the solute reduced mass which is clearly not satisfied in the I_2/Xe system and furthermore, their crossing model takes no account for solvent dependent effects other than mass. Xe may increase nonadiabatic curve crossing through heavy atom effects. Finally, the gas phase potential surfaces are not accurately known at large r where the crossing points occur, nor are the intermolecular potentials for the excited states. These factors will effect the relative energies of the surfaces in solution. Slight changes in these surfaces will dramatically alter the calculated lifetimes and possibly the density effects. Thus, the Kramers' regime to which the curve crossing belongs is not clear, nor is the expected density dependence.

The temperature dependence of the A' lifetimes in the 3.0 g/ml Xe density solution does little to clarify the Kramers' regime to which the crossing belongs. The lifetime shortens from 12 nsec at 253 K to 4.5 nsec at 323 K. Since the viscosity change is negligible over this temperature range, the data might be expected to show Arrhenius behavior. An Arrhenius plot of the temperature data (figure 26) reveals an activation barrier of 850 cm^{-1} and a preexponential factor of 0.01 $psec^{-1}$ which may be compared to the gas phase well depth of 2400 cm^{-1} and the A' vibrational period of 0.3 $psec^{-1}$. While these are reasonable parameters, the plot does not fit the data particularly well and the data should not necessarily be considered to display Arrhenius behavior.

Figure 26 Arrhenius plot of the A′ state lifetime temperature dependence over a temperature range of 253 to 323 K at a Xe density of 3.0 g/ml.

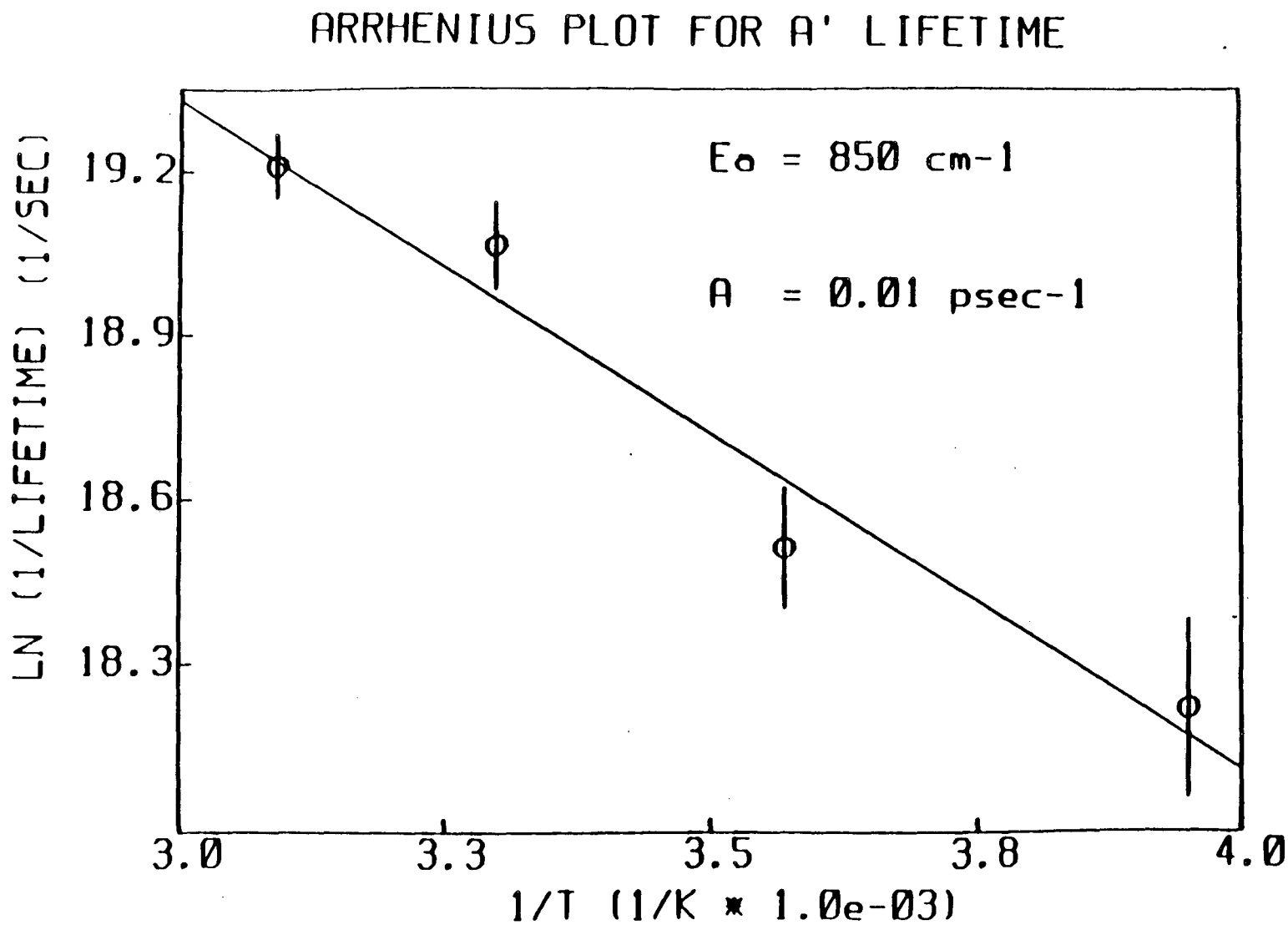
ARRHENIUS PLOT FOR A' LIFETIME
Ea = 850 cm-1
A = 0.01 psec-1
LN (1/LIFETIME) (1/SEC)
19.2
18.9
18.6
18.3
3.0
3.3
3.5
3.8
4.0
1/T (1/K * 1.0e-03)

Figure 26

B. Deuterium Isotope Effect on A' Lifetime

The A'→X curve crossing time varies from 100 psec in hydrocarbon solvents to 8 nsec in liquid xenon (see table 9). The reason for this large variation in curve crossing time is not yet understood. As previously stated, attempts to correlate this lifetime with solvent characteristics such as viscosity or ionization potential have shown that no simple relationship can explain this phenomenon. Thus, little understanding of the dynamics underlying this curve crossing process has been gained from comparison of the experimental results in the different solvents. In this section, a surprising deuterium isotope effect on the A' state lifetime is reported which elucidates the mechanism of this curve crossing.

Within experimental error, the A' state lifetimes in the deuterated solvents are 2.0 times longer than those found in the corresponding hydrogenated solvent (see table 9) while the ground state vibrational relaxation is unaffected by deuteration. This isotope effect on the trap state lifetime cannot be attributed to enhanced I_2 activation occurring through more efficient energy transfer from the solvent vibrational modes to the I_2. The lowering of solvent vibrational frequencies upon deuteration most largely changes the C-H stretch frequencies in the these solvents, lowering the frequency from about 3000 cm^{-1} to 2100 cm^{-1}. The other solvent vibrational frequencies which are lowered to any appreciable extent by deuteration are all over 400 cm^{-1}.[72,73,74] The ground vibrational frequency of the A' state is approximately 100 cm^{-1}.[24] Thus, none of the largely affected solvent

Table 9

Solvent	[CH] (M)	τ_H (psec)	τ_D (psec)	τ_D / τ_H
Cyclohexane	110	94 ± 24	193 ± 37	2.05 ± 0.21
Octane	111	114 ± 25	222 ± 34	1.95 ± 0.52
CS_2		150		
CH_2Cl_2	31.3	540 ± 41	1078 ± 53	2.00 ± 0.18
$CHCl_3$	12.4	998 ± 103	1826 ± 183	1.83 ± 0.26
$CFCl_3$		2300		
CCl_4		2700		
Xe		8000		

Table Caption: I_2 A'/A state 1/e lifetimes in various solvents (τ_H) and their deuterated analogs (τ_D). [CH] denotes the density of solvent CH stretching modes. $CFCl_3$ results are from ref. 75 and CCl_4 results are from ref. 26.

vibrational modes are near resonance with the $I_2(A')$ vibrational frequency. In addition, if the energy transfer from the solvent modes to the excited I_2 were important, the transfer would become more efficient in the deuterated solvent since the vibrational energy mismatch would be smaller. Since the lifetimes lengthen upon deuteration, direct vibration to vibration energy transfer from these solvent modes to the I_2 does not occur. The change in the solvent mass and moments of inertia upon deuteration is not very large and does not alter the translational and rotational solvent frequencies appreciably. The insensitivity of the ground state vibrational relaxation rate to deuteration reflects this fact. Thus, this deuterium effect is not due to enhanced energy transfer from the solvent to the I_2.

Clearly though, since deuteration would not electronically alter the A' potential surface, this isotope effect indicates that the solvent's hydrogens are directly involved in an energy transfer process with the I_2. This effect can be explained with the hypothesis that electronic to vibrational energy transfer is occurring from the excited I_2 to the solvent. For example, the process might be as follows:

$$I_2(A') + M(v=0) \rightarrow I_2(X) + M(v=1)$$

Presumably, this process would involve the Franck-Condon overlap of the I_2 vibrational wavefunctions in the two electronic states and would therefore occur near the region of maximum wavefunction overlap (near the classical turning points for high vibrational levels). In addition, this process would be resonance enhanced when the difference in energy between the two I_2 states was equal to a solvent vibrational quanta. At the A'

surface minimum, the energy difference between the gas phase RKR A' and ground state surfaces at constant internuclear separation is 6100 cm^{-1}.[20,24] This energy gap monotonically decreases as the internuclear separation increases until the two surfaces cross. However, as this energy gap between the two potential surfaces decreases, the activation energy required to reach the appropriate I_2 internuclear separation for the Franck-Condon transition increases. The activation energy factor ($e^{-E/kT}$) from the A' potential surface minimum to reach the classical turning point transition region as a function of the energy difference between the RKR gas phase A' and ground state surfaces is shown in figure 27. Since the C-H stretch frequency is the highest vibrational frequency in the solvents studied, transfer of energy to this mode would require less activation energy on the A' surface than would transfer to other solvent modes. Deuteration lowers this stretch frequency and the process then requires more activation energy to reach the resonant transition region, thereby lengthening the A' lifetime. According to figure 27, the activation time required to reach the C-H resonance region is 4 times shorter than for C-D resonance although the lifetime in the hydrogenated solvents is only 2 times shorter than that in the deuterated solvents. This discrepancy appears to indicate that if the activation energy were held constant, the energy transfer occurs more readily as the electronic energy difference between the two I_2 states becomes smaller. Alternatively, the transition may involve a two quanta vibrational excitation of the solvent. From figure 27, the activation factor ($e^{-E/kt}$) in the deuterated solvent for a resonant two quanta transition is twice as small as that in the hydrogenated solvent. This factor of 2 in

Figure 27 The activation energy factor relative to thermal energy at room temperature is shown as a function of the energy difference between the RKR A′ and X state surfaces of I_2 at the classical turning points. This plot is essentially a logarithmic plot of the total activation factor $e^{-E/kt}$. The vibrational frequencies of various solvent modes are noted on the figure.

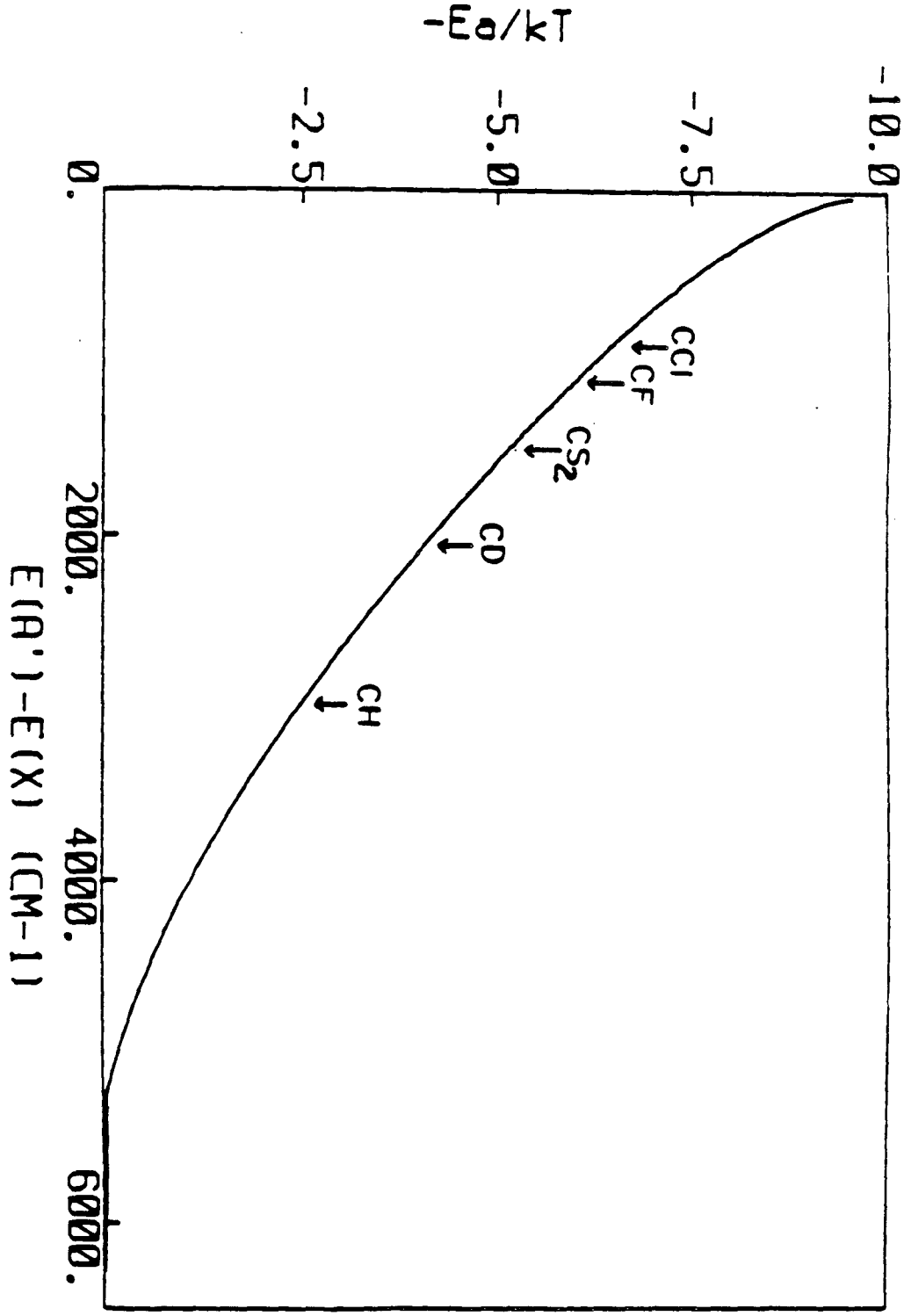

Figure 27

activation probability matches the difference in A′ lifetime observed in the deuterated and hydrogenated solvents. However, putting aside activation energy considerations, excitation of multiple quanta of vibrational energy is presumably less favorable than one quanta excitation and the agreement regarding the factor of 2 may be fortuitous. The relative efficiency of one quanta versus multiple quanta transitions requires a comparison of the shorter activation time for the two quanta transition versus the increased probability of a one quanta transition once the necessary activation has occurred. The relative activation time ($e^{-E/kt}$) for the one quanta excitation is approximately 10 times longer than that for the two quanta process for the hydrogenated solvent.

This proposed mechanism of the A′→X nonadiabatic curve crossing explains the trend of shorter A′ state lifetimes with increasing density of concentration stretching modes (see table 9). The activation time required for transfer of energy to solvent vibrational modes other than the C-H stretch will take substantially longer since the C-H frequency is the highest frequency in these solvents and thus, the resonant turning point region for other solvent modes is at higher vibrational energy in the A′ state or requires a greater change in solvent vibrational quanta. Alternatively, the coupling of the C-H stretch with the A′→X electronic transition (which is not yet understood) may be larger than it is with other solvent modes. Thus, in solvents containing a C-H bond, transfer of energy to the C-H stretching mode is the dominate mechanism of the nonadiabatic curve crossing even when there are many other vibrational modes present. This dominance of the C-H energy acceptance is indicated by the constant factor of 2 change in A′ lifetime between the

hydrogenated and deuterated solvent, regardless of the number of C-H bonds in the solvent. The density of C-H modes directly controls the rate of the energy transfer. Notice that with the exception of CS_2 which is known to form a charge transfer complex with I atoms and may strongly electronically interact with A' state I_2, the longest A' lifetimes occur in the hydrogen free solvents which contain no high frequency modes, with the longest lifetime occurring in the monatomic solvent Xe.

Quantitative calculations of the electronic to vibrational energy transfer rates from this data will require specific knowledge regarding the alteration of the potential surfaces by the solvent. These alterations include electronic interactions as well as the effect of the solvent force along the bond axis. Furthermore, modeling of the activation process via Langevin or generalized Langevin equations of motion may be necessary rather than assuming a Boltzman distribution of vibrational states. Lastly, the coupling mechanism between the I_2 electronic states and the solvent vibrational modes is not yet understood. However, suitable alternative explanations of this isotope effect of the A' lifetime are not apparent. Observations of intermolecular electronic to vibrational energy transfer have been extremely rare (except from electronically excited atoms)[76-80] and thus, this system provides a unique opportunity for studying such a process.

VI. Summary and Conclusions

Careful consideration of the solvent effects on the I_2 ground state spectroscopy have revealed that there are some slight differences between the gas phase extinction coefficients and those calculated for I_2 in liquid Xe. In this sense, Xe is an ideal solvent as it perturbs the I_2 potential surface minimally at energies well below the dissociation limit and does not appear to change intermolecular potential with the I_2 when the I_2 is electronically excited. However, large spectroscopic effects will occur in other solvents if the intermolecular solvent-solute potential changes when the molecule is excited from the ground state.

The studies of I_2 relaxation in liquid Xe have shown that vibration to translation energy transfer in this system is an inefficient process when compared to the relaxation rates observed in molecular solvents. In the upper half of the potential surface, relaxation is fairly rapid (< 300 psec) which demonstrates that vibration to translation energy transfer can play an important role in stabilizing a newly formed bond. However, the relaxation in Xe is particularly slow in the lower half of the I_2 ground state potential surface where the vibrational frequencies (> 170 cm^{-1}) do not overlap well with the intermolecular force spectrum. These results do not imply that vibration to translation energy transfer will be an inefficient process in this part of the potential surface in other solvents. The fast relaxation observed in CS_2 indicates that with a more repulsive solute-solvent intermolecular potential, vibration to translation energy transfer alone can bring the relaxation rate to within

a factor of 2-3 of that occurring when other energy pathways are available.

The observed slow relaxation in Xe is in agreement with the qualitative predictions of theorists. The quantitative agreement between molecular dynamics simulations and experiment though is far from satisfactory. A large part of this discrepancy is due to an inaccurate characterization of the intermolecular potential as a Lennard-Jones surface. However, agreement between experimental results and molecular dynamics simulations regarding the density and temperature dependence of the relaxation is good. Thus, a theoretical model which can accurately describe the simulation results will be useful for describing the real system when the intermolecular potential becomes better characterized and efforts at developing such a model are encouraged. Current theoretical predictions of the density and temperature dependence of the relaxation rate by Stote and Adelman using a generalized Langevin model show a much greater density variation than was observed experimentally or in computer simulations and indicates that further work is needed on their model.

A new manner in which to test the validity of the isolated binary collision (IBC) model of relaxation at liquid densities which eliminates the ambiguities associated with a collision frequency determination has been presented. This test is performed by observing the relaxation over many vibrational levels and verifying whether the energy decay curve for this multilevel relaxation process can be linearly scaled with time in order to describe the relaxation as a function of density. Deviations from linear scaling indicate nonbinary behavior. This test of the IBC model for the I_2/Xe system surprisingly revealed that the model was

consistent over the entire liquid Xe density range. This result is startling because the IBC model is not expected to be valid for such a low frequency oscillator in solution or when the large amplitude motions of the oscillator rather than random solvent motions are driving the collisions. Thus, the IBC model has more theoretical validity in describing vibrational relaxation in the liquid phase then has been generally been thought.

However, the IBC model still lacks predictive value in the liquid phase because a model of calculating the collision frequency remains undetermined. A simple contact distance model of collision frequency was employed in this study in order to assess the value of this notion. The collision frequency tabulated through molecular dynamics simulations did describe the relative difference in relaxation rate for 2 of the 3 densities examined. This simple concept of collision frequency may merit further attention for theoretical development. Gas phase measurements of the relaxation in I_2/Xe system would be a great help in addressing this issue.

Measurements of the A′ state lifetime as a function of Xe density showed that the lifetime is independent of density. This result is rather puzzling since the solvent force along the I_2 bond axis increases with density, thereby increasing the activation barrier. The increase in activation energy with density may be offset by a simultaneous increase in collision frequency. However, at liquid density the reactant is typically considered to be in thermal equilibrium with the transition state and an increase in density only serves to hinder the forward reaction because of viscous effects. Further theoretical work is

required on this system in order to understand the insensitivity to solvent density of this curve crossing process. Specifically, simulation of the process using the generalized Langevin equation and a model of nonadiabatic transitions are required.

Experiments in deuterated hydrocarbons and chloromethanes revealed that the mechanism of A'→X curve crossing occurs through electronic to vibrational energy transfer from the I_2(A') to the solvent. This energy transfer process substantially reduces the activation energy required to make the A'→X transition. Specifically, the higher the solvent vibrational frequency involved is the lower the activation energy. The C-H stretch is the highest vibrational frequency in the solvents which have been studied thus far and thus, is the dominant mode involved in the transfer process for hydrogen containing solvents. The A' state lifetime in the hydrogen containing solvents is directly related to their hydrogen content. Further investigation into this phenomenon through temperature dependence studies or in other solvents may reveal more details about this interesting process which has been rarely observed between two molecules.

Finally, the results presented in this thesis on the density and temperature dependence of the I_2 dynamics in Xe should stimulate further theoretical work on this system. There have been few experiments in the past which have investigated the effects of density and temperature on vibrational relaxation or nonradiative curve crossing in solution with such a simple system. Given the complexity inherent to the liquid phase, the I_2 recombination reaction in Xe is an ideal system for quantitative modeling since accurate theoretical description of the reaction dynamics

is much more realizable.

Appendix

Data file format for CAMAC.MAC

Files on the LSI11 are occupy an integer number of segments known as blocks. Each block consists of 256 sixteen bit words. The data files are binary files in which the first block known as "block 0" contains all information regarding the setting of program parameters during the data collection. The data is listed beginning at the start of the next block and fills the remaining blocks in the file.

Block 0 format

Word	Contents
0	45502 (octal) - Camac.mac data file identifier ("KB" in ASCII)
1	Delay/Gate Settings for Channel A
2	Delay/Gate Settings for Channel B
3	Number of A/D Channels in data file (excluding normalizations)
4	Date (RT11 Format)
5	Number of Laser Shots/Data Point
6-11	1 Byte labels for A/D Channels (further description given below)
12	Number of Data Points in Scan (stage stops)
13	Number of Steps/Point for Triplemate
14	Scan Mode (0=normal, 1=dly/gate sweep, 2=difference, 3=transmission, bit 3 set means Ten Step option enabled)
15	Stepper Motor Start Position
16	Stepper Motor End Position
17	Stepper Motor Steps/Data Point

18	Triplemate Start Wavelength (Å)
19	Triplemate Stop Wavelength (Å)
20	Number of Normalized A/D Channels in data file
21	Overflow error
22	Sum error
23	Normalization error
24-26	Filename (packed Radix 50)
27-38	Backgrounds for A/D Channel 0 → A/D Channel 11
39	Grating Number (1=150 grove/mm, 2=300, 3=600, 4=1200, 5=1800, 6=2400, 7=3600)
40-75	Comment Field for data file (72 characters)
76-90	Comment Field for data Set 1 (30 characters)
91-105	Comment Field for data Set 2 (30 characters)
106-120	Comment Field for data Set 3 (30 characters)
121-135	Comment Field for data Set 4 (30 characters)
136-150	Comment Field for data Set 5 (30 characters)
151-165	Comment Field for data Set 6 (30 characters)
166-180	Comment Field for data Set 7 (30 characters)
181-195	Comment Field for data Set 8 (30 characters)
196-210	Comment Field for data Set 9 (30 characters)
211-225	Comment Field for data Set 10 (30 characters)
226-240	Comment Field for data Set 11 (30 characters)
241-255	Comment Field for data Set 12 (30 characters)

<u>Format of Data Blocks</u>

The data is listed in sequential words with no gaps left between points. Each A/D and normalized channel for a particular stage stop is listed before proceeding to the data at the next stage stop. The order in which the A/D and normalized channels are listed follows the order in which the one byte labels in words 6-11 of Block 0 are listed. A/D channels are alloted 1 word/data point while normalized channels are alloted 2 words/data point (listed low word then high word). The data points are all unsigned integers. The data for the A/D channels is the sum of the number of counts whereas the normalized channels are multiplied by 1024 for each division performed in the normalization in order to preserve resolution with the integer format.

1 Byte Labels for A/D and Normalized Channels (words 6-11 in Block 0)

The bytes in each word should be read in the order low byte then high byte. The lower four bits in each byte are the number of the A/D or normalized channel being described. Each A/D channel only requires a 1 byte description whereas a normalized channel requires as many bytes as there are operations in the calculations plus one. The upper four bits in each byte are used only for normalized channels and each have a specific purpose in describing the normalization string as listed here:

Bit	Meaning when Set
5	This is the last byte in the normalization string
6	Indicates that this A/D should now be divided into the normalization string

7 Indicates that this A/D should now multiply the normalization string

8 Indicates that this byte is part of a normalization string

Example (words given in binary - high byte, low byte):

Word 6: 100 000 000

Storing A/D Channel 0 (low byte)

Storing A/D Channel 1 (high byte)

Word 7: 1 011 000 010 000 001

Start of a normalization string using A/D Channel 1 (low byte)

End of a normalization string - division by A/D Channel 0 (high byte)

Word 8: 10

Storing A/D Channel 2

In this example the normalization string 1 is:

A/D Channel 1 / A/D Channel 0

Order of storing the data would be in the order listed by the bytes (low byte then high byte) with 1 word for each A/D channel and 2 words for the normalized channel.

The following is a subroutine used on the LSI11 to read CAMAC.MAC data files:

```
C
C     THIS PROGRAM READS CAMAC OR CAMSUM OUTPUT FILES
C
C     CREATED 3/86 BY MARK PAIGE
C
C
      SUBROUTINE READMP
C
      COMMON/LIST1/ COMENT,DATA,DATE,DPTS,FNAME
      COMMON/LIST2/ MEND,MSTART,SCTYPE,SHOTS,STEPS,TZERO
      INTEGER ADDRES,ADCHAN,ADD,ADLBL(12),ANS
      INTEGER BKG,BLANK,BLKNUM,BLOCK(256)
      INTEGER CHAN,COMENT(36),COUNT
      INTEGER DATE,DPTS,DOT,E
      INTEGER FILE(12),FNORM,HWORD
      INTEGER I,ICHAN,J,KB,LEFT,LOC,LWORD
      INTEGER MEND,MSTART,NNORM,NUM,NUMBER(3)
      INTEGER SCTYPE,SHOTS,SPACE,STEPS,TZERO,Z
      LOGICAL*1 FNAME(16),CSINAM(12)
      REAL*4 DATA(500),HNUM,LNUM,TEMP
C
C     **** INITIALIZATION ****
C
700   NUM=-1
      FNAME(1)='A'
C
C     **** CALL FILE ****
C
14    WRITE(5,15)
15    FORMAT('$ENTER COMPLETE FILENAME:  ')
12    CALL GETSTR (5,FNAME,14)
C
C     **** PUT FILENAME INTO CSI FORM ****
C
50    CALL MPNAME(FNAME,CSINAM)
      ICHAN=7
      IF (IFETCH(CSINAM).EQ.0) GO TO 75
      WRITE(5,70)
70    FORMAT('$NO SUCH DEVICE EXISTS.  ')
      GO TO 14
75    I=LOOKUP(ICHAN,CSINAM)
      IF (I.GE.0) GO TO 80
      WRITE(5,78)
78    FORMAT('$FILE NOT FOUND.  ')
      GO TO 14
80    Z=IREADW(256,BLOCK,0,ICHAN)

C
C     **** VERIFY FILE TYPE ****
C
      KB=BLOCK(1)                    !FILE IDENTIFIER
      IF (KB.EQ."45502) GO TO 29
```

```
      WRITE (5,20)
20    FORMAT('$ARE YOU SURE THIS FILE HAS THE CORRECT FORMAT? ')
      READ (5,25) ANS
25    FORMAT(A1)
      IF (ANS.EQ.'Y') GO TO 29
      CALL ICLOSE(ICHAN)
      WRITE(5,26)
26    FORMAT($' TRY AGAIN. ')
      GO TO 14
C
C     **** PROMPT FOR CHANNEL NUMBER ****
C
29    IF (NUM.NE.-1) GO TO 100
      WRITE(5,30)
30    FORMAT('$WHICH CHANNEL DO YOU WANT TO PLOT?  ')
      READ(5,31)CHAN
31    FORMAT(A2)
      IF (CHAN.EQ.1H0) NUM=0
      IF (CHAN.EQ.1H1) NUM=1
      IF (CHAN.EQ.1H2) NUM=2
      IF (CHAN.EQ.1H3) NUM=3
      IF (CHAN.EQ.1H4) NUM=4
      IF (CHAN.EQ.1H5) NUM=5
      IF (CHAN.EQ.1H6) NUM=6
      IF (CHAN.EQ.1H7) NUM=7
      IF.(CHAN.EQ.1H8) NUM=8
      IF (CHAN.EQ.1H9) NUM=9
      IF (CHAN.EQ.2H10) NUM=10
      IF (CHAN.EQ.2H11) NUM=11
      IF (CHAN.EQ.2HN1) NUM=21
      IF (CHAN.EQ.2HN2) NUM=22
      IF (CHAN.EQ.2HN3) NUM=23
      IF (CHAN.EQ.2HN4) NUM=24
      IF (CHAN.EQ.2HN5) NUM=25
      IF (CHAN.EQ.2HN6) NUM=26
C
C     **** READ FILE PARAMETERS ****
C
100   ADCHAN=BLOCK(4)           !# OF A/D CHANNELS
      DATE=BLOCK(5)
      SHOTS=BLOCK(6)       !# OF SHOTS/PT
      DPTS=BLOCK(13)       !# OF DATA PTS
      SCTYPE=BLOCK(15)     !SCAN TYPE
      MSTART=BLOCK(16)     !MOTOR START
      MEND=BLOCK(17)
      STEPS=BLOCK(18)           !MOTOR STEP/PT
      NNORM=BLOCK(21)           !# OF NORM CHANNELS
      ADDRES =IADDR(BLOCK(7))
      DO 110 I=0,11
110   ADLBL(I+1)= IPEEKB(ADDRES+I)
      DO 111 I=1,3
111   FILE(I)=BLOCK(I+24)
```

```
      DO 112 I=1,36
112   COMENT(I)=BLOCK(I+40)
      BKG=0
      IF (NUM.LT.12) BKG=BLOCK(28+NUM)
C
C     **** FIND LOCATION OF FIRST DATA POINT ****
C
      COUNT = 1
      FNORM = 0
      NORMN = 20
      DO 205 I=1,12
      IF ((ADLBL(I).LT.16).AND.(ADLBL(I).EQ.NUM)) GO TO 250 !A/D TYPE
                                                            !FOUND
      IF (ADLBL(I).LT.16) GO TO 205       !A/D TYPE CHANNEL
      IF (FNORM.EQ.0) COUNT=COUNT + 1          !FIRST IN NORM STRING
      IF (FNORM.EQ.0) NORMN=NORMN + 1          ! SO INCREMENT NORMN
      IF (NORMN.EQ.NUM) GO TO 250         !NORM TYPE FOUND
      FNORM=1
      IF (INT((MOD(ADLBL(I),32)/16)).EQ.1) FNORM=0 !LAST IN NORM STRING
205   IF (FNORM.EQ.0) COUNT=COUNT + 1
C
C     **** READ IN DATA POINTS INTO DATA ****
C
250   BLKNUM=1
      Z=IREADW(256,BLOCK,BLKNUM,ICHAN)
      SPACE= ADCHAN + 2*NNORM        !SPACING OF DATA POINTS
      LOC= COUNT                 !LOCATION OF FIRST POINT
      DO 350 I=1,DPTS
      IF (NUM.LT.13) GO TO 310            !A/D TYPE
      IF (LOC-1.GT.256) BLKNUM=BLKNUM+1
      IF (LOC-1.GT.256) Z=IREADW(256,BLOCK,BLKNUM,ICHAN)
      IF (LOC-1.GT.256) LOC=LOC-256
      LWORD=BLOCK(LOC-1)                  !LOW WORD
      IF (LOC.GT.256) BLKNUM=BLKNUM+1
      IF (LOC.GT.256) Z=IREADW(256,BLOCK,BLKNUM,ICHAN)
      IF (LOC.GT.256) LOC=LOC-256
      HWORD=BLOCK(LOC)                       !HIGH WORD
      HNUM =HWORD                !CONVERT TO REALS
      LNUM =LWORD
      IF (HNUM.LT.0) HNUM=HNUM + 65536.  !FIX SIGN BIT
      IF (LNUM.LT.0) LNUM=LNUM + 65536.
      DATA(I) =HNUM*65536. + LNUM
      GO TO 350
310   IF (LOC.GT.256) BLKNUM=BLKNUM+1
      IF (LOC.GT.256) Z=IREADW(256,BLOCK,BLKNUM,ICHAN)
      IF (LOC.GT.256) LOC=LOC-256
      LWORD=BLOCK(LOC)
      DATA(I)= LWORD - BKG
350   LOC= SPACE + LOC
409   CALL ICLOSE(ICHAN)
      RETURN
      END
```

```
C
C     **** PUTS ASCII FILENAME STRING AND PUTS IN CSI FORM
C
      SUBROUTINE MPNAME(ASCII,CSINAM)
      LOGICAL*1 ASCII(14),CSINAM(12)
      INTEGER DOT,I
      DO 5 I=4,9                !PUT BLANKS IN FOR NAME
5     CSINAM(I) = ' '
      DOT = 0
      DO 10 I=1,11              !FIND DOT POSITION
      DOT =DOT + 1
10    IF (ASCII(I).EQ.'.') GO TO 15
15    DO 20 I=1,3               !COPY DEVICE NAME
20    CSINAM(I) = ASCII(I)
      DO 30 I=5,DOT-1                !COPY NAME
30    CSINAM(I-1) = ASCII(I)
      DO 40 I=1,3               !COPY RUN NUMBER
40    CSINAM(I+9) = ASCII(DOT+I)
      CALL IRAD50(12,CSINAM,CSINAM) !PUT INTO RADIX50
      END
```

References

1) See for example: J. Tellinghuisen, J. Chem. Phys. 76, 4736(1982). and references contained therein.

2) E. Rabinowitch and W.C. Wood, Trans. Faraday Soc. 32, 1381(1936).

3) R.M. Noyes, Z. Electrochemie 64, 153(1960).

4) D. Booth and R.M. Noyes, J. Am. Chem. Soc. 82, 1868(1960).

5) H. Rosman and R.M. Noyes, J. Am. Chem. Soc. 80, 2410(1958).

6) F.W. Lampe and R.M. Noyes, J. Am. Chem. Soc. 76, 2140(1954).

7) R.M. Noyes, J. Chem Phys. 18, 999(1950).

8) R.M. Noyes and J. Zimmerman, J. Chem. Phys. 18, 656(1950).

9) J. Zimmerman and R.M. Noyes, J. Chem. Phys. 18, 658(1950).

10) K. Luther, J. Schroeder, J. Troe, and U. Unterberg, J. Phys. Chem. 84, 3072(1984).

11) B. Otto, J. Schroeder, and J. Troe, J. Chem. Phys. 81, 202(1984).

12) K. Luther and J. Troe, Chem. Phys. Lett. 24, 85(1974).

13) H. Hippler, K. Luther, and J. Troe, Chem. Phys. Lett. 16, 174(1972).

14) T.J. Chuang, G.W. Hoffman, and K.B. Eisenthal, Chem. Phys. Lett. 25, 201(1974).

15) D.L. Bunker and B.S. Jacobson, J. Am. Chem. Soc. 94, 1843(1972).

16) J.N. Murrell, A.J. Stace, and R. Dammel, J. Chem. Soc. Faraday Trans. II 74, 1532(1978).

17) A.J. Stace and J.N. Murrell, Mol. Phys. 33, 1(1977).

18) D.J. Nesbitt and J.T. Hynes, J. Chem. Phys. 77, 2130(1982).

19) G. Herzberg, Molecular Spectra and Molecular Structure I. Spectra of Diatomic Molecules. (Van Nostrand Reinhold Co., Cincinnati: 1950) p. 541.

20) R.J. LeRoy, J. Chem. Phys. 52, 2683(1970).

21) R.F. Barrow and K.K. Yee, J. Chem. Soc. Faraday II 69, 684(1973).

22) D.F. Kelley, N.A. Abul-Haj, and D.J. Jang, J. Chem. Phys. 80, 4105(1983).

23) K.S. Viswanathan, A. Sur, and J. Tellinghuisen, J. Mol. Spec. 86, 393(1981).

24) J. Tellinghuisen, J. Mol. Spec. 94, 231(1982).

25) P. Bado, C. Dupuy, D. Magde, K.R. Wilson, and M.M. Malley, J. Chem. Phys. 80, 5531(1984).

26) A.L. Harris, M. Berg, and C.B. Harris, J. Chem. Phys. 84, 788(1985).

27) M. Berg, A.L. Harris, and C.B. Harris, Phys. Rev. Lett. 54, 951(1985).

28) G. Herzberg, Molecular Spectra and Molecular Spectra II. Infrared and Raman Spectra of Polyatomic Molecules. (Van Nostrand Reinhold Co., New York: 1945).

29) D.F. Kelley and P.M. Rentzepis, Chem. Phys. Lett. 85, 85(1982).

30) C.L. Brooks and S.A. Adelman, J. Chem. Phys. 80, 5598(1984).

31) P. Bado, P.H. Berens, J.P. Bergsma, M.H. Coladonato, C.G. Dupuy, P.M. Edelsten, J.D. Kahn, K.R. Wilson, and D.R. Fredkin, Laser Chem. 3, 231(1983).

32) A.J. Ledbetter and H.E. Thomas, Trans. Faraday Soc. 61, 10(1965).

33) D. Vidal, L. Guengant, and J. Vermesse, Physica 116A, 227(1982).

34) Alexander Lowe Harris, Ph.D. thesis, Picosecond Spectroscopy of Chemical Reactions in Liquids. University of California, Berkeley, 1985.

35) Mark Allen Berg, Ph.D. thesis, Picosecond Dynamics of Reactions in

the Liquid Phase: Studies of Iodine Photodissociation and Development of New Laser Techniques. University of California, Berkeley, 1985.

36) W.B. Street, L.S. Sagan, and L.A.K. Staveley, J. Chem. Thermodynamics 5, 633(1973).

37) A. Michels, T. Wassenaar, and P. Louwerse, Physica 20, 99(1954).

38) C.A. Langhoff, K. Gnadig, and K.B. Eisenthal, Chem. Phys. 46, 117(1980).

39) W.F. Sherman and A.A. Stadtmuller, Experimental Techniques in High Pressure Research. (John Wiley and Sons, Ltd., Chichester, England: 1987).

40) High Pressure Technology. I.L. Spain and J. Paauwe, eds. (Marcel Dekker, Inc., New York: 1977).

41) D.E. Smith and C.B. Harris, J. Chem. Phys. 87, 2709(1987).

42) J. Tellinghuisen, J. Chem. Phys. 82, 4012(1985).

43) J. Tellinghuisen, Adv. Chem. Phys. 60, 299(1985).

44) R.J. LeRoy, Computational Physics Comm. 52, 383(1989).

45) J.C.D. Brand, A.R. Hoy, A.K. Kalkar, and A.B. Yamashita, J. Mol. Spec. 95, 350(1982).

46) S. Gerstenkorn, P. Luc, and J. Sinzelle, J. Physique 41, 1419(1980).

47) M.S. Child, Molecular Collision Theory. (Academic Press, London: 1974) p. 235.

48) J. Tellinghuisen, J. Chem. Phys. 76, 4736(1982).

49) J.B. Koffend, R. Bacis, and R.W. Field, J. Chem. Phys. 70, 2366(1979).

50) O.J. Walker, Trans. Faraday Soc. 31, 1432(1935).

51) J.K. Brown, C.B. Harris, and J.C. Tully, J. Chem. Phys. 89, 6687(1988).

52) Tabulations of the mean force were less noisy than tabulations of absolute energy, thus saving computer time. However, a constant of integration is needed to convert the force tabulations to information regarding energy. This constant was determined by evaluating the energy at one distance in the simulations.

53) J.A. Blazy, B.M. Dekoven, T.D. Russell, and D.H. Levy, J. Chem. Phys. 72, 2439(1980).

54) P.B. Beeken, E.A. Hanson, and G.W. Flynn, J. Chem. Phys. 78, 5892(1983).

55) W.H. Press, B.P. Flannery, S.A. Teukolsky, and W.T. Vetterling, Numerical Recipes, The Art of Scientific Computing. (Cambridge University Press, Cambridge: 1986) p. 52.

56) R. Sension and H. Strauss, J. Chem. Phys. 85, 3791(1986).

57) S. Hirayama and D. Phillips, J. Photochem. 12, 139(1980).

58) S.R. Polo and M.K. Wilson, J. Chem. Phys. 23, 2376(1955).

59) M. Chatelet, J. Kieffer, and B. Oksengorn, Chem. Phys. 79, 413(1983).

60) M. Chatelet, B. Oksengorn, G. Widenlocher, and Ph. Marteau, J. Chem. Phys. 75, 2374(1981).

61) Nesbitt and Hynes have applied their gas phase model to the I_2/Xe system also as reported in: D.J. Nesbitt and J.T. Hynes, J. Chem. Phys. 76, 6002(1982). However, specific details regarding the results of these calculations are not presented.

62) J. Chesnoy and G.M. Gale, Ann. Phys. Fr. 9, 893(1984).

63) R.H. Stote and S.A. Adelman, J. Chem. Phys. 88, 4415(1988).

64) K. Herzfeld, J. Chem. Phys. 36, 3305(1962).

65) For a general review of this field see Ref. 62 and D.W. Oxtoby, Adv. Chem. Phys. 47, 487(1981).

66) D.J. Russell and C.B. Harris, paper in preparation.

67) L.J. Lowden and D. Chandler, J. Chem. Phys. 61, 5228(1974).

68) D.J. Tildesley and P.A. Madden, Mol. Phys. 48, 129(1983).

69) H.A. Kramers, Physica 7, 284(1940).

70) J.M. Dawes and M.G. Sceats, Chem. Phys. 96, 315(1985).

71) The viscosity has been estimated using the reduced state correlation method from O.A. Uyehara and K.M. Watson, Natl. Petroleum News 36, R714(1944) and H. Shimotake and G. Thodos, A.I.Ch.E.J. 4, 257(1958).

72) K.B. Wiberg and A. Schrake, Spectrochim. Acta 27, 1139(1971).

73) T. Shimanouchi and I. Suziki, J. Mol. Spectrosc. 6, 277(1961)

74) J.H. Schachtschneider and R.G. Synder, Spectrochim. Acta 19, 117(1963).

75) N.A. Abul-Haj and D.F. Kelley, J. Chem. Phys. 84, 1335(1986).

76) A.B. Callear and P.M. Shiundu, Chem. Phys. Lett. 136, 342(1987).

77) W.W. Rice, J.E. Barefield II, R.T. Pack, and B.A. Dye, J. Chem. Phys. 82, 58(1985).

78) G.E. Hall, W.J. Marinelli, and P.L. Houston, J. Phys. Chem. 87, 2153(1983).

79) R.J. Butcher, R.J. Donovan, and R.H. Strain, J. Chem. Soc. Faraday Trans. 2 70, 1837(1974).

80) L.J. Volk and E.K.C. Lee, J. Chem. Phys. 67, 242(1977).

Acknowledgments

My prolonged stay here has been greatly enhanced by working alongside some incredibly bright people from whom I have learned a great deal of science. Foremost among these people, I wish to thank Keenan Brown who has been a mentor as much as a colleague. Discussions with Keenan were always very illuminating and his influence pervades this work. In addition, he has either written or taught me how to write many of the data collection and analysis programs. Keenan did all of this in spite of the teasing he had to endure because of the total and crushing dominance the NY Giants have had over the Washington Hogs while he and I were here.

I owe much to Mark Berg, Alex Harris, and Dor Ben-Amotz who taught me the picosecond technology used in these experiments. Mark, in particular, spent several months teaching me the experimental techniques. Mark and Alex also performed the early I_2 experiments in this laboratory and it was at their suggestion and that of my advisor, Charles Harris, that I extended these experiments which turned into this thesis project. I hope that the results presented here are a source of satisfaction to Mark and Alex as it is as much a culmination of their work as it is mine.

I am very grateful to Flight Captain Dan Russell who was always willing to think over a problem or question (provided he had his minimum daily caffeine intake) and who has taught me a great deal of quantum and statistical mechanics. Dan also endured with me through many long late nights of data collection in the low density Xe experiments and could always interpret my unintelligible babble (e.g., battery = flashlight).

Rebecca Hoff collaborated with me on the I_2/CS_2 project and I thank her for her efforts on this project, particularly since the results of this work will not be published. Mr. Comedian (Dave Smith) and Eric Peterson lent helping hands in the Xe experiments for which I am grateful. I hope Dave has recovered his breath from the innumerable explanations of GLE I implored of him. I thank Jin Zhang and Karen Schultz for proofreading this document and for their helpful suggestions regarding it. I understand that their insomnia problems have now been cured.

In addition, I am grateful for the sense of humor which pervades the group and has injected a great deal of levity to the somber 2 AM atmosphere of D level. Aside from those already mentioned, these personalities include convicted fruit abuser Walt Merry(•••-) and Robert "Pumpkin Pie" Jordan(••••) from Walbert Welding Co., Inc.®, the Truc. Karen Monster Schultz(••-), Jennifer "the Whoop" Hane(•••-), the CAP of operator fame (Craig Parsons), Ben "Frozen Yogurt" Schwartz (- - - -) who along with Walt formed the famous Food Hotline, Dee "Popcorn" Pennington(--), Eric Avocado Haas, Avogadro the Skiing Mole (also ••••), and, of course, the Moose.

Lastly, I want to thank Mom and Dad who may not have understood what I have been doing, but were always very supportive throughout this long "educational" process. I am very appreciative of their efforts and sacrifices on my behalf and particularly recall my mom saving money from her job since I was 12 years old in order to put me through college.

Funding for this work was provided by the National Science Foundation and the Office of Naval Research. The U.S. Department of

Energy, Office of Basic Energy Sciences, Chemical Sciences Division, under Contract No. DE-AC03-76SF00098 provided some specialized equipment which was used in these experiments.

LAWRENCE BERKELEY LABORATORY
TECHNICAL INFORMATION DEPARTMENT
1 CYCLOTRON ROAD
BERKELEY, CALIFORNIA 94720